INVESTIGATION AND PROPOSED REMEDY OF VIBRATION PROBLEM IN INDUSTRIAL CRANE SYSTEM DUE TO HUMAN OPERATION

by

DUSTIN C. LORANCE

Presented to the Faculty of the Graduate School of

The University of Texas at Arlington in Partial Fulfillment

of the Requirements

for the Degree of

MASTER'S OF SCIENCE IN CIVIL ENGINEERING

THE UNIVERSITY OF TEXAS AT ARLINGTON

August 2017

ACKNOWLEDGEMENTS

I would like to thank anyone who has supported myself throughout this journey. Special thanks to my advisor, Dr. Chao, for agreeing to be my advisor on this minimally researched topic. Dr. Chao accommodated my work schedule and made it possible for me to complete this project. I would also like to extend gratitude a towards the support team at LUSAS. Learning the program and running the numerous models would not have been possible without the personal one-on-one experience and help they provided. Lastly, a special thanks to my girlfriend, Racia Ratliff, who tirelessly waited for me to finish and supported me with everything I needed in the process.

Dustin Lorance
July 31, 2017

ABSTRACT

INVESTIGATION AND PROPOSED REMEDY OF
VIBRATION PROBLEM IN INDUSTRIAL CRANE
SYSTEM DUE TO HUMAN OPERATION

Dustin Lorance, MS

The University of Texas at Arlington, 2017

Supervising Professor: Shih-Ho Chao

A recent investigation of a crane system began when a facilities manager reported a runway beam under-going torsional vibration during operations. The investigation revealed the runway beam's twisting was caused by resonance vibration due to "inching" of the crane hoist. A Fourier spectrum analysis revealed that one of the harmonic frequencies of this rhythmical motion coincided very close to the natural frequency of the crane system. The runway beam, although met strength requirements, failed to meet serviceability criteria due to the resonance vibration. Resonance vibration issues due to human activity in crane operation (inching, sway, etc.) is often encountered by engineers when designing crane runways. These issues are even more familiar in long-span crane runways where limited bracing opportunities exist. While vibration resonance issues, of all modes, may be known to many designers of crane structures, the time required to run an in-depth dynamic analysis is usually not economical for such a simple structure. Possible critical vibration issues coupled with the inability to perform an in-depth analysis requires design engineers to use very conservative design recommendations regarding vibration. The few design recommendations found in current standards are very broad and offer little-to-no commentary, and the application of such design recommendations may or may not support a critical vibration mode. The resulting overdesign may reinforce a vibrational mode

which is not necessarily an object of concern. The cost associated with the overdesign could have possibly been directed towards a more vibrational sensitive mode. This study first investigated the cause of the resonance vibration. Secondly, through extensive finite element analyses (FEA), a practical solution is recommended. Lastly, using the FEA results, alongside current standards, a set of design equations are formulated to aid in future crane runway vibration design in addition to the limited vibration research.

TABLE OF CONTENTS

LIST OF FIGURES

LIST OF TABLES

CHAPTER 1

INTRODUCTION

1.1 OBJECTIVES

- To investigate the general structural performance of the crane system presented herein.
- To investigate the general stability of the crane system presented herein
- To evaluate the cause behind the presented crane system's instability
- To investigate critical variables in the crane systems stability
- To propose design solutions to alleviate any instability within the crane system
- To introduce approximate equations to be used in preliminary design

1.2 THESIS OUTLINE

Chapter 2 of this thesis presents the commonly used methods and equations used in crane runway design. This chapter will investigate the difference between the standards, articles, methods, and "rules of thumbs" and their shortcomings. General recommendations are made to a design format based on all the compiled information.

Chapter 3 of this thesis reviews an industrial crane in which the runways exhibited torsional rotations due to vibration from human operation. A hypothesis is made as to why the vibration occurred in the crane runways. Likewise, the design of the crane system is reviewed with respect to code compliance.

Chapter 4 of this thesis discusses the finite element model used to model the crane system. The processes and assumptions made while constructing the model are investigated. The assignments made within the model are discussed.

Chapter 5 of this thesis introduces the results of the finite element model. Likewise, the results obtained through the crane system are examined. Both the model's results and analytic crane system's actions are compared. Any error between the two are discussed and possible interpretations of such are made.

Chapter 6 of this thesis investigates a variety of possible design solutions for the crane structure. Each investigation is modelled and analyzed through the analysis software. The results of each solution are compared to the original model. Each solution is discussed based on economics, structural integrity, and performance under vibration.

Chapter 7 of this thesis investigates possible preconstruction design equations. The proposed equations are simplified methods able to be calculated quickly for possible torsional vibration concerns. Each method is compared to the analytic crane structure and the finite element model.

CHAPTER 2

CRANE DESIGN REVIEW

2.1 INTRODUCTION

There are a variety of governing organizations that offer guidance, recommendations, and analysis procedures in the design of overhead bridge crane runway beams. Some of these guidelines and requirements vary between each organization. Such differences may lead to different design outcomes. The discussion presented below will present a summary of the standards most commonly used in the design of overhead bridge cranes per the load factor resistance design (LRFD). The reader should be aware that although many of the standards vary, there is no evidence that any guideline or specification will result in an under-designed runway beam. A few miscellaneous topics may be mentioned as needed.

2.2 CRANE CLASSIFICATIONS

The operation frequency and type, working period, traveling speed and precision of handling, to name a few, are important factors that need to be considered in the design. The classifications of cranes attempt to predict the amount of work performed by the crane, which in-turn, allows the designer to establish how the crane will be affected under normal operating conditions over the service life of the structure particularly about fatigue. Two standards, Crane Manufacturers Association of America (CMAA) and Association of Iron and Steel Technology (AIST), provide crane classifications that will be listed below.

2.2.1 CMAA CRANE CLASSIFICATION

The following classifications have been taken directly from CMAA (CMAA, 2010):

Class A (Standby or Infrequent Use): This service class covers cranes which may be used in installations such as powerhouses, public utilities, turbine rooms, motor rooms and transformer stations where previse handling of equipment at slow speeds with long, idle periods between lifts are required. Capacity loads may be handled for initial installation of equipment and for infrequent maintenance.

Class B (Light Service): This service covers cranes which may be used in repair shops, light assembly operations, service buildings, and light warehousing [to name a few] where service requirements are light and the speed is slow. Loads may vary from no load to occasional full rated loads with 2 to 5 lifts per hour, averaging 10 feet per lift.

Class C (Moderate Service): This service covers cranes which may be used in machine shops or papermill machine rooms, etc., where service requirements are moderate. In this type of service the crane will handle loads which average 50 percent of the rated capacity with 5 to 10 lifts per hour, averaging 15 feet, not over 50 percent of the lifts at rated capacity.

Class D (Heavy Service): This service covers cranes which may be used in heavy machine shops, foundries, fabricating plants, steel warehouses, container yards, and lumber mills [to name a few] and standard duty bucket and magnet operations where heavy duty production is required. In this type of service, loads approaching 50 percent of the rated capacity will be handled constantly during the working period. High speeds are desirable for this type of service with 10 to 20 lifts per hour averaging 15 feet, not over 65 percent of the lifts at rated capacity.

Class E (Severe Service): This type of service requires a crane capable of handling loads approaching a rated capacity throughout its life. Applications may include magnet, bucket, magnet/bucket combination cranes for scrap yards, cement mills, lumber mills, fertilizer

plants, and container handling [to name a few] with twenty or more lifts per hour at or near the rated capacity.

Class F (Continuous Severe Service): This type of service requires a crane capable of handling loads approaching rated capacity continuously under severe service conditions throughout its life. Applications may include custom designed specialty cranes essential to performing the critical work tasks affecting the total production facility. These cranes must provide the highest reliability with special attention to ease of maintenance features.

2.2.2 AIST CRANE CLASSIFICATION

The following classifications have been taken directly from AISE (AISE, 2003).

Class A: Buildings in this category are those in which members might experience either 500,000 to 2,000,000 repetitions in the expected service life of the structure.

AIST lists a set of building types which AIST recommends to be considered as Class A. See AISE 13, 2003 for the list.

Class B: Buildings in this category are those building in which members experience 100,000 to 500,000 repetitions of a specific loading during the expected service life of the structure.

Class C: Buildings in this category are those building in which members experience 20,000 to 100,000 repetitions of a specific loading during the expected service life of the structure.

Class D: Buildings in this category are those building in which no member will experience more than 20,000 repetitions of a specific loading during the expected service life of the structure.

2.2.3 CRANE CLASSIFICATION COMPARISON

The CMAA crane classification is based on a specific cranes use, service speed, number and height of lifts on a day-to-day basis. The AIST crane classification is based on a loading classification and repetition over the course of the service life of the structure; AIST recommends a service life of 50 years for the structure. Because the crane classification is used to determine, for the most part, fatigue provisions, the more specific CMAA crane classification may be more useful in determining related criteria based on the function of the structure. The CMAA crane classification will be used as the standard in this thesis.

2.3 CRANE RUNWAY LOADS & LOAD COMBINATIONS

The dimensions of the crane, rated capacity, bridge wheel loads, weight of trolley, total weight of crane, bridge and trolley speed, cab clearances, bridge bumper forces, lifted load, size of runway rail, and type of crane should be supplied by the owner or crane manufacturer (AISE, 2003). With the previously listed information, the design forces imposed on the crane runway can be calculated. Crane runway loads/forces consist of vertical, lateral, and longitudinal forces which account for the forces generated statically and/or dynamically during the travelling and/or hoisting process. For simplification purposes, only forces specific to cranes and crane loads will be reviewed. Other vertical, lateral, or longitudinal loads not specific to cranes such as wind or seismic should be analyzed and applied accordingly. Engineering judgement should be used in the combination of wind and seismic forces with crane loads.

2.3.1 VERTICAL LOADS

The vertical loads are a combination of the bridge, trolley, and hoist weight of the crane as well as the rated capacity of the crane as shown in *Figure 2-1* below.

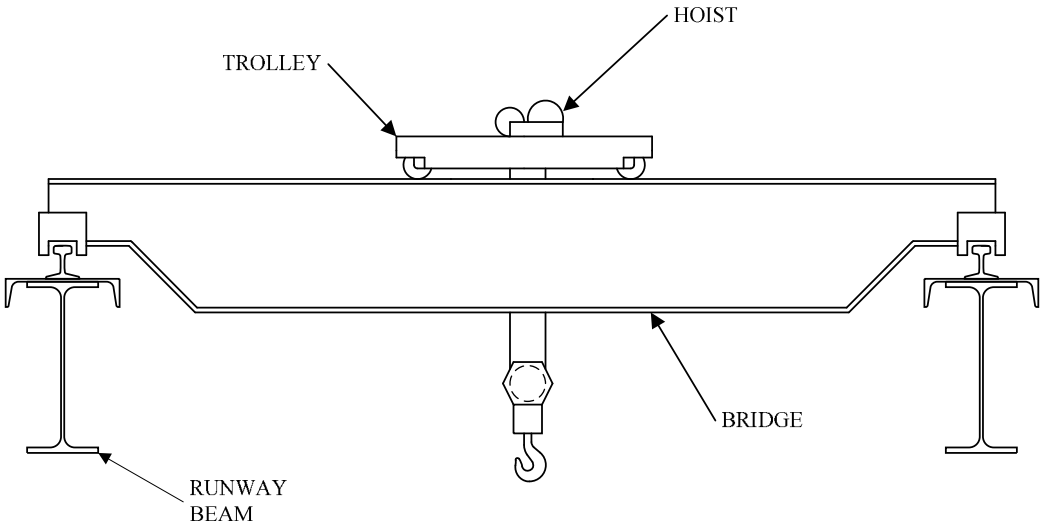

Figure 2-1 Overhead Bridge Crane Assembly

Chapter 4, Section 9 of ASCE7-10 (Crane Loads) addresses the use of design loads for runway beams. The maximum wheel load as defined by ASCE7-10 4.9.2 (Maximum Wheel Load) is the “wheel loads produced by the weight of the bridge plus the sum of the rated capacity and the weight of the trolley with the trolley positioned on its runway at the location where the resulting load effect is maximum” (ASCE, 2010). The component weights supplied by the crane manufacturer are given as the full weight, and most often the weight of the trolley and hoist will be given as a total combined weight. The maximum wheel load does not include the hoist weight, so for the most economical design the hoist weight should be subtracted from the combined weight of the trolley and hoist weight. A conservative approach could be made where the combined trolley and hoist weight provided by the manufacturer is taken as the trolley weight in the design.

To calculate the maximum wheel-load the total weights must be converted into individual wheel loads. The bridge weight is equally proportioned between the two runway beams and so the bridge weight per individual wheel will be equal to the weight divided by the total number of wheels. The trolley and hoisted load (rated capacity) can be positioned such that weight of these components is centralized on one side such as when lifting a load near one of the runway beams. For this reason, the trolley and hoisted load weight per individual wheels is equal to the total weight (of the three components) divided by the number of wheels per runway beam. The vertical load induced can be translated in equation form as;

$$W_{trolley} = P_{max} - W_{bridge} - W_{capacity} \quad (2\text{-}1)$$

$$P_{max} = W_{bridge} + W_{trolley} + W_{capacity} \quad (2\text{-}2)$$

Where,

W_{bridge} = Weight of the bridge per individual wheel load

$W_{trolley}$ = Weight of the trolley per individual wheel load

$W_{trolley+hoist}$ = Combined weight of the trolley and hoist per individual wheel load

$W_{capacity}$ = Weight of the rated capacity per individual wheel load

In addition, all design specifications make use of a vertical impact factor or percentage increase in the vertical force. The impact factor is a static force equivalent to account for the acceleration in hoisting loads, as shown in *Figure 2-2*, and impact produced by wheels traveling over irregularities in the rail (MBMA, 2006). In addition to acceleration and rail irregularities, the vertical impact factor to accounts for vibration force (ASCE, 2010).

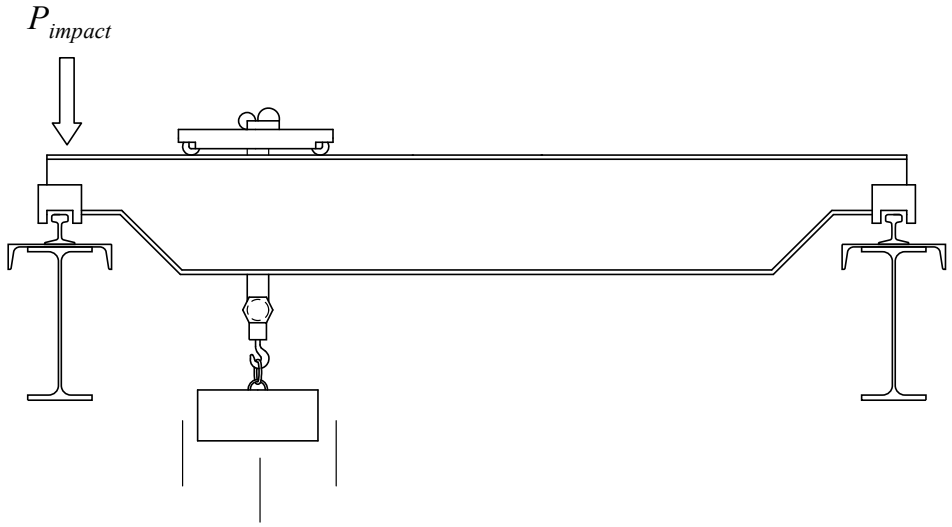

Figure 2-2 Vertical Impact

The vertical impact is to be multiplied by the maximum wheel load previously defined. *Table 2-1* summarizes the percentage increase in the vertical forces (ASCE, 2010);

Crane Type	Vertical Impact (%)
Monorail cranes (powered)	25
Cab-operated or remotely operated bridge cranes (powered)	25
Pendant-operated bridge cranes (powered)	10
Bridge cranes or monorail cranes with hand-geared bridge trolley, and hoist	0

Table 2-1: ASCE 7-10 Vertical Impact Percentage

The vertical impact factor can be expressed in equation form as;

$$P_{impact} = f_{impact} \cdot P_{max} \quad \text{(2-3a)}$$

Or in expanded form;

$$P_{impact} = f_{impact} \cdot \left(W_{bridge} + W_{trolley} + W_{capacity}\right) \quad \text{(2-3b)}$$

Where,

f_{impact} = Vertical impact factor per ASCE

The Association of Iron and Steel Engineers (AISE) (previously Association of Iron and Steel Technology, AIST) also provides vertical impact factors for a variety of cranes such as mill, ladle, clamshell/magnet, soaking pit, stripping, motor room, and stacker cranes. *Table 2-2* taken from *AISE Guide for the Design and Construction of Mill Buildings,* includes the vertical impact factor per AIST's requirements. The vertical impact, like that in ASCE, is a percentage of the maximum wheel load (same definition as ASCE).

Crane Type	Vertical Impact (%)
Mill Cranes	25
Ladle Cranes	25
Clamshell bucket and magnet cranes (including slab and billet yard cranes)	25
Soaking pit cranes	25
Stripping cranes	25
Motor room maintenance cranes, etc.	20
Stacker cranes (cab-operated)	25

Table 2-2: AISE Vertical Impact Percentage

2.3.2 LATERAL LOADS (SIDE THRUST)

The lateral load generated on crane runways, in general, come from the trolley running into the bridge end stops, runway misalignment, crane skew, trolley acceleration and braking, and crane steering (Fisher, DG 7, 2004) as shown in *Figure 2-3*. "Drive mechanisms provide either equal drive wheel torque on each side of the crane or they are

balanced to align the center of the tractive force with the center of gravity of the crane and lifted load. If the drive mechanism is not balanced, acceleration and deceleration of the bridge crane results in skewing of the bridge relative to the runways. The skewing imparts lateral loads onto the crane girder. Oblique [skewed] travel may be thought of as being similar to the motion of an automobile with one tire underinflated. The tendency of the crane to wander can be minimized by properly maintaining the end trucks and the rails. The wheels should be parallel and they should be in similar condition of wear. The rails should be kept aligned and the surfaces should be smooth and level. A poorly aligned and maintained runway can result in larger lateral loads. The relatively larger lateral loads will in turn reduce the service life of the crane girder" (MBMA, 2006).

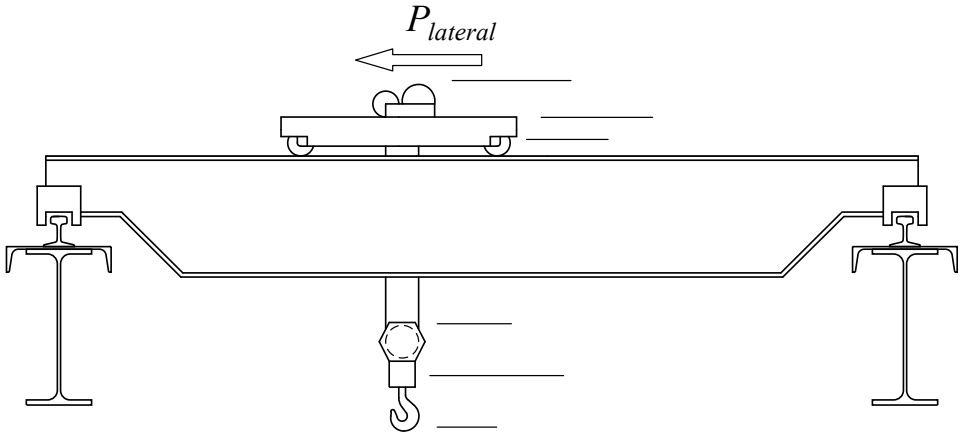

Figure 2-3 Lateral Load

ASCE specifies the lateral force on crane runway beams with electrically powered trolley as "20 percent of the sum of the rated capacity of the crane and the weight of the hoist and trolley" (ASCE, 2010). ASCE stipulates that "the lateral force shall be assumed to act horizontally at the traction surface (top of the rail) of a runway beam in either direction

perpendicular to the beam, and shall be distributed with due regard to the lateral stiffness of the runway beam and supporting structure" (ASCE, 2010).

The lateral force can be translated in equation form to (assuming equal stiffness, and therefore, distributed equally);

$$P_{lateral} = 0.20 \cdot \left(W^{T}{}_{trolley+hoist} + W^{T}{}_{capacity} \right) \qquad \text{(2-4a)}$$

$$\frac{P_{lateral}}{wheel} = \frac{0.20 \cdot \left(W^{T}{}_{trolley+hoist} + W^{T}{}_{capacity} \right)}{\#_{wheels}} \qquad \text{(2-4b)}$$

Where;

$W^{T}{}_{trolley+hoist}$ = Total weight of the trolley and hoist (not per individual wheel)

$W^{T}{}_{capacity}$ = Total weight of the rated capacity (not per individual wheel)

$\#_{wheels}$ = Total number of trolley wheels

AISE also provides side thrust or lateral forces. "The total side thrust should be distributed with due regard for the lateral stiffness' of the structures supporting the rails" (AISE, 2003). The total lateral load, per AISE, should be the greatest of a percentage of the lifted load (found in *Table 2-3*), 20% of the combined weight of the lifted load and trolley (40% of the combined weight of the lifted load, trolley, and rigid arm for stacker cranes), and 10% of the combined weight of the lifted load and the crane weight (15% of the combined weight of the lifted load and the crane weight for stacker cranes) (AISE, 2003). For pendant-operated cranes, the lateral force shall be "10% of the combined weight of the lifted load and crane weight" (AISE, 2003). The lifted load, per AISE, is defined as "a total weight lifted by the hoist mechanism, including working load, all hooks, lifting beams, magnets or other appurtenances required by the service but excluding the weight of column

ram or other material handling device which is rigidly guided in a vertical direction during hoisting action" (AISE, 2003).

Crane Type	Lateral Force (%)
Mill Cranes	40
Ladle Cranes	40
Clamshell bucket and magnet cranes (including slab and billet yard cranes)	100
Soaking pit cranes	100
Stripping cranes	100
Motor room maintenance cranes, etc.	30
Stacker cranes (cab-operated)	200

Table 2-3: AISE Lateral Force Percentage

2.3.3 LONGITUDINAL LOADS

"Longitudinal crane forces are due to either acceleration or deceleration of the crane bridge or the crane impacting the bumper" (MBMA, 2006) as shown in *Figure 2-4*. The longitudinal force percentage can be rationalized as proportional to the friction coefficient between the wheels of the bridge crane and rail atop the runway beam. The longitudinal force required by ASCE is to be taken as 10 percent of the maximum wheel loads of the crane. Likewise, the longitudinal force "shall be assumed to act horizontally at the traction surface of a runway beam in either direction parallel to the beam" (ASCE, 2010). ASCE does not require a longitudinal load in crane runway beams in which the bridge is hand-geared.

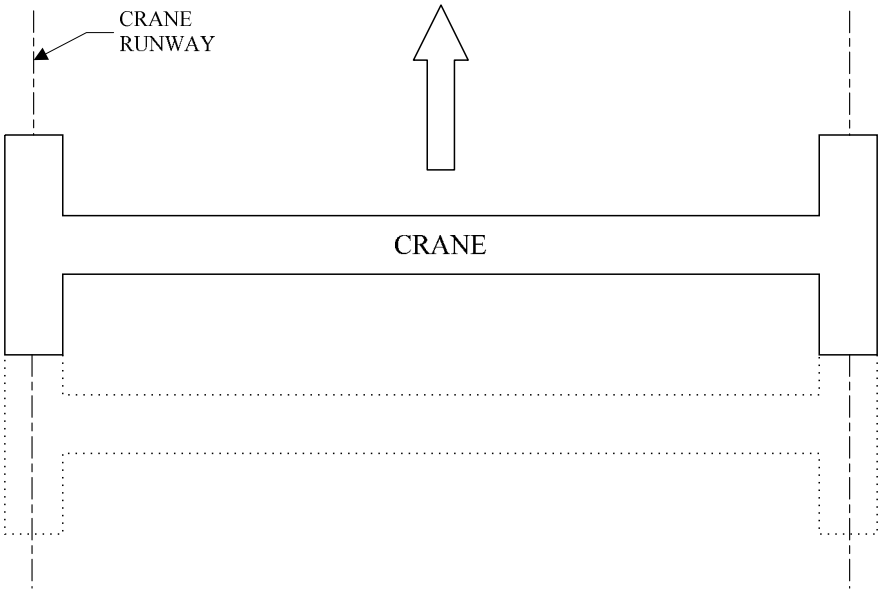

Figure 2-4 Longitudinal Load

The longitudinal force can be translated in equation form to;

$$\frac{P_{longitudinal}}{wheel} = 10\% \cdot (P_{max}) = 0.10 \cdot (P_{max}) \qquad \text{(2-5a)}$$

Or in expanded form;

$$\frac{P_{longitudinal}}{wheel} = 0.10 \cdot (W_{bridge} + W_{trolley} + W_{load}) \qquad \text{(2-5b)}$$

Where;

$\frac{P_{longitudinal}}{wheel}$ = Longitudinal force per wheel

In lieu of creating another table for the longitudinal force per AIST, AIST requires "20% of the maximum load on the driving wheels" (AISE, 2003) for the longitudinal (tractive) force for all crane types as well as pendant-operated cranes.

2.3.4 LOAD COMBINATIONS

ASCE gives no specific load combinations regarding cranes or crane loads nor does ASCE offer any insight on the appropriate factors to use. James Fisher, recommends using a load factor of 1.2 for the bridge weight and a load factor of 1.6 for the hoist and trolley (Fisher, DG 7, 2004). Both *AISE Guide for the Design and Construction of Mill Buildings* (AISE, 2003) and MBMA *Low Rise Building Systems Manual* (MBMA, 2006) provide load combinations specific to crane loads for single and multiple cranes in a variety of configurations: The AISE and MBMA provide very similar load combinations. The load combinations in both AISE and MBMA are in ASD loading format. The LRFD load combinations will be chosen based off the ultimate load factors recommended by Fisher (Fisher, DG 7, 2004).

For the vertical ultimate load combination (ULC);

$$ULC_{vertical.1} = 1.2 \cdot \left(W_{bridge}\right) + 1.6 \cdot \left(W_{trolley+hoist} + W_{load}\right) \qquad (2\text{-}6)$$

$$ULC_{vertical.2} = 1.2 \cdot \left(DL\right) \qquad (2\text{-}7)$$

For the vertical ultimate load combination including impact;

$$ULC_{vertical+impact} = ULC_{vertical.2} + \left(1 + f_{impact}\right) \cdot ULC_{vertical.1} \qquad (2\text{-}8)$$

Where;

DL = Combined dead-load of the runway beam and rail

For the lateral ultimate load combination;

$$ULC_2 = 1.6 \cdot P_{lateral} \qquad (2\text{-}9a)$$

Or in expanded form;

$$ULC_2 = 1.6 \cdot \left(0.20\right) \cdot \left(W_{trolley+hoist} + W_{load}\right) \qquad (2\text{-}9b)$$

$$ULC_2 = (0.32) \cdot (W_{trolley+hoist} + W_{load}) \quad \text{(2-9c)}$$

As well as providing load combinations specific to cranes, AIST and MBMA each provide load combinations for crane loads combined with rain, snow, seismic, and wind (ASD format). As mentioned before, this thesis will only cover loads specific to cranes. For more information on crane load combinations including rain, snow, seismic, and/or wind refer to *AISE Guide for the Design and Construction of Mill Buildings* (AISE, 2003) and MBMA *Low Rise Building Systems Manual* (MBMA, 2006)

2.4 SIMPLE VS. CONTINUOUS SPAN

Although the discussion is focused on simple span crane beams, the information presented throughout can be used or adopted easily for continuous spans. In addition, the reader may benefit from knowing the advantages and disadvantages between the simple span and continuous span runway beams. Cantilever spans will not be covered.

2.4.1 SIMPLE SPAN

Listed below are the advantages of simple span crane beams mentioned by Fisher (Fisher, DG 7, 2004);

- *Much easier to design for various load combinations*
- *Generally unaffected by differential settlement of the supports*
- *More easily replaced if damaged*
- *More easily reinforced if the crane capacity is increased.*

The simple span has the advantage of simplicity. Crane runway beams need to be analyzed for a variety of combinations (when rain, snow, seismic, and wind are included)

under both ultimate and service states. Likewise, the crane runway beam must be analyzed under sever different wheel positions under each combination to find the maximum stresses and deflections. The simple span, a determinant system, is easier to analyze, compared to the continuous non-determinant system, under multiple loads for various load combinations. A single crane runway supporting multiple cranes is another frequently encountered situation where the simplicity of analysis would be largely beneficial. Much like differential settlement, simple span cranes are less affected (compared to the continuous span) to expansive (primarily shrinking) (or collapsible) soil movement. In addition to the advantages listed above, simple span crane beams offer the greater performance when fatigue is considered due to having no reverse stress considerations when the crane bridge moves along the runway beam. Simple span crane beams may also be the most economical choice when various spans are involved.

2.4.2 CONTINUOUS SPAN

Listed below are the advantages of continuous span crane beams mentioned by Fisher (Fisher, DG 7, 2004);

- *Continuity reduces deflections that quite often control*
- *End rotations and movement are reduced.*
- *Generally result in lighter weight shapes and a savings in steel cost when fatigue considerations are not a determining factor*

"Continuous girders should not be used if differential settlement of the supports is of the magnitude that could cause damage to the continuous members (Fisher, DG 7, 2004). Although not specifically mentioned, expansive and collapsible soil movement follows the same principle. The designer, when using continuous runways need also to investigate fatigue issues and any reductions in stress should be accounted for in the design.

Special note should be made that AISC discourages the use of continuous crane runway girders because “they are subject to many problems and a short fatigue life” (ASIC, 2010). Likewise, AIST states, “direct interconnection that would restrain relative rotation between adjacent ends of successive girders is not recommended” (AISE, 2003).

2.5 CRANE RUNWAY MEMBERS

If the vertical, lateral, and longitudinal imposed forces mentioned previously permit, the use of a wide flange beam (“W” shape per AISC) is often times most economical and practical. However, due to the stresses and deflections imposed by the lateral loads in heavier cranes, a wide flange beam with a channel welded to the top, as shown in *Figure 2-5*, is commonly used. The built-up member consisting of a channel (“C” shape per AISC) welded atop a wide flange beam can be found in AISC’s *Steel Construction Manual* page 1-115 (ASIC, 2010). Studies have found that a steel savings of approximately 25 lb/ft. is required to justify the cost of welding a cap to a structural shape (Fisher, DG 7, 2004).

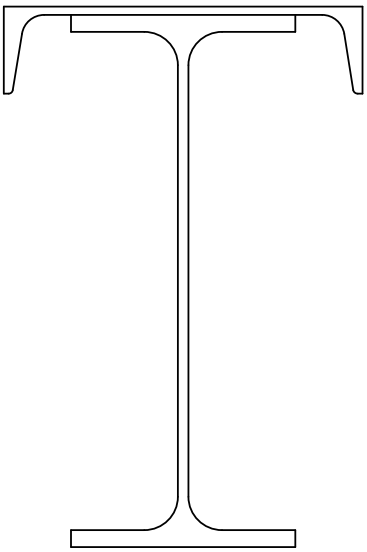

Figure 2-5 Cap Channel Section

"It should be noted that the cap channel or plate does not fit perfectly with 100% bearing on the top of the wide flange. The tolerances given in ASTM-A6 allow the wide flange member to have some flange tilt along its length, the plate may be cupped or slightly warped, or the channel may have some twist along its length. These conditions will leave small gaps between the top flange of the girder and the underside of the top plate or channel. The passage of the crane wheel over these gaps will tend to distress the channel or plate to top flange welds. Because of this phenomenon, cap plates or channels should not be used with class E or F cranes" (MBMA, 2006).

2.6 MISCELLANEOUS DETAILS

The intent of this chapter is for the reader to further their knowledge on the design of overhead crane runways. The assumptions made in design, however, must be analogous to the actual characteristics and performance of the structure. The unbraced

length term, L_b, used in the lateral-torsional buckling provision, for example, is defined as the “length between points that are either braced against lateral displacement of the compression flange or braced against twist of the cross section” (ASIC, 2010). A crane runway beam bearing on support columns (each end) will, by definition, have no resistance to lateral displacement or twisting of the cross section; the unbraced length would theoretically approach infinity. Likewise, due to fatigue issues, many details are special for crane beams; developed by rational mathematical methods, research, and years of experience. The following sections will address certain details that are specific to overhead crane runway beams and the assumptions made in the design process.

2.6.1 RUNWAY END CONNECTIONS

2.6.1.1 Tiebacks

Tiebacks are a type of connection serving two purposes: 1) transfer the lateral forces from the runways beams top flange to the support (such as a column) and 2) the tieback must provide adequate lateral restraint against buckling of the compression flange (Fisher, DG 7, 2004). The connection must be designed sufficiently to transfer the lateral loads from the crane to the column, however, the connection must be detailed in such a way to accommodate the longitudinal movement due to the beam end rotation. A common example presented in DG-7 can illustrate the magnitude of longitudinal movement: “The end rotation of a 40-foot girder that has deflected 0.8 inches (span over 600) is about 0.005 radians. For a 36-inch deep girder, this results in 0.2 inches of horizontal movement at the top of the girder” (Fisher, DG 7, 2004). In additional to longitudinal movement, tiebacks must be flexible enough to allow for vertical movement due to axial shortening which can be in the range of a quarter of an inch (Fisher, DG 7, 2004).

For a typical tie-back connection, any configuration of detail is acceptable “if the flange is connected directly for transverse forces and allowed to move longitudinally” (Mueller, 1965). Tieback connections that do not allow for the vertical and horizontal movement of the crane girder should be avoided. A common past connection, the diaphragm plate, attempts to retrain the beam movement which it was not designed for (Mueller, 1965). “The lateral load path for this detail causes bending stresses in the girder web perpendicular to the girder cross section” (Fisher, DG 7, 2004). The localized stress due to this detail often results in fracturing of the diaphragm and loosening and/or shearing of the fasteners (Mueller, 1965). Mueller suggests for repairs or retrofits of old crane girders, the diaphragm connection should be eliminated and replaced with a direct top flange connection such as a tieback (Mueller, 1965).

2.6.1.2 Bearing Stiffeners

A pair of transverse stiffeners, or bearing stiffeners, is required by AISC Specification J10.7 (pg-138) at any unframed ends of beams and girders not otherwise restrained against rotation about their longitudinal axes (ASIC, 2010). The transverse stiffeners are required per AISC to extend the full depth of the web. Likewise, AISE (AISE, 2003) recommends bearing stiffeners be welded to the top and bottom flange using full penetration (beveled) welds. The use of the less expensive, in comparison to full penetration, fillet welds are not forbidden by AISC. Fatigue criteria is available in AISC to design fillet welds in shear (developed by the passage of the crane wheel), however, the “determination of the actual stress state in the welds is extremely complex” (Fisher, DG 7, 2004). Likewise, fatigue cracks have been observed to in runway beams which utilized a bearing stiffener fillet welded to the top flange of the girder (Fisher, DG 7, 2004). AISE recommends that all bearing stiffeners to girder web welds be continuous (AISE, 2003).

2.6.2 INTERMEDIATE BRACING

2.6.2.1 AISE-13 Bracing Requirements

AISE requires girders with spans equal to or greater than 36 feet (or 40 feet in Class D or greater buildings) to have the “bottom flanges stiffened by means of a bracing system connected to an adjacent girder or stiffening truss” (AISE, 2003). The bracing requirements set by AISE are still commonly referenced in literature. AISE, however, gives no commentary on the nature of this bracing requirement. Although the requirements of this provision are not known, the AISE limitation on the length of the unbraced tension flanges was likely created to address the web sidesway buckling phenomena (MBMA, 2006). “The sidesway buckling criteria was introduced into the AISC ASD Specification in the Ninth Edition. Runway girders designed prior to this time would not have been checked for this criteria” (MBMA, 2006). Common industry practice is to ignore this requirement if the provisions of web sidesway buckling are satisfied. Note should be made that AISE is not a legal requirement and should be used as a guideline.

2.6.2.2 Lacing

Lacing is a method to connect the top flange of the runway beam to an adjacent structural member to provide, or rather increase, the lateral stability and buckling resistance of runway beams (Fisher & Van De Pas, 2002). The intermediate members (laces) typically are composed of angles; however, lacing can also be achieved using a top plate. Special precaution should be taken in using these details. The crane runways beam will deflect vertically as the crane travels along the member, however, the structural member who the runway is laced will not experience the same vertical deflection. The lacing system must be designed flexible to accommodate the differential vertical deflection. “If the lacing is not

flexible, stresses will be produced which could cause a fatigue failure of the lacing system, thereby losing the lateral support for the girder" (Fisher, DG 7, 2004).

2.6.2.3 Intermediate Stiffeners

Intermediate stiffeners may be used to increase the shear buckling strength of the member as well as resist torsional forces. Intermediate, or nonbearing, stiffeners permitted to be stopped short of the tension flange in accordance with AISC Specification G2.2 (pg.16.1-60). AISE (AISE, 2003) requires that intermediate stiffeners be connected to the compression flange using a full penetration weld. AISE recommends that all intermediate stiffeners to girder web welds be continuous, and the stiffeners to have clipped corners to provide clearance for the web to flange welds (AISE, 2003). The designer considering the use of intermediate stiffeners should first think of a member with a thicker web without intermediate stiffeners as a better solution; the "simplicity, more rugged web-to-flange connection, elimination of details subject to fatigue in the tension zone of the web and distortion-induced to fatigue" (MacCrimmon, 2009). Utilizing intermediate stiffeners may be a good option for the upgrading or repair of runway beams (MacCrimmon, 2009).

2.7 CRANE RUNWAY BEAM DESIGN

The crane runway beam, consisting of a wide flange beam, can be designed using the standard equations from the AISC *Steel Construction Manual*. Because of the popularity in using the WC section for crane runways, and the slight modification of AISC's equations needed for the design of WC sections, the following design review will focus on the WC section.

2.7.1 STRENGTH (ULTIMATE) DESIGN

The wide flange beam denoted here by “W”, and the wide flange beam with a channel welded to the top denoted here by “WC”, are the two most common shapes chosen as runway beams. The design for the WC is not well established in AISC’s *Steel Construction Manual*. The current design practice of a WC section has been to use the monosymmetric equations from Chapter F5 of AISC’s *Specification for Structural Steel Buildings* (Specification for Structural Steel Buildings, 2010). The equations from Chapter F5, however, are for three plated monosymmetric structures. Moreover, these equations use section properties not found in the *Steel Construction Manual* and therefore must be arduously calculated or found by approximations which can have considerable error.

2.7.1.1 Major Flexure

A common method to design crane runways has been to use the provisions from AISC’s *Steel Construction Manual* Chapter F4 “Other I-Shaped Members with Compact or Noncompact Webs Bent about Their Major Axis” (ASIC, 2010). Under this section, the limit states of compression flange yielding, lateral torsional buckling, compression flange local buckling, and tension flange yielding are investigated. Although compactness criteria for these shapes is not addressed in the AISC shapes table (pg.1-114). Verification of web compactness/slenderness could be verified manually using the cases 16 and 18 in Table B4.1b of the *Steel Construction Manual* (AISC 2011) for the web and flange respectively.

The lateral torsional buckling equation under “Chapter F4” is derived from rolled (or welded) three-plate section monosymmetric beams which do not apply to Cap Channel beams, likewise, the equations require the tedious and time consuming calculation of section properties (Elifritt & Lue, 1998). Similarly, the wheel loads are not applied through the shear center. When the wheel loads are applied above the shear center, the loads exert

a torque about the shear center which augments the rotation from lateral torsional buckling thereby reducing the buckling resistance (Galambos, 2008). AISC addresses when loads are not applied through the shear center and directs the designer to the SSRC Guide and other references (ASIC, 2010). The SSRC Guide, however, only addresses the height of load application for doubly symmetric beams. For the limit state of lateral torsional buckling, a suggested design procedure proposed by Ellifritt (Elifritt & Lue, 1998) will be utilized. The design procedure proposed for the limit state of lateral torsional buckling is based off section properties readily available within the AISC Steel Construction Manual (Elifritt & Lue, 1998). For shapes not listed in AISC, the equations by Ellifritt (Elifritt & Lue, 1998), which are presented here, offer good results. To address the effect of the load height relative to the shear center a modified version of the C_b variable from Nethercot & Rockey (Nethercot & Rockey, 1972) will be used. The summary of the lateral torsional buckling design procedure can be found below. The lateral torsional buckling strength equations here, much like those in chapter F, are derived from the nominal moment transition from a plastic design to inelastic and elastic lateral torsional buckling based on the unbraced length.

The reader should note, for simplification purposes, the section properties will be listed as normal (usual format of AISC) with an additional “W” or “C” superscript indicating the section property of the wide flange beam (W), or channel (C) respectively. The use of the superscript is to avoid section properties with competing variables: mistaking “S_{xc}” (elastic section modulus of the compression flange of the cap channel beam) for the elastic section modulus of the channel. Any section property without a superscript is a property of the cap channel member.

The plastic moment is defined as;

$$M_P = Z_x \cdot F_y \leq 1.6 \cdot S_{xc} \cdot F_y \quad (2\text{-}10)$$

The elastic moment is defined as;

$$M_r = min\left(F_L \cdot S_{xc}, F_y \cdot S_{xt}\right) \quad (2\text{-}11)$$

Where,

S_{xc} & S_{xt} = Elastic section modulus of the compression and tension flanges of the WC respectively

In the elastic moment equation, *Equation 2-11*, the limiting stress, F_L, is multiplied by the elastic section modulus of the compression flange, S_{xc}, under the assumption of a simple supported beam. If the stress distribution were reversed (tension on top and compression on bottom) the limiting stress would then need to be multiplied by the section modulus of the tension flange, S_{xt}.

$$F_L = F_y - F_R \quad (2\text{-}12a)$$

$$F_R \text{ (residual stress)} = 10 \text{ to } 16.5 \text{ ksi}$$

The reduction of stress is based on the residual stress due to welding the channel to the wide flange beam; 10-ksi for rolled shapes and 16.5-ksi for welded shapes (Elifritt & Lue, 1998). The specification, however, does not address the case where rolled shapes are welded together (Elifritt & Lue, 1998). The residual stress was changed from a constant 16.5-ksi in the 1999 Specification to $0.3F_y$ found in the 2005 Specification. This change, to update to current standards, will be adopted here. Ellifritt (Elifritt & Lue, 1998) suggested using a residual stress of 10-ksi because of a low heat input required to join the two members. The 10-ksi residual stress was lower than the suggested value of 16.5-ksi, which the specification recommended. Fisher (Fisher, DG 7, 2004) used the value the

Specification recommended of 16.5-ksi. The value of $0.3F_y$ will be used in this thesis in lieu of a reduced equivalent used by Ellifritt (Elifritt & Lue, 1998).

$$F_R = 0.3 \cdot F_y$$

$$F_L = F_y - F_R = F_y - 0.3 \cdot F_y = 0.7 \cdot F_y$$

$$F_L = 0.7 \cdot F_y \qquad \text{(2-12b)}$$

The nominal moment capacity, based on the unbraced length, is defined as;

$$M_n = M_p - \left(M_p - M_r\right) \cdot \left(\frac{L_b - L_p}{L_r - L_p}\right) \qquad \text{(2-13)}$$

Where the limiting laterally unbraced length for the limit state of yielding is;

$$L_p = \frac{300 \cdot r_{yc}}{\sqrt{F_y}} \qquad \text{(2-14)}$$

The radius of gyration of the flange components;

$$r_{yc} = \sqrt{\frac{I_{yc}}{A^c + \left(b_f^w \cdot t_f^w\right)}} \qquad \text{(2-15)}$$

The second moment of inertia of the flange components;

$$I_{yc} = \frac{I_y^w}{2} + I_x^c \qquad \text{(2-16)}$$

The elastic buckling moment can be defined as;

$$M_e = \frac{\pi \cdot C_b}{K \cdot L_b} \cdot \sqrt{E \cdot I_y \cdot G \cdot J} \cdot \left(B_1 + \sqrt{1 + B_2 + B_1^2}\right) \qquad \text{(2-17a)}$$

In the previous equation (*equation 2-17a*), “because the shear center and centroid do not coincide in the monosymmetric shapes, the C_b indicated is somewhat lower than would be calculated by the current AISC specification” (Elifritt & Lue, 1998). For *Equation*

2-17a, a C_b value of 1.0 would be appropriate, and the effective length factor, *K*, is to be taken as 1.0 (Elifritt & Lue, 1998) Based on the two variable definitions mentioned above, *Equation 17a* has been simplified into *Equation 17b*.

$$M_e = \frac{\pi}{L_b} \cdot \sqrt{E \cdot I_y \cdot G \cdot J} \cdot \left(B_1 + \sqrt{1 + B_2 + B_1^2} \right) \qquad \text{(2-17b)}$$

Where the two factors, B_1 and B_2, are expressed as;

$$B_1 = \frac{\pi \cdot \beta_x}{2 \cdot K \cdot L_b} \cdot \sqrt{\frac{E \cdot I_y}{G \cdot J}} \qquad \text{(2-18a)}$$

Making use of the previously defined effective length factor (taken as 1.0),

$$B_1 = \frac{\pi \cdot \beta_x}{2 \cdot L_b} \cdot \sqrt{\frac{E \cdot I_y}{G \cdot J}} \qquad \text{(2-18b)}$$

$$B_2 = \frac{\pi^2 \cdot E \cdot C_w}{L_b^2 \cdot G \cdot J} \qquad \text{(2-19)}$$

The previous three equations have variables that have no yet been introduced which can be found below.

The warping constant can be approximated as;

$$C_w = C_w^w \cdot \left(0.79 + 1.79 \cdot \sqrt{\frac{A^c}{A^w}} \right) \qquad \text{(2-20)}$$

In addition, the monosymmetric parameter, β_x, for a section with a lipped top flange can be approximated as;

$$\beta_x = 0.87 \cdot (R - 1) \cdot \left(d^w + \frac{b_f^c}{2} \right) \qquad \text{(2-21)}$$

$$\text{Where, } R = 2 \cdot \frac{I_{yc}}{I_y} \qquad \text{(2-22)}$$

Finally, the torsional constant, can be expressed as;

$$J = \int_A r^2 dA \qquad \text{(2-23a)}$$

$$J \approx \frac{1}{3}\sum_{1}^{n}\left(b_i \cdot t_i^3\right) \qquad \text{(2-23b)}$$

Ellifritt (Elifritt & Lue, 1998), to provide an equation with readily available section properties, developed the following modified formula for the torsional constant expressed in section properties and dimensions of wide flange beams and channels found in the AISC *Steel Construction Manual* (Elifritt & Lue, 1998).

$$J = J^w + J^c + \left(b_f^w \cdot t_f^w \cdot t_w^c \cdot \left(t_f^w + t_w^c\right)\right) \qquad \text{(2-23c)}$$

Equations 2-23b and *Equation 2-23c* are both approximations, and *Equation 2-20a* may be too tedious and difficult to reliably calculate. To aid in the design procedure, the torsional constant property has been calculated using *IES Shape Builder 8.0* for each section included in *AISC Steel Construction Manual*. The section properties used in the calculation example will be based on *IES Shape Builder*. A full table of section properties will not be presented in this thesis.

Up to this point the limiting laterally unbraced length for the limit state of elastic lateral-torsional buckling (LTB), L_r, has not been defined because L_r cannot be found directly. In this design procedure, as is used in the design example in ASIC DG-7 (Fisher, DG 7, 2004), L_r must be found through an iterative process. The iterative process involves making use of the assumed transitions between limit states of buckling. The elastic LBT length, L_r, therefore, is the length used in the elastic buckling moment, M_e, which results in a value equal to the elastic moment, M_r. For clarity, the unbraced length, L_b, must be iterated in *Equations 2-17* through *Equation 2-19* until $M_e = M_r$; L_r will be the unbraced length to which $M_e = M_r$.

The calculation of the nominal moment capacity is no more difficult than that of the equations presented in the AISC *Steel Construction Manual* up until the iterative process of calculating L_r. To avoid this, Ellifritt (Elifritt & Lue, 1998) also came up with another approximate method to calculate the nominal moment capacity for lateral torsional buckling based on the introduction of another variable, lambda (λ). *Equation 2-24* eliminates the need perform multiple iterations to calculate L_r, however, "obscures the unbraced length a bit" (Elifritt & Lue, 1998).

Under this formulation, the nominal moment capacity is defined as;

$$M_n = M_p - \left(M_p - M_r\right) \cdot \left(\frac{\lambda - 0.49}{1.15 - 0.49}\right) \qquad \text{(2-24)}$$

Where;

$$\lambda = \sqrt{\frac{M_p}{M_e}} \ , \ 0.49 < \lambda < 1.15 \qquad \text{(2-25)}$$

Based on the value of lambda, the nominal moment capacity is then M_n, M_p, or M_e.

$$\phi_b M_{nx} = \phi_b \cdot M_{nx} \qquad \text{(2-26)}$$

Where, $\phi_b = 0.90$

2.5.1.2 Minor Flexure

Recall from *Section 2.3.2 Lateral Loads*, the lateral loads are to be taken at the traction surface; the traction surface is the top of the rail as shown in *Figure 2-6*. The lateral load, $P_{lateral}$, however, will not act through the shear center. Torsion results from the lateral load not passing through the shear center. The difficulty in the torsional analysis will be discussed in a later section. In this section, and the method most often used in design, the

flexure analogy will be used to decompose the forces. As shown in *Figure 2-6*, the eccentric lateral load is decomposed into equivalent flange forces. The method used here is the same outlined in *Crane-Supporting Steel Structures Design Guide* (MacCrimmon, 2009). Another popular method used in crane design, a type of simplified flexure analogy, is to assume the lateral load is carried entirely by the top flange component (channel plus top flange of wide flange section).

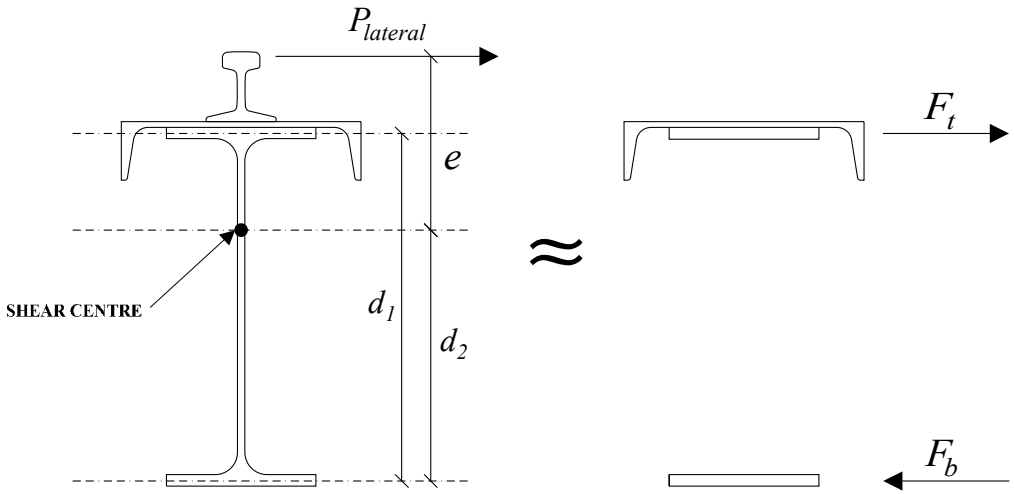

Figure 2-6 Lateral Load Flexure Analogy

The equivalent flange horizontal forces can be found by the following equilibrium equations;

$$\sum M_b = 0 = P_{lateral} \cdot (e_v + d_2) - F_t \cdot (d_2)$$

$$\sum F_x = 0 = F_b + P_{lateral} = F_t$$

Solving the above two equilibrium equations for the two unknowns, F_b and F_t;

$$F_t = P_{lateral} \cdot \left(\frac{e_V + d_2}{d_1} \right) \qquad \text{(2-27)}$$

$$F_b = P_{lateral} \cdot \left(\frac{e_V + d_2}{d_1} - 1 \right) \qquad \text{(2-28)}$$

Where,

F_t = Equivalent top flange lateral force

F_b = Equivalent bottom flange lateral force

e_v = Vertical eccentricity of lateral load

d_1 = Distance between flange centroids

d_2 = Distance from the bottom flange centroid to the shear centre

Alongside the lateral load, the rail misalignment must be taken into account because of the resulting eccentric wheel load, as shown in *Figure 2-7,* which will result in additional beam torsion. The allowable offset from the centerline of the runway beam is given by Fisher (Fisher, DG 7, 2004) and here as *Equation 2-29*.

$$e_H = 0.75 \cdot t_w \qquad (2\text{-}29)$$

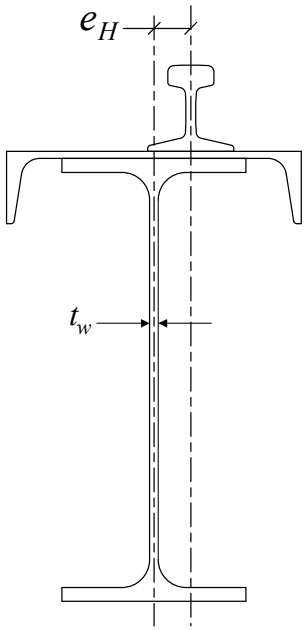

Figure 2-7 Rail Misalignment

Similar to the lateral load not acting through the shear center, the rail misalignment will cause the vertical load to be applied at a distance equal to *Equation 2-31* away from the shear center of the runway beam. The resulting action will cause torsion on the beam. To avoid the tedious derivations and calculations of torsion, the flexure analogy can be applied to find equivalent flange lateral forces. From *Figure 2-7*, the equivalent flange horizontal forces can be found by the following equilibrium equations;

$$\sum M_b = 0 = P_{max} \cdot (e_H) - F_t \cdot (d_1)$$

$$\sum F_x = 0 = F_b = F_t$$

Solving the above two equilibrium equations for the two unknowns, F_b and F_t,

$$F_t = P_{max} \cdot \left(\frac{e_H}{d_1} \right) \qquad (2\text{-}30)$$

$$F_b = F_t = P_{max} \cdot \left(\frac{e_H}{d_1} \right) \qquad (2\text{-}31)$$

If the resulting torsion rail misalignment is such that it supplements the eccentric lateral load, the total equivalent lateral load acting on the flanges can be found by combining *Equation 2-27* and *Equation 2-30* for the top flange, and *Equation 2-28* and *Equation 2-31* for the bottom flange. Thus, the equivalent lateral load for the top and bottom flange are,

$$F_t = P_{lateral} \cdot \left(\frac{e_V + d_2}{d_1} \right) + P_{max} \cdot \left(\frac{e_H}{d_1} \right) \qquad (2\text{-}32)$$

$$F_b = P_{lateral} \cdot \left(\frac{e_V + d_2}{d_1} - 1 \right) + P_{max} \cdot \left(\frac{e_H}{d_1} \right) \qquad (2\text{-}33)$$

The designer must remember that the flexure analogy is a useful analogy that simplifies and aids in the understanding of the torsion phenomenon. The flexure analogy,

however, is not torsion, and as such, is not a complete representation of beam torsion. The use of the flexure analogy is of engineering judgement; and the designer must determine whether this method is appropriate. The flexure analogy tends to overestimate the normal stress due to warping. When considering the strength of the WC section to the lateral loads half of the plastic modulus about the y-axis, Z_y, of the wide flange plus the plastic modulus about the x-axis, Z_z, of the channel for the top flange and half of the plastic modulus about the y-axis of the wide flange for the bottom flange.

The lateral design strength of the top flange;

$$M_{ny} = F_y \cdot \left(Z_x^c + \frac{Z_y^w}{2} \right) \qquad (2\text{-}34)$$

$$\phi_b M_{ny} = \phi_b \cdot M_{ny} \qquad (2\text{-}35)$$

2.7.1.3 Torsion

Assuming pin-pin torsional boundaries, normal stress due to warping will develop within the span of the beam; normal stress due to warping will not occur at the end restraints of the beam. The normal stress was accounted for using the flexure analogy in the previous section. The torsional analysis of the WC section is not often preformed due to difficulty and time-consuming calculations. For more information on the torsional analysis, the reader should see *Torsional Analysis of Structural Steel Members* (Seaburg & Carter, 2003).

2.7.1.4 Biaxial Bending

The interaction between major and minor axis bending can be found using equation H1-1b of the AISC Steel Construction Manual as shown here as *Equation 2-36a*.

$$\frac{M_{rx}}{M_{cx}} + \frac{M_{ry}}{M_{cy}} \leq 1.0 \qquad \text{(2-36a)}$$

Equation 2-36a can be formatted as *Equation 2-36b*, which is consistent with the notations, used here.

$$\frac{M_{ux}}{\phi_b M_{nx}} + \frac{M_{uy}}{\phi_b M_{ny}} \leq 1.0 \qquad \text{(2-36b)}$$

The reader should note that the above two equations, *2-36a* and *2-36b*, are only appropriate to use only if the axial forces on the beam are small by engineering judgement. If the axial stresses are not small, then the interaction equation including axial force should be adopted.

2.7.1.5 Web Sidesway Buckling

Web sidesway buckling is a criterion “included to prevent buckling in the tension flange of a beam where flanges are not restrained by bracing or stiffeners and are subject to concentrated loads” (Fisher, DG 7, 2004). Web sidesway buckling may control the design when the “compression flange is braced at closer intervals than the tension flange or when a monosymmetric section is used with the compression flange larger than the tension flange” (ASIC, 2010) such the case of WC sections. The following equations can be found in AISC *Steel Construction Manual*;

If the compression flange is restrained against rotation;

When $\left(h/t_w^w\right)/\left(L_b/b_f^w\right) \leq 2.3$;

$$R_n = \frac{C_r \cdot \left(t_w^w\right)^3 \cdot t_f^w}{h^2} \cdot \left[1 + 0.4 \cdot \left(\frac{h/t_w^w}{L_b/b_f^w}\right)^3\right] \qquad \text{(2-37a)}$$

When $\left(h/t_w^w\right)/\left(L_b/b_f^w\right) > 2.3$, web sidesway buckling does not apply.

If the compression flange is not restrained against rotation;

When $\left(h/t_w^w\right)/\left(L_b/b_f^w\right) \leq 1.7$;

$$R_n = \frac{C_r \cdot \left(t_w^w\right)^3 \cdot t_f^w}{h^2} \cdot \left[0.4 \cdot \left(\frac{h/t_w^w}{L_b/b_f^w}\right)^3\right] \qquad \text{(2-37b)}$$

When $\left(h/t_w^w\right)/\left(L_b/b_f^w\right) > 1.7$, the limit state of web sidesway buckling does not apply.

$$\phi R_n = \phi \cdot R_n \qquad \text{(2-38)}$$

Where,

C_r = 960,000 ksi when $M_u < M_y$ at the location of the force or 480,000 ksi when $M_u \geq M_y$ at the location of the force

L_b = Largest laterally unbraced length along either flange at the point of load

h = Clear distance between flanges less the fillet or corner radius for rolled shapes; distance between flanges when welds are used for built-up shapes.

$\phi = 0.85$

As stated in ASIC Steel Construction Manual, the equations provided for web sidesway buckling (pg.16.1-135), are for single-concentrated forces (ASIC, 2010). Although cranes are usually supported at the ends by two wheel trucks, Fisher 2004 stated, “[he] is not aware of any reported problems with runway beams that are designed using these criteria with a single wheel load” (Fisher, DG 7, 2004). For crane runways controlled

by web sidesway buckling, the outward stress distribution from the concentrated wheel loads, spaced at a distance equal to the wheel spacing, may never overlap. If the wheels are spaced relatively close, the designer should be encouraged to use precaution in using the web sidesway buckling equations provided in the AISC *Steel Construction Manual*.

2.7.2 SERVICEABILITY DESIGN

2.7.2.1 Vertical & Lateral Deflection Criteria

The serviceability criterion for each crane is determined based on the crane classification for each standard. Each standard uses the 100% maximum vertical wheel load without impact and 100% of the maximum vertical load for the vertical and lateral deflection respectively. In the table below, the vertical and lateral allowable deflection limits are summarized based on the crane classification. The classifications of the standards may not be the same, in this event, such standard's deflection criteria were best fitted to the CMAA crane classification. The CMAA crane classification was used as the standard. *Table 2-6* is in relation to the span length of the runway beam. For the examples provided at the end of this chapter, the deflection criteria suggested by Fisher (Fisher, DG 7, 2004) will be used.

DEFLECTION CRITERIA

	Crane Class	DG-7	CMAA	MBMA	AIST
VERTICAL	A	600	600	800	1000
	B	600	600	600	1000
	C	600	600	600	600
	D	800	600	600	600
	E	1000	600	1000	600
	F	1000	600	1000	600
LATERAL	ALL	400	400	400	--

Table 2-6: Allowable Vertical Deflection Requirements

2.7.2.4 Vibration Requirements

The vertical impact factor, as stated in ASCE previously, a vertical impact factor is required to account for vertical impact or vibration force (ASIC, 2010). Other standards also require an increase in the vertical force to account for such actions as vibration. Due to the simplification of the vertical impact factor, and the difficulty associated with dynamic analyses little is mentioned about vibration. AIST, however, states the following: “Both static and dynamic loads generated by the equipment shall be supplied by the equipment supplier. Structures to be designed for problem-free installations of rotating and vibrating equipment should be designed so that the lowest approximate natural frequencies of installed equipment (equipment/ support/ structure and/or soil configurations) as determined by dynamic analysis is 1.5 times the operating frequency of the equipment.” (AISE, 2003)

CHAPTER 3

VIBRATIONAL ISSUES IN CRANE OPERATION– CRANE INCHING

3.1 INTRODUCTION

In most cases, overhead bridge crane supporting structures are composed of two runway frames. Typically, for simplification purposes, the supporting structure is analyzed and designed as one frame, and the hoisting elements (bridge, end-truck, trolley, and hoist) are idealized as point loads on the runway beam. Although the crane supporting structure may be idealized as a simple structure, and most often designed as one, the designer must be aware that crane supporting structures are unique and a comprehensive knowledge of structural engineering is required to achieve an economical, reliable, and long-term design. For instance, cranes are one of the most commonly designed structures in which fatigue considerations have such a predominant role in the performance and lifespan. More critical than fatigue, however, are the dynamic loads induced by the crane and sustained by the runway beam. Engineers can become misguided when dealing with dynamic loads. Such as the case with cranes, dynamic loads are expressed in a static equivalent force to simplify the analysis and design; as the case with ASCE's vertical impact factor, $f_{impact,}$ mentioned in *Chapter 2* of this thesis. The designer needs to remember, much like the flexural analogy in torsion, that static load equivalents are not a true representation of the dynamic action or response of a structure. The use of these loads should be dealt with carefully, especially when current codes may not depict the full nature of the dynamic load.

3.2 CRANE CASE STUDY

A recent investigation of a crane system began when a facilities manager reported a runway beam under-going “twisting” motions during operations. The motion occurred when crane was loaded to an estimated half capacity as reported by the present crew (facilities manager was absent).

3.2.1 DESCRIPTION OF SYSTEM

The crane was reported to have been constructed months’ previously with no prior issues or concerns. The crane system was an outdoor crane consisting of a three-span (non-continuous) beam-column system. The crane runways were composed of a two WC16×36, and one WC27×84 (all capped with a C15×33.9) spanning a length of 27 feet 6 inches, 29 feet 8 inches, and 59 feet 4 inches, respectively. The two shorter spans varied due to matching existing column locations of an engineered metal building (not pre-engineered) to which the crane runway columns were laced. The longer span was required to avoid drive isles in a traffic heavy area. Tie-backs were provided at all the column intersections. The crane was a single bridge crane with a capacity of “5T” (10 kips). The length between the two runway bays (or length of the crane bridge) spanned 30-feet. The crane was controlled via pendant operation.

3.2.2 DESIGN INVESTIGATION

The design of the crane supporting system was carried out through a few companies including a staff engineer, the crane manufacturer, and an independent party. The design was deemed adequate and capable of resisting the loads. The crane runways

manufacturer material's sheet was provided and deemed to correlate with both the assumptions made in design and the material on the structural plans.

3.2.2.1 125% Load Rating

Documentation was provided of the "Rated Load Test" required by OSHA (29 CFR 1910.179(k)). "Overhead and gantry cranes should not be rated in excess of 80 percent of the test load. Therefore, in order to rate a crane to 100 percent of the design intended loading, the test load must be 125 percent of the rated load. The only exception to this requirement would be when a crane manufacturer specifies a different test loading criteria. In that case, the crane manufacturer's procedures shall be adhered to" (OSHA 2016). The "Rated Load Test" inspection forms were provided for the system and no concerning remarks or observations were noted.

3.2.2.2 Field Examination

A site visit was made to further review the structural integrity of the structure. Firstly, the rail and track were inspected to verify the rail alignment. The rail and track were checked for both the culprit of the "twisting" motion reported, possibly due to an intolerable offset, and/or make sure the "twisting motion" had not caused any misalignment. The rail clamps were also inspected to make sure the clamps had not moved or loosened during the reported "twisting motion". No misalignments were found in the rail and no clamps were found to be loose or moved. Since no safety concerns were yet found, the crane was driven along the railway. For safety reasons, the crane was initially loaded with an object approximately weighing 500 pounds (twentieth of the crane's nominal rated capacity). The crane was driven along the runway, and was found to have no issues. The crane was

slowly and incrementally loaded to 5 kip (half the crane's nominal rated capacity). With the crane loaded with 5 kip, the procedures of OSHA's 125% loaded test were conducted (with 5 kips instead of 125% capacity); the hoist and trolley were placed closest to one side on the bridge and driven the length of the runway (all three spans) for maximum concentration on the runway beams. To measure/verify the structural performance, at various points, the crane was stopped, and manual (simplified) calculations were compared to actual measured deflections; all the calculations, when compared to actual deformations, were found to be within an accurate and suspected magnitude. Likewise, the hoisted load was continuously hoisted, from the resting position on the ground, and continuously lowered to the ground. During the test, no "twisting" movements or otherwise unusual movements were observed.

3.2.2.3 Hoisting/Lifting "Test"

No abnormal responses were found using standard testing protocols. Since the movement or action was not known (observable) nor the severity, the repair (if any was needed) was not known. The exact movement of the runway beam was to be known so a repair solution could be advised and possibly avoid any possibly dangerous/deadly accidents in the future. Up to this point, the goal was to avoid any replication, for safety reasons, and preform standard safety tests and inspection to identify any problem. Since the crane was verified in the previous tests to be in good and safe working order, the decision was made to replicate the scenario during the time the "twisting action" was reported. The workers were found to be inching or jogging the crane during precise material handling. Jogging, or inching, is referred to the action of "switching of the crane's motion from on to off quickly, to move in small increments" (Inching, 2017) or to "move the hook,

trolley, or bridge in a series of short, discontinuous, increments by momentary operation of a controller" (Inching, 2017) as depicted in *Figure 3-1a* and *Figure 3-1b*.

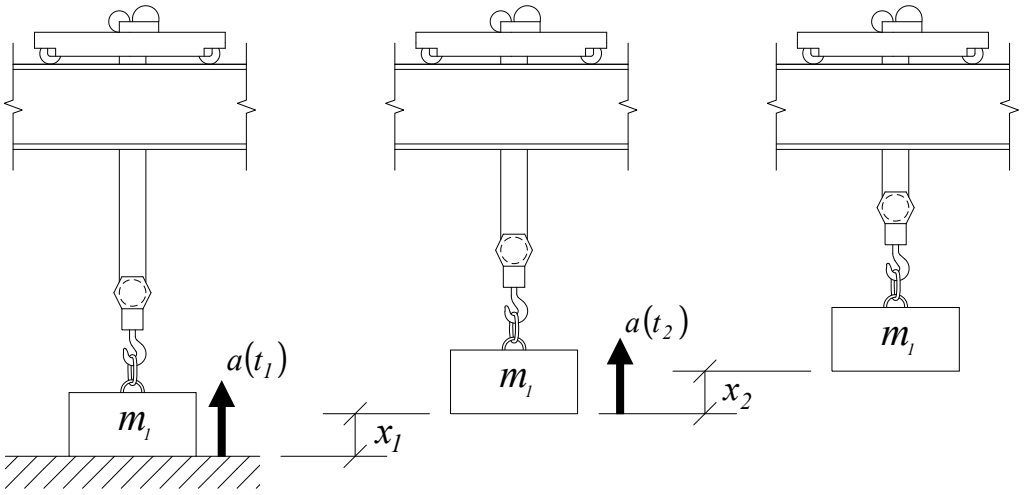

Figure 3-1a: Crane Inching

Jogging, or inching, is often used to control the movement, and slow the crane speed so a load can be carefully placed (Inching, 2017). Although inching is known to possibly cause damage to the bridge, trolley, and/or hoist, the movement may be necessary when accurate load placement is required, or when tight movements to avoid obstructions are required (Inching, 2017). The reader should be made aware that the material handled at this specific company, in general, do not necessarily require precision handling. For this particular case, however, the situation did require precise handling.

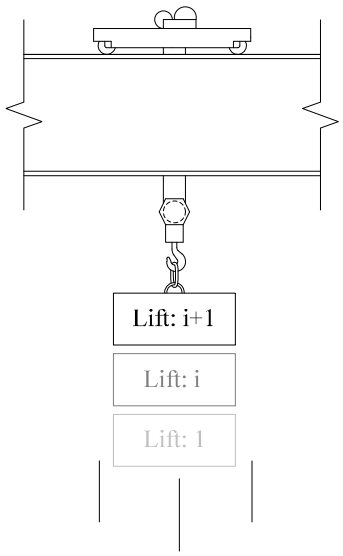

Figure 3-1b: Crane Inching

3.2.2.4 Movement/Rotation of Beam

With the 5-kip weight still attached, the bridge was travelled to the mid-span of the longer-span runway beam and the hoist and trolley placed as close as possible to one side (concentrating the load on one runway beam). The load, after being fully suspended in the air (full tension on hoist), was jogged using quick and successive taps of the lift key on the control pendant. At the beginning of the jogging process, a few successive taps of pendant were spaced at multiple seconds apart in which movement, but very limited, was seen to occur. The decision was made to speed up the jogging (quicker successive taps of the pendant). Using a video recording of the process (video stills not shown due to copy-right purposes), a time-chart has been put together as shown in *Table 3-1. Table 3-1* only shows the times of the quicker pendant lifting; the times of the lifting which were spaced multiple seconds apart are not included. The “Time” column in *Table 3-1* describes the “time in

space" or time noted on the video footage of when the crane lifting was actuated. The "$\Delta t_{i,i+1}$" column in *Table 3-1* describes the "resting time" or time between crane lifts.

LIFT #	TIME (sec)	$\Delta t_{i,i+1}$ (sec)	
1	11.8	--	
2	12.93	1.13	
3	14.15	1.22	
4	15.93	1.78	
5	16.8	0.87	***Most Critical Lifts***
6	17.68	0.88	
7	18.58	0.9	
8	19.46	0.88	
9	21.2	1.74	

Table 3-1: "Jogging" Times

During the jogging process described in *Table 3-1*, which occurred over a period of roughly 10 seconds, the beam can be seen exhibiting small vibrations which slowly become more evident after several jogs. When the intervals between jogs shorten, as identified in *Table 3-1* as "most critical lifts" (lifts 5-8), the bottom flange of the beam exhibits a distinct swaying motion transverse to the span. The bottom flange deformation is best described as similar too movement expected in web distortional buckling where the top flange is restrained. The swaying of the bottom flange, depicted in *Figures 3-3a-3-3c,* was more predominant near the center of the span. For visualization purposes, *Figure 3-2* represents the crane system (not to scale) in an un-deformed state.

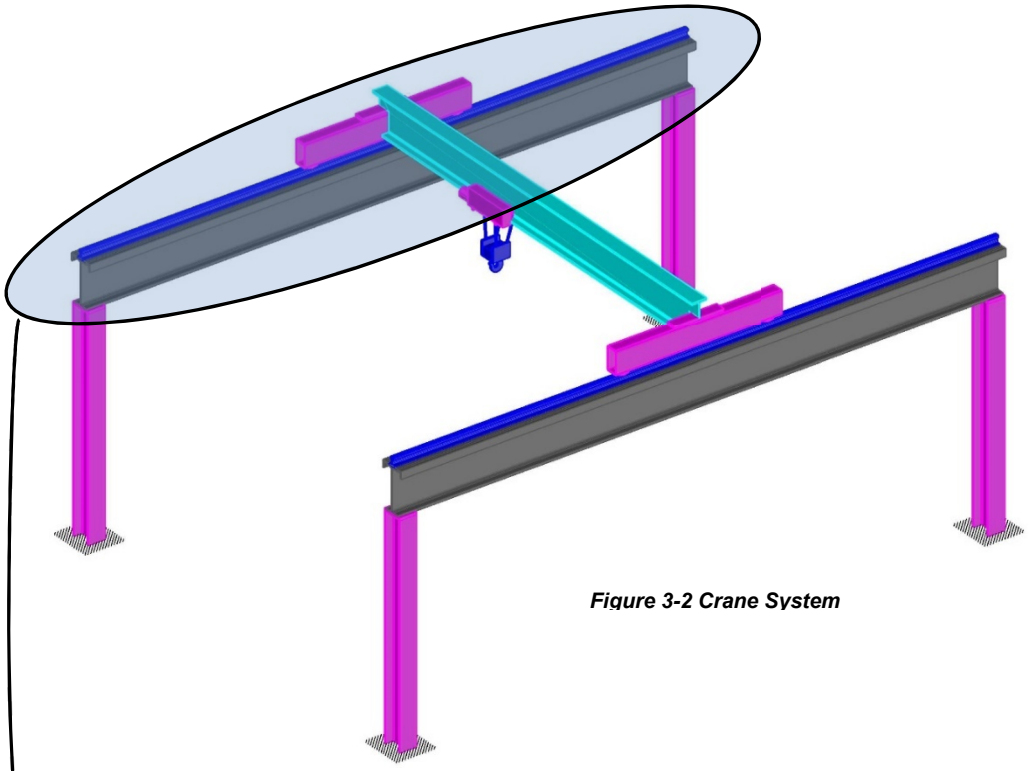

Figure 3-2 Crane System

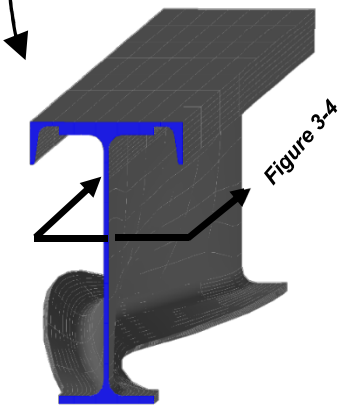

Figure 3-3(a) Flange Sway, Isometric View

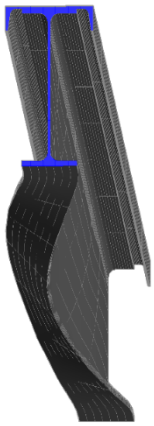

Figure 3-3(b) Flange Sway, Bottom Isometric View

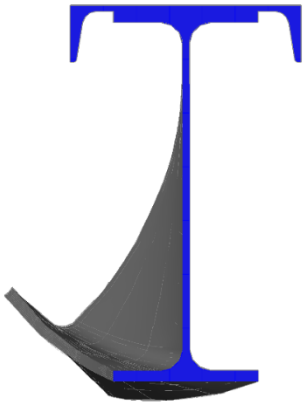

Figure 3-3(c) Flange Sway, Elevation View

The loading and supports are not shown in *Figures 3-3a-3-3c*, and the blue colored face of the beam is for visualization purposes only. The top flange of the girder appeared to be vibrating but did not appear to be swaying like that of the bottom flange. For clarity, *Figure 3-4* represents a cross-section about the mid-span of the above beam; the dashed lines represent the cyclic back-and-forth movement of the bottom flange.

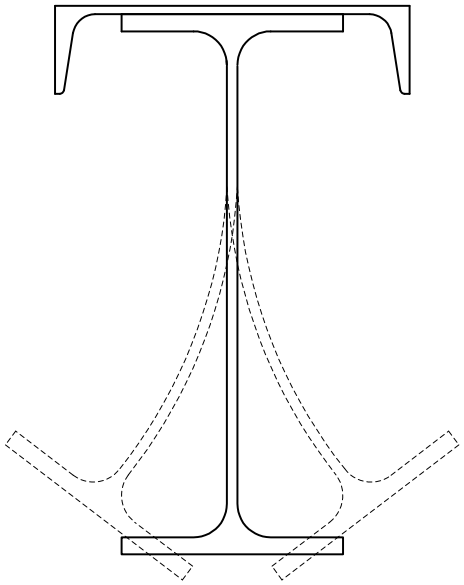

Figure 3-4: Runway Girder Mid-Span Cross-Section Bottom Flange Sway

The reason behind the limited swaying of the top flange was unclear, however, the crane bridge may have been providing some lateral restraint to the top flange as suggested by Ellifritt (Elifritt & Lue, 1998). The ends of the runway beam did not appear to undergo any rotation/twisting. The runway end rotation restraint was due to the end stiffener plates (at the column-runway beam intersection), which are often times going to be required from AISC J4.4, and the tie-back connection.

3.2.2.5 Movement Determination

The rotation/twisting of the crane girder, although not measured, was deemed unsuitable. The most major concern was the stability of the crane. The crane bridge rides along the rail on two wheels spaced at a set increment (6 feet in this case). The rotation of the crane girder became more predominant the closer to the center of the span. The rotation, subsequently, will lead to differential movement about the longitudinal axis (laterally) of the crane girder. Since the bridge wheels are “fixed” in position (the bolted bridge to truck connection would allow some rotational movement), and will not accommodate the lateral movement during the twisting action, if the twisting is severe enough, a crane wheel could slip off the track as shown depicted *Figure 3-5*. The designer must keep in mind that friction is the only mechanism keeping the wheel from slipping off the track.

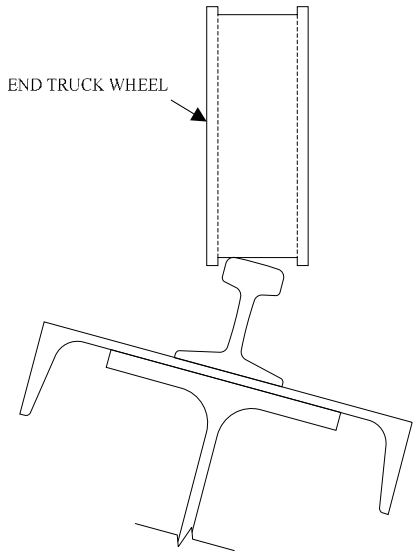

Figure 3-5: Runway Rotation

As mentioned before, the top flange of the girder did not seem to undergo the same magnitude of movement as the bottom flange. Although this may be the case, the future movement of the top flange if the jogging was to continue could have led to a higher magnitude of rotation. The top flange could have also exhibited more movement if the jogging was done at different time step intervals or if the jogging involved a different weight. If a wheel was to slip off the track, then the weight would be redistributed to a single point load acting on the wheel in contact and create loads not considered in design. Likewise, if a wheel was to slip off the track, the crane could possibly collapse. From a serviceability standpoint, regardless if the system was structurally sufficient and stable, the workers were alarmed of the movement.

Mention should be made that prior to the “jogging” test preformed on the long-span crane runway, the same test was performed at the same weight and similar time intervals on the two shorter span runways. Expected small movements were noted, however, no stability issues nor concern were found. Neither the top flange nor bottom flange exhibited the movement as the longer-span runway beam.

3.3 LONG SPAN CRANES

3.3.1 OUTDOOR CRANES

A common situation where bracing may be limited is outside cranes which “often require longer spans than interior cranes” (Fisher, DG 7, 2004). In typical new building construction, the building columns (which the crane typically shares) is usually dictated by the building design, and the runway beam designed accordingly. For outside cranes both the span and bracing are dependent on “drive aisles, railways and other similar restrictions” (Fisher, DG 7, 2004). In these situations, the designer must make the decision, dependent

on the limit state, of whether to use a heavier (possibly built-up section – e.g. WC section), lacing a horizontal member to brace the runway, or a truss system. As previously mentioned in Chapter 2, if the bracing members of a lacing system are to fatigue then the runway girder will lose the lateral support, and the joints on trusses are “highly susceptible to fatigue problems” (Fisher, DG 7, 2004). Both the analysis and design of a truss system are complicated due to secondary stresses which must be calculated and included in the fatigue analysis for trusses used as crane girders (Fisher, DG 7, 2004).

3.3.2 RETROFITS

A popular ongoing trend is for businesses, rather than buy a new metal building, to purchase and retrofit existing metal buildings to meet the new owner’s needs. If the crane structure was to run along an existing bay, then beam bracing could easily be incorporated into the design. Problems with beam bracing may arise if the crane structure was oriented to span perpendicular to the bays leaving few options to brace the crane off the existing structure. Similarly, if the crane was to run along an existing bay but the bracing members had to span a large distance, either due to variations in height and/or large offset distance from the bay, then the stiffening equations per ASIC J4.4 may require these members to be uneconomically large.

3.4 ISSUES IN VIBRATION

The issue with the case described above was the frequency of the repetitive lifting of the load possibly coincided, or closely so, with a natural frequency of the crane system. The two-matching frequencies led to the system vibrating in resonance. When resonance vibration occurs, the system (bridge beam and runway beam) will begin to vibrate with

increasing amplitudes (Bucholdt & Nejad, 2012). As the resonance vibration continues, the increasing amplitudes may lead to a build-up of very large displacements and corresponding large stresses greater than that found by a traditional static analysis (Bucholdt & Nejad, 2012). Most commonly, the unaccounted-for force from this vibration can have detrimental effects regarding instabilities, fatigue, possible plastification, and serviceability.

For bridge cranes the issues with vibrations depend among many variables including, to name a few, the bridge beam, bridge span, runway beam, runway span, magnitude of the lifted load, repetition and duration of the lifted load. With so many dependent variables, the few cases of resonance vibration in bridge cranes encountered by professionals is understandable. Although the problem may be unique, the costs associated with possible upgrades, repairs, and especially downtime can be large.

3.4.1 FATIGUE

As is the case with the travel of the crane along the rail, the repeated loading causing vibrations in the structure can cause stress fluctuations which can critically impair the strength of the runway beam after a certain number of cycles (Bucholdt & Nejad, 2012). Likewise, aside from the runway beam, fatigue can also lead to increased wear of mechanical parts and loosening of fasteners (Rao, 2004). The loosening of the fasteners can be critical, especially in the case of lateral torsional buckling or web sideway buckling where the beam is designed based on bracing among interval points.

3.4.2 PLASTIFICATION

Small plastic deformation may result due to excessive vibrations. In many situations, localized deformations may be accepted to enable an economical design such

as the case with earthquake design. Localized plastic deformations in the case of crane runway beam vibrating in resonance may lead to instabilities from damaged bracing members, or even cracking at the runway beam ends due to the end rotation of the girder in high deflections.

3.4.3 SERVICEABILITY

"The serviceability is impaired when the vibration of the structure under dynamic load causes disturbance and discomfort to the occupants" (Bachman & Walter, 1987). One importance of resonance vibration on the runway beam is the expected (or calculated deflection) does not consider the deflection due to vibrations. The impact factor which accounts for vibrational effects is not used in deflection calculations. A runway beam, especially one which is designed based on deflection, such as a long-span runway beam, may have detrimental consequences if the resonance vibration causes a large increase in deflection than that which is expected. As the case of the runway beam described above, the resonance vibration may lead to excessive rotation about the longitudinal axis of the runway beam. The longitudinal rotation of the runway beam, which does not have a published acceptable limit, should be considered for reasons mentioned previously. Regardless of whether these deflections are indications of the structures stability, workers may not feel safe.

3.5 VIBRATION DESIGN CONSIDERATIONS

Quasi-static forces can be used, and have been used for many years, to successfully to represent the dynamic response of a structure. The quasi-static vertical impact factor, does not align with many other quasi-static loads found in ASCE.

Up to this point, the design for dynamic movement (acceleration and deceleration of the crane and counterparts) has been accounted for using the impact factor. The impact factor is a quasi-static load, or static load equivalent, used to mimic the dynamic forces such as “wheel impact” (MBMA, 2006) and “vibration forces” (ASCE, 2010) which was previously covered in *Section 2.3.1* of this thesis. Quasi-static forces can be used, and have been used for many years, to successfully to represent the dynamic response of a structure. Quasi-static forces, however, are only applicable when the frequency of the dynamic load and the natural frequency of the structure do not coincide or fall within the same range. In cases where the forcing frequency and the natural frequency of the system coincide, quasi-static forces may not accurately predict the amplified response of the structure due to the dynamic load. The quasi-static vertical impact factor, does not align with many other quasi-static loads found in ASCE. Many quasi-static loads used in code account for the structures natural frequency, in some manner, for applicability or require an increase in load magnitude when the natural frequency is in a problematic range (known as dynamic amplification). For example, when calculating the design wind force for a dynamic sensitive structure, such as a tall single post pylon sign, the fundamental natural frequency (n_1 – variable as named in ASCE7-10) is included in the calculation of the gust effect factor (G – variable as named in ASCE7-10). Likewise, for the seismic analysis, the seismic response coefficient (used to calculate the base shear) calculation includes the fundamental period of the structure (inverse of the frequency). Unlike the wind and seismic quasi-static forces, the vertical impact factor for crane runways does not account for the structures natural frequency.

In a more congruent relationship between quasi-static loads, the vertical impact factor for crane runways is not like the “Hoist Load Factor (HLF)” for cranes given by *Crane Manufacturers Association of America (CMAA) Specification-74*. CMAA’s hoist load factor

is the “result of normal operating inertia forces, loads due to the sudden lifting of the load, and other loading uncertainties that occur during normal crane operation.” (CMAA-74). The definition and reasoning of CMAA’s hoist load factor coincide very closely to ASCE’s vertical impact factor. The hoist load factor equation can be found below as *Equation 3-1 (Section 3.3.2.1.4.2).*

$$\text{HLF} = 0.15 \le 0.005 \times \text{HoistSpeed(ft/min)} \le 0.5 \qquad \textit{Equation 3-1}$$

The section number listed after *Equation 3-1* is the respective section where the equation can be found in CMAA-74; CMAA-74 does not number or letter equations. As shown, the CMAA hoist load factor includes the hoist lifting speed. An average hoist lifting speed (for common bridge spans) is generally around 30 feet per minute. For a crane with a 30 feet per minute hoist lifting speed, the hoist load factor equates to a factor of 0.15.

$$HLF = 0.005 \times 30 = 0.15$$

The hoist load factor in the above example falls short of the vertical impact factor assuming pendant operated. The hoist load factor is important in that the factor is variable; relating a variable (lifting speed) which has direct implication with dynamic effects. Likewise, the British Standard (EN1991-3:2006) contains dynamic factors for vertical loads to be applied to specifically cranes and crane supporting structures. The British Standard contains four dynamic factors; each applied to different crane components under different load conditions. The focus here, however, will be on the vertical load dynamic factor φ_2 whose formula can be found below.

$$\varphi_2 = \varphi_{2,\min} + \beta_2 \cdot \nu_h \qquad \textit{Equation 3-2}$$

In *Equation 3-2*, ν_h is the steady hoisting speed in meters per second. The other two variables, $\varphi_{2,\min}$ and β_2, are based on the hoisting class (like the crane classification

outlined in *Chapter-2* of this thesis) and can be found in the British Standard which has been copied below as *Table 3-2*.

Hoisting Class of Appliance	β_2	$\varphi_{2,\min}$
HC1	0.17	1.05
HC2	0.34	1.10
HC3	0.51	1.15
HC4	0.68	1.20

Table 3-2: Values of β_2 and $\varphi_{2,\min}$

In reference to the previous example with 30 feet-per-minute hoist lifting speed the British Standard vertical load dynamic factor can range from 1.08 to 1.30, or rather a 0.08 to 0.30 increase in the nominal vertical load. In comparison, the British Standard dynamic factor is on a scale of half to double that of CMAA's hoist load factor.

$$v_h = 30\,(\text{ft/min}) = 0.152\,(\text{m/s})$$

$$\varphi_{2,\min} = \varphi_{2,\min} + \beta_2 \cdot v_h = 0.17 + 1.05 \cdot 0.152 = 1.08$$

$$\varphi_{2,\max} = \varphi_{2,\min} + \beta_2 \cdot v_h = 0.68 + 1.20 \cdot 0.152 = 1.30$$

Aside from the vertical impact factor not following similar processes as other quasi-static forces, crane runways do not follow vibration limitations/recommendations as other similar structures. The British Standard (EN1993-6:2007) contains specific criteria regarding vibration of the bottom flange. The standard states "the possibility of noticeable lateral vibration of the bottom flange of a simply supported crane runway beam, induced by crane operation or movement, should be avoided" (EN1993-6:2007). The standard states no lateral vibration of the bottom flange can be assumed "if the slenderness ratio L/i_z of the bottom flange is not more than 250" (EN1993-6:2007) which is presented in equation form below as *Equation 3-3*.

$$L/i_z \leq 250 \qquad \textit{Equation 3-3}$$

Where,

L = The runway beam's length between lateral restraints

i_z = The radius of gyration of the bottom flange

If the radius of gyration of the bottom flange, i_z , is taken as approximately equal to the radius of gyration of the bottom flange components then for the crane presented in this chapter;

$$i_z \approx \sqrt{\frac{\left(\frac{I_y^w}{2}\right)}{\left(\frac{A^w}{2}\right)}} = \sqrt{\frac{\left(I_y^w\right)}{\left(A^w\right)}} = r_y^w$$

$$L/i_z \approx L/r_y^w = 712/2.07 = 343 >> 250$$

The value obtained (343) is much greater than the recommended value of 250. For comparison, if the designer was to follow this recommendation (excluding other design checks), the most economical beam (top channel will have no affect) is a W27×146. The equation results in a much larger beam (equating to more cost). Even with the large weight/cost increase, the natural frequency of the beam is still unknown to the designer. While the formula may be useful for initial design assumptions, the designer is still unaware of the natural frequencies and corresponding modal shapes. Likewise, this provision may not be sufficient enough to control vibration during resonance. The most economical and safe beam can be designed when the target natural frequencies (bottom flange lateral movement) are avoided with respect to common/troublesome lifting frequencies. Although the slenderness of the bottom flange may be related to the potential for bottom flange

lateral vibrations, the lifting frequency of the payload and natural frequency (relating to bottom flange vibration) would be a more reliable relationship. Unfortunately, no equation exists for the natural frequency related to bottom flange lateral vibration.

Designing structures based on avoiding troublesome forcing frequencies with respect to the structures frequency is a common principal in design. Pedestrian bridges, with respect to AASHTO 2009 design, for example, are similar in types of supporting systems used (girder and truss), loadings (lateral, vertical, longitudinal, and sometimes magnitude if the bridge supports vehicular traffic), and dynamic considerations. Pedestrian bridges are required to have a fundamental frequency (in a vertical mode without live load) greater than 3.0 Hz to avoid the first harmonic (AASHTO, 2009). Likewise, the fundamental frequency in the lateral direction must be greater than 1.3 Hz (AASHTO, 2009). AASHTO further states that “if the fundamental frequency cannot satisfy these limitations, or if the second harmonic is a concern, an evaluation of the dynamic performance shall be made” (AASHTO, 2009).

The reader should note that the above comparison between dynamic factors is only to show the difference in dynamic criteria with respect to impact factors and vibration limitations. The impact factor is important in that it is a standard value where other quasi-static forces in code are standard, variable, and with limitations. The designer would benefit in knowing the limitations of the impact factor with regards to vibration. While the use/limitation of quasi-static forces may be known by some, the absence of explicit limitations and/or alternative methods within the code (ASCE and other published crane design texts) may lead the designer to believe there is no limitations. The reader should also not take the comparison as a suggestion of adopting these formulas for crane design especially as a solution for the bottom flange lateral sway discussed in this chapter. The implementation of an impact factor based on major dynamic variables (hoist

velocity/acceleration, bridge span, and/or runway span) may lead to a higher design force in specific dynamic sensitive crane and crane supporting structures. While the higher design force may result in a larger WC section used as the runway, the vibrational issues may remain. In a standard WC section, based on current crane runway design practices, large forces will typically result in a larger transverse (I_x) while the lateral stiffness (I_y) and the longitudinal stiffness (J) typically remains, comparatively, unchanged. Take the case presented in this chapter as an example: The existing runway beam consist of a WC27×84 (15×33.9 channel), however, if the designer was to choose a WC27×94, the next largest WC section in the AISC manual, the results are as follows;

Section	WC27×84	WC27×94	Percent Difference
I_x (in^4)	4056.91	4550.18	11.46 %
I_y (in^4)	422.59	439.79	3.99 %
J (in^4)	6.51	8.57	27.32 %

Table 3-3a: Comparison 1

Section	WC27×84	WC30×99	Percent Difference
I_x (in^4)	4056.91	5589.34	31.77 %
I_y (in^4)	422.59	445.34	5.24 %
J (in^4)	6.51	7.85	18.66 %

Table 3-3b: Comparison 2

As seen from the two tables, *Table 3-3a* and *3-3b*, the transverse stiffness in largely increased. The lateral stiffness is only slightly increased even when a section two sizes larger (per AISC sections) is chosen. The torsional stiffness may appear to have a large increase between sections. While this is true, the magnitude is not linear among

larger sections. If a larger impact factor was utilized, and the design forces required the section to be upgraded to a WC30×99 where the current impact factor used a WC27×94, the torsional stiffness would be decreased and possibly more susceptible to torsional vibration issues. For this reason, the use of the impact factor should not be relied upon as a measure against vibrational issues. Likewise, a beam with more torsional stiffness may still undergo vibrational issues under resonance. To try to codify the runways allowable rotational movement for serviceability purposes would be difficult and extremely dangerous. In addition, the degree of twisting under dynamic loads, especially under resonance vibration, would be difficult if not impossible to calculate without a time consuming finite analysis. Such an in-depth and time consuming analysis, especially the associated cost, would probably not be warranted for such a usually simple design. For safety and simplification reasons, runway beams should avoid a natural vibration frequency (primarily one associated with the natural mode of longitudinal twisting) with common crane lifting frequencies.

CHAPTER 4

FINITE ELEMENT SIMULATION

4.1 INTRODUCTION

As the case with most vibration issues, the competitive push among engineers from clients for lighter smaller structures (where lighter is often equivalent to less costly) can be intrusive to vibration resistance. Resonance vibration issues due to human activity (from inching, sway, etc.) is often encountered by designers when designing crane runways especially long span crane runways. While vibration resonance issues, of all modes, is known to many crane designers, the time required to run an in-depth dynamic analysis is usually not economical. The possible critical vibration issues coupled with the inability to perform an in-depth analysis requires the design engineer to use very conservative design recommendations regarding vibration. These design recommendations, however, may or may not be for the exact vibration issue. The resulting overdesign may reinforce a vibrational mode which is not necessarily an object of concern to which the overdesign could have been focused on a more vibrational sensitive mode. As presented in this Thesis, the suspect crane passes the required/common design checks for a crane runway and the designer may have even considered many other recommendations. The runway, however, would be unacceptable if that particular client commonly uses an “inching” technique. Unfortunately, there is very little to no information (possibly *Eurocode 2012* mentioned in *Chapter 3*) regarding torsional vibration in crane runways due to “inching”. As such, an in-depth finite element analysis was conducted to study the behavior of the crane system, mentioned in *Chapter 3*, under the dynamic “inching” action. There are two primary goals of this research: (a) to identify the cause behind the vibrational issue where there is currently very limited research, and (b) to, based on repetitive analysis results, provide

remediation retrofit solutions for the runway (or crane system) which still meets the clients' expectations of the system. Secondary goals include (c) introducing other common runway members into the crane system and analyzing the response of the member, and (d) using the analysis results, along with theoretical derivations, produce equations which may aid in crane design.

4.2 MODEL DEVELOPMENT

The general-purpose finite element analysis program LUSAS, version 15.2, Civil and Structural Plus application product, was chosen to perform the three-dimensional finite element analysis of the crane system. While this research is focused on the behavior of the runway beam(s), the modelling of the entire crane system must first be analyzed. The crane system is composed of many intricate members which may have a large impact on the behavior of the runway beam. A single runway beam was later modelled and compared to that of the system which will be discussed later. The modelling of the single runway beam was done to check if a simplified finite element model for beams with appropriate boundary conditions can obtain reasonable results as compared to that from a complicated model of the entire runway system.

In general, the model is dimensionally recreated in LUSAS using point (one-dimensional geometry), line (one-dimensional geometry), surface (two-dimensional geometry), and volume elements (three-dimensional geometry) as shown in *Figure 4-1*. *Figure 4-1* shows the geometry (unmeshed) of the full system of the runway crane. The colors of each structure within the crane system have been shown based on their respective grouping; the color has no implication on the structure other than the group within LUSAS to which the author has assigned. These elements are assigned material,

geometric, and restraint/support features. To analyze the model, each piece of geometry is assigned a mesh which resolves the geometry into elements interconnected by nodes. All the modeled members where based off the structural engineer's plan set in terms of geometric and material properties. In the proceeding subsections, each member will be discussed individually. Each discussion will focus on how the member was modelled as well as any assumption, if any, which went into the construction of the model. Post discussion of the individual members the entire crane system will be presented. construction of the model. Post discussion of the individual members the entire crane system will be presented.

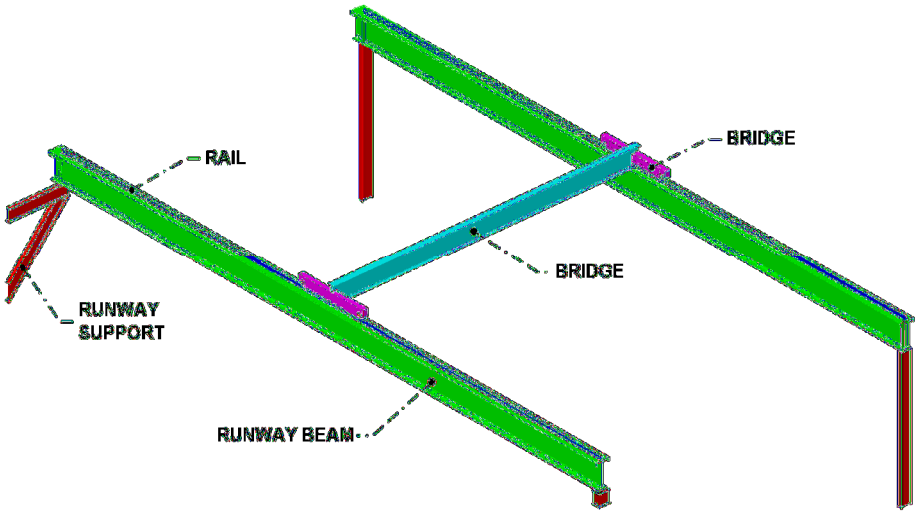

Figure 4-1 Crane

4.2.1 RUNWAY AND RAIL

For personal ease-of-drawing, both the wide-flange (W27x84) and channel section (C15x33.9), which compose the runway section, was developed in AutoCAD, based off AISC's geometric dimensions, and then imported into LUSAS. The runway beam, as the focus of this research, was chosen to be modelled as a volume. The meshed volume will

allow for the most realistic and precise results compared to that of a two-dimensional element. Likewise, the rail was developed as a volume. While the specific stress and displacements of the rail are not of specific interest in this research, the load transfer must be carefully considered. The implication of how the load is transferred into the runway section (through the centerline or off-center, even or uneven pressure distribution, etc.) can possibly have a direct effect on the torsional mode of vibration. Ultimately, the volume was chosen to reduce any possible risk of error and increase precision to the analytical results.

The runway beam section (wide-flange with channel) contains many intricacies especially within the fillet joints between the flanges and web. To mesh the section using only the perimeter lines of the section would reveal an unreasonably required number of elements in the cross section to avoid a high aspect ratio; a visual example of this is presented with the rail further in this section. A high aspect ratio, which will affect the accuracy of stress distribution, can lead to ill-conditioning issues within the stiffness matrix when solving, and further lead to poor iteration convergence. To control the mesh, the cross section was subdivided into different volumes as shown in *Figure 4-2*.

To limit the length-to-curve ratio of each subdivided volume mesh, the fillet arc section of the channel flange tip should be removed as done in *Figure 4-2* and *Figure 4-3* in greater detail. To keep the fillet arc on the channel's flange tips the subdivision would have resulted in a large number of elements with small geometry. The exclusion of the arc would constitute a difference in area of 0.029 in^2. Because the change does not change the identity of the cross section, the filleted flange tips of the top channel were chamfered as shown in *Figure 4-2* and *Figure 4-3*. Although other parts of the cross section do contain small length geometry, which presents difficulties when controlling the aspect ratio, such as the center base volume of the rail, these volumes either have no option to be simplified or any simplification would greatly change the identity of the section.

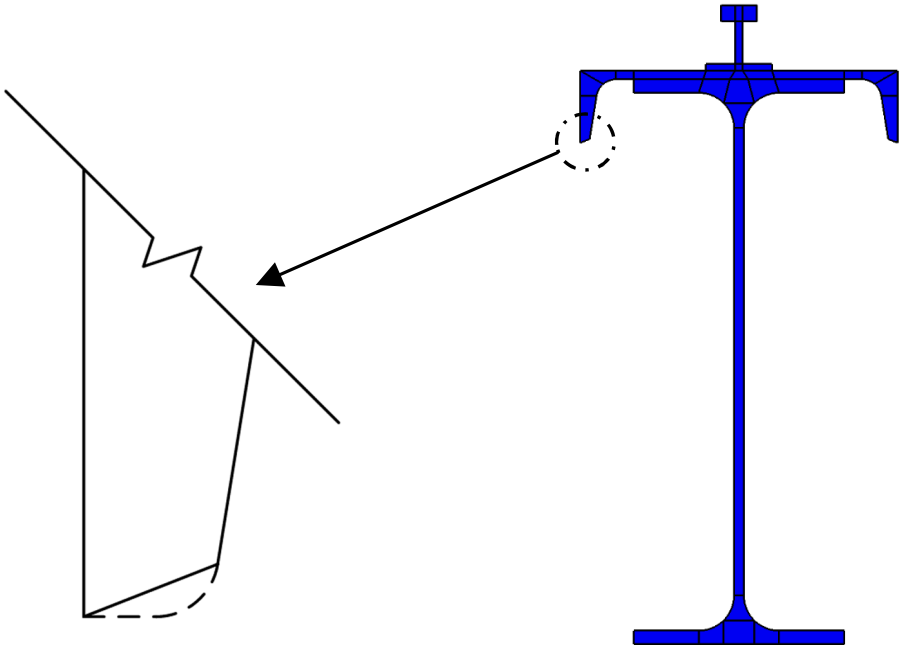

Figure 4-3 WC Simplification

Figure 4-2 WC Section

Like the runway section, the rail's geometry was slightly modified to attain a more reasonable mesh within the cross section. The rail section's geometry is much less structurally significant compared to the runway beam. The rail serves two major functions which, for this research, must be preserved for accurate results which was discussed previously. *Figure 4-5* shows the actual, or unmodified, rail cross-section mesh created by the LUSAS Support Team. The mesh has been refined such that the aspect ratio between elements within the cross-section are reasonable uniform. As shown in *Figure 4-5*, for the single rail cross-section, to maintain a reasonable aspect ratio along the length, the rail would be composed of an estimated 712,000 solid elements which equates to over three million degrees of freedom. Because the rail is not of specific interest the extra disk space nor processing time required is not desirable. To simplify the rail while maintaining the required functions, discussed previously, the rail section was modified as shown in *Figure*

4-2 and in greater detail in *Figure 4-6*. *Figure 4-6* shows the modified geometry (solid black line) contrast against the actual rail section (dashed grey line).

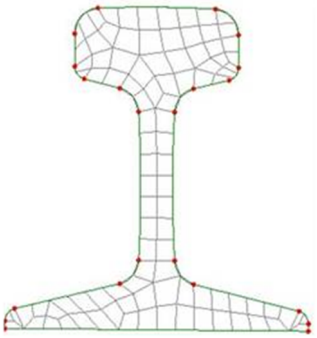

Figure 4-5 Unmodified Rail Mesh

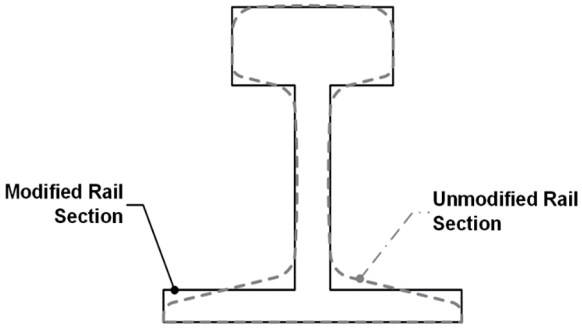

Figure 4-6 Rail Modification

The rail and runway section were meshed using 3D isoparametric solid continuum hexahedral (16 node) elements with a quadratic interpolation order along mesh lines. The mesh division was scheduled such that a maximum aspect ratio of 5:1 was maintained. An excessive aspect ratio is defined by LUSAS as 10:1. The controlling aspect ratio, the small square element at the base of the rail as seen in *Figure 4-4*, equates to an aspect ratio of 4.92:1 which is just under the target goal and well within the suggest program parameters.

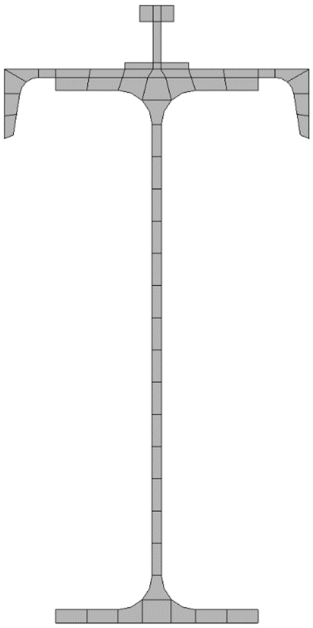

Figure 4-4 Runway Beam Mesh

4.2.2 END-TRUCK & WHEELS

The geometry of the end-truck was modelled following the crane manufacturers specification sheet which called out a HSS 10x6x3/8 steel tube as shown in *Figure 4-7*. Surfaces, or two-dimensional geometry (2D), were used to model the member, so the geometry drawn in LUSAS was made along the actual members' centerline. The specification sheet also revealed the wheel base distance along with the end distance to the centerline of the wheel. Using these two dimensions the overall length of end-truck was formulated. The location and size of wheel fittings were also provided with the coping length on each end of the end-truck.

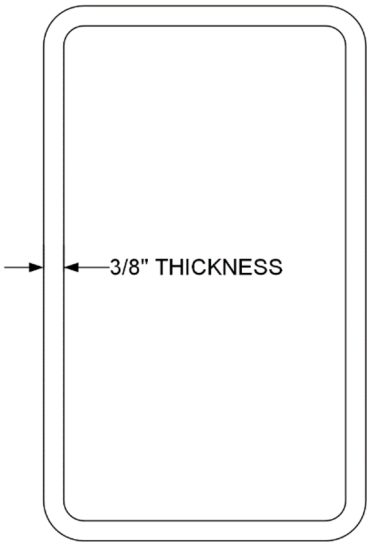

Figure 4-7 End-Truck Cross-Section

The end-truck is composed of three unique thicknesses. The standard section utilizes the standard 3/8-inch (0.375 inch) thickness as shown in the green areas in *Figure 4-8*. *Figure 4-8* is a depiction of the surface elements composing the end-truck. The mesh has been turned off so that the selected surfaces (grey areas), which will be discussed later, can be more easily shown. Multiple surface section can be seen as indicated by the grey division lines (and black lines which are simply selected grey lines). Multiple surface sections were used to model the element which allowed a more easily controlled meshed at area where the end-truck interacts with other objects of the crane structure such as the wheels and bridge. In a typical end-truck, and the end-truck used in this case-study, a mounting plate for the motor is often used and attaches to the side-wall of the end-truck. For simplification purposes, the wheel walls of the member, as labeled in *Figure 4-8* ("Wheel Walls") and shown in the grey highlighted areas near the wheel openings, were assigned a thickness of 0.75 inches to account for the mounting plate (assumed 0.375 inches) and end-truck wall thickness (0.375 inches). The connection between the mounting

plate and end-truck is either bolted or welded and, for this study, can be assumed rigid and modelled as a single element of uniform thickness. Likewise, in real construction, for ease of attaching the bridge to the end truck, another mounting plate is utilized. A 0.75-inch plate attached to the end-truck and another 0.75-inch plate attached to the bridge are connected at time of construction. For modelling simplification, the section shown by the grey highlighted areas at top of the end-truck in *Figure 4-8* and labeled “Bridge Mounting Area” was modelled as a single surface with an assigned thickness of 1.875 inches which is an equivalent thickness of the assumed rigidly connected two mounting plates (0.75 inches each) and the end-truck thickness (0.375 inches).

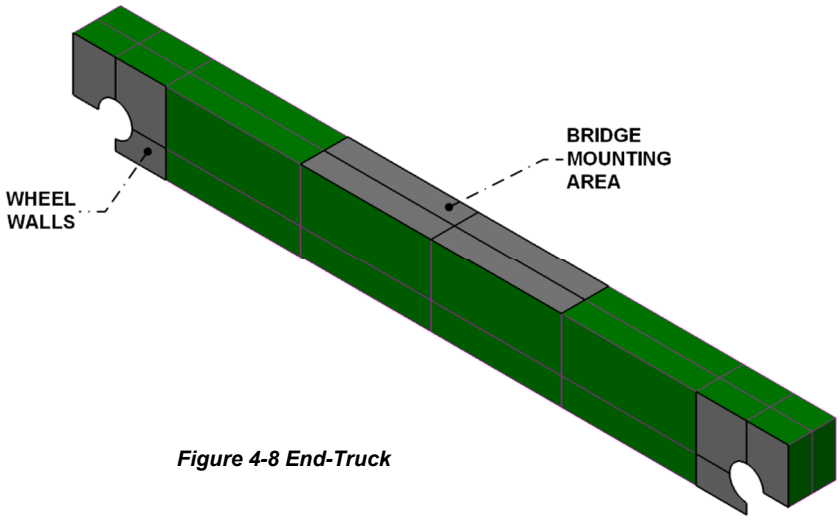

Figure 4-8 End-Truck

The mesh of the end-truck was created using 3D thick shell quadrilateral elements with a quadratic interpolation order along mesh lines. The 3D thick shell mesh elements are utilized here because, as stated previously, the bridge was modelled using surfaces (2D) where the rail and runway beam was composed of volume elements (3D). The mesh was densified in areas connecting to the wheel because of the concentration of stress which will develop in these areas as shown in *Figure 4-9* and *Figure 4-10*. Both *Figure 4-9*

and *Figure 4-10* represent the same meshed end-truck, however, *Figure 4-9* is an elevation view and *Figure 4-10* is an isometric view. The denser mesh was also controlled by the wheel which share a geometric line which was used to control the mesh.

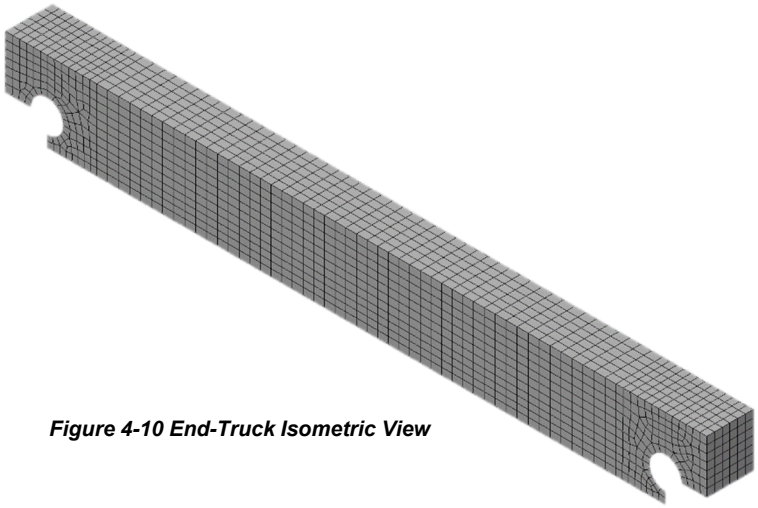

Figure 4-10 End-Truck Isometric View

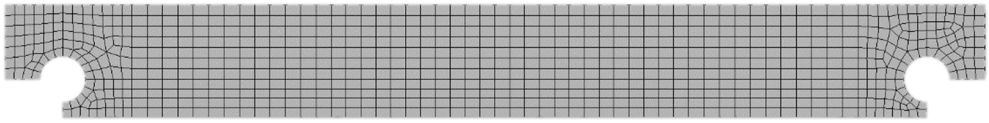

Figure 4-9 End-Truck Elevation View

The wheel was geometrically derived based on the crane manufacturers specification sheet which called for an eight-inch diameter wheel. End-truck wheels contain a “lip” around the diameter of the wheel which fits past the rail and acts as a guide during travel as shown in *Figure 4-44*. The reader should note that *Figure 4-44* is just an annotated drawing and is not part of the LUSAS model. As shown in *Figure 4-11*, the “lip” was excluded from the model. The “lip”, in terms of structural importance or integrity of the wheel, provides little significance for this research. The “lip” as a function of a guide can be

achieved by restraint joints which will be of accurate load transfer reasons discussed previously. Likewise, like the other volumes, the discussed in detail further in this chapter.

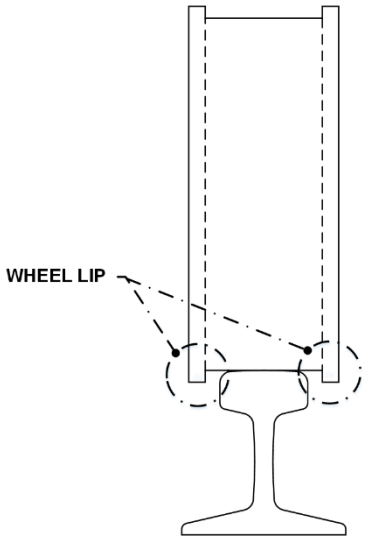

Figure 4-44 Wheel Lip

The wheels were chosen to be modelled as volumes for reasons wheels were meshed using 3D isoparametric solid continuum hexahedral (16 node) elements with a quadratic interpolation order along mesh lines.

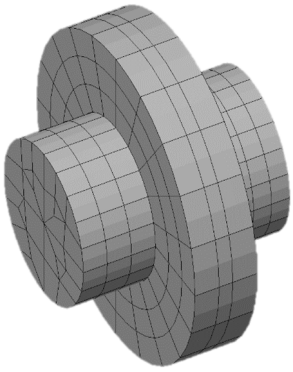

Figure 4-11 Wheel Isometric View

4.2.3 BRIDGE

The geometry of the bridge was modelled following the crane manufacturers specification sheet which called out a W18x71 standard wide-flange. The geometry of the bridge was developed using surfaces along the centerlines of the actual shape. The coping length was also specific in the sheet and modelled accurately. Per AISC shape specifications, the flange was assigned a thickness of 0.81-inches and the web a thickness of 0.495-inches. The mesh of the bridge was created using 3D thick shell quadrilateral elements with a quadratic interpolation order along mesh lines. As shown in *Figure 4-12*, the mesh was densified at the ends where the bridge and end-truck connect.

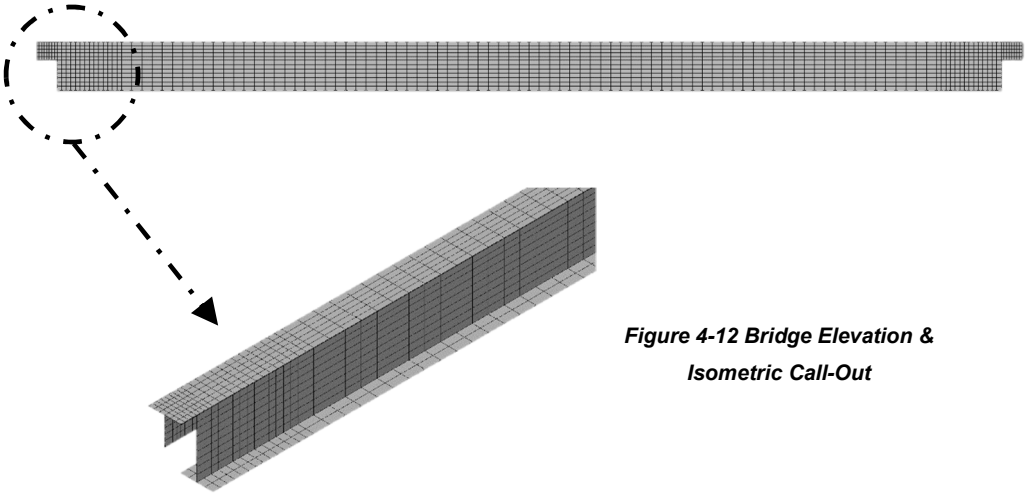

Figure 4-12 Bridge Elevation & Isometric Call-Out

4.2.4 COLUMNS

The columns were geometrically modeled based off the construction documents submitted by the structural engineer. The columns, or rather runway beam supports, for this case study are not very typical. Along one of the runways, nearest the building, the runway support was constructed off the existing structure. Reportedly, due to an excess

number of members, the columns were constructed of S12x35's. One of the runway supports was constructed off the engineered building. The runway support, as shown in *Figure 4-13*, spanned thirteen inches and consisted of (2)S12x35.

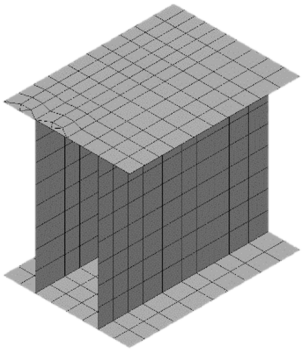

Figure 4-13 Runway Support

On the opposite side of the runway span, the support was fabricated off an existing crane column. The existing 50T crane column was reportedly designed with the assumption of supporting a future 50T crane. The support, as shown in *Figure 4-14*, has a span (top beam) of six foot. The support also consisted of an angled strut member. Both the support members were designated as S12x35.

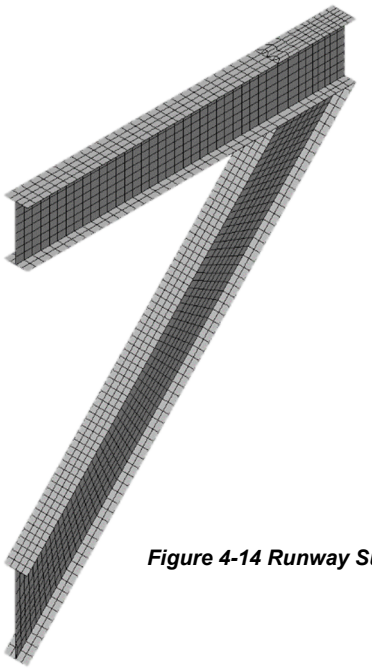

Figure 4-14 Runway Support

On the other runway, no existing construction obstructed the crane supporting system. Therefore, the runway was supported by a S12x35 on each side as shown in *Figure 4-15*. The length of the columns was twelve foot. As shown in *Figure 4-15*, the column was also modelled with a cap plate for the runway beam.

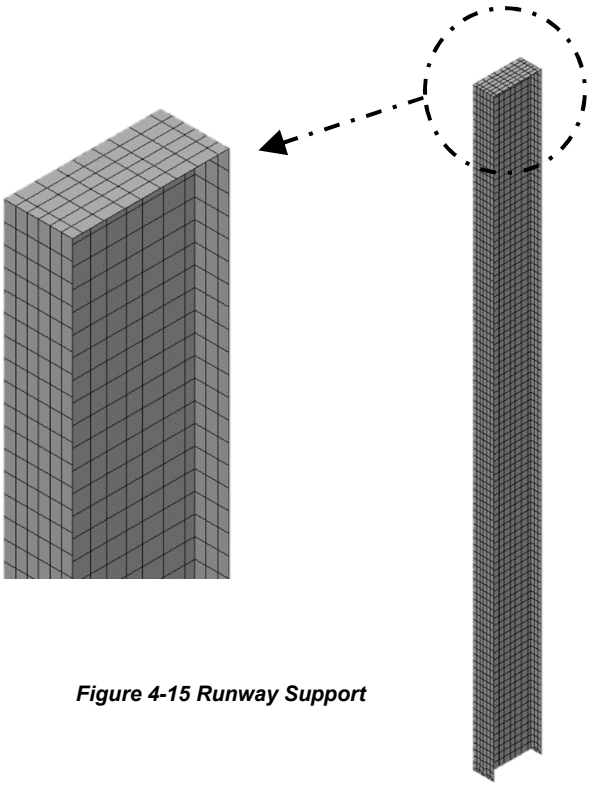

Figure 4-15 Runway Support

All the columns and cap plates were meshed using 3D thick shell quadrilateral elements with a quadratic interpolation order along mesh lines. Each of the meshes were dominated by shared mesh lines with the supported runway beam. The mesh division about the length was assigned such that the average element would have a square geometry. The thicknesses of the flanges were assigned a thickness of 0.544-inches and the webs a thickness of 0.428-inches per AISC specification. The column cap plates were assigned a thickness of 0.5 inches.

4.3 RESTRAINTS

No support or restraint was modelled directly. Using the structural plans along with the author's construction experience, assumptions can be made to simplify the restraints within the model. The restraints of the system are vital in concluding meaningful results. The assumptions made about the restraints must behave similarly to actual restraint.

Some of the following figures are of the crane system, where two or more structural members are discussed. *Figure 4-7*, for visualization purposes, has been included and denoted with labels respective to the figure which will be described later.

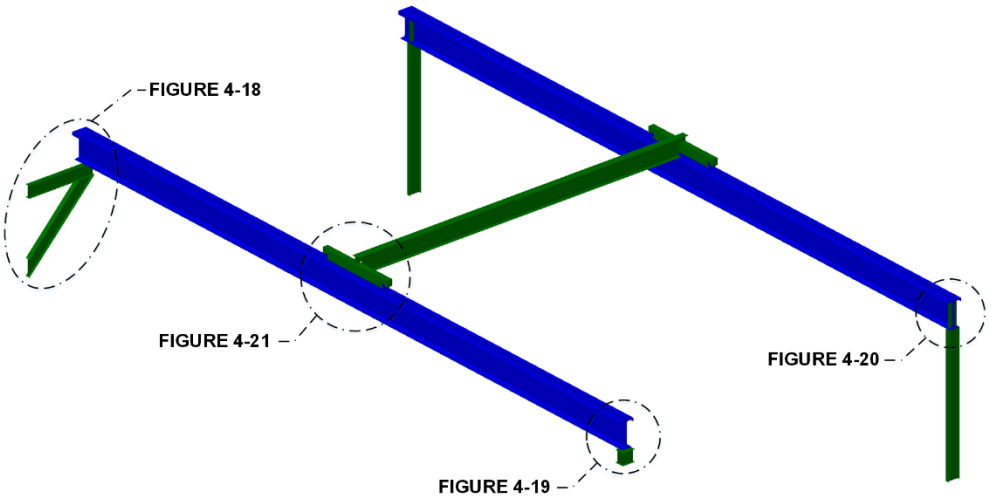

Figure 4-7 Crane System

The runway support shown in *Figure 4-16*, or previously in *Figure 4-14*, was welded (all around) to an existing 50T crane column's flange (strong axis). The size of the existing column, which is not known to the author, was approximated as a large wide-flange section with flanges which measured to close to two inches. The existing column, which had a top elevation of over twenty foot, was designed to withstand a moment, produced by

the lateral force from the existing crane, much larger than the coupled moment produced from the runway support's fixed restraints. Due to these reasons, the existing column is likely to undergo very minimal translation or rotation at the welded restraints, and can reasonably be replaced by fixed restraint supports.

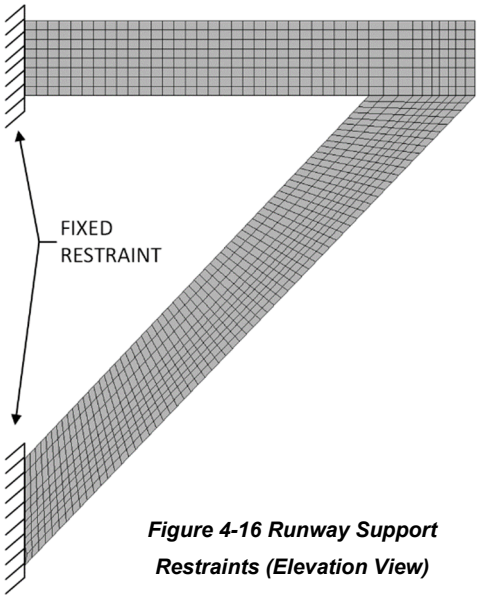

Figure 4-16 Runway Support Restraints (Elevation View)

Similar to the runway support shown above, the other runway supports, shown in *Figure 4-13* and *Figure 4-15,* were modelled with fully fixed restraints. The runway support shown in *Figure 4-13* was fully welded to an existing building column. The runway columns shown in *Figure 4-15* were supported on individual concrete deep piers twenty-four inches in diameter. The columns' base plate was designed as a moment resisting connection.

The rail was attached to the runway beam using rail hook bolts. Aligned with the same principal as the structural design of the runway, since the crane is attached using hook bolts the runway beam and the rail are assumed to act non-compositely. As indicated by EN.1993.6.2007. Joint elements are used to account for the effect of slip between the plane two members as shown in *Figure 4-17* (joint elements labeled as white "X"'s). The

joint material (of no rotational stiffness) was assigned a value of 500,000 lbf-in for the axis in the gravity direction and for the other axis in the plane of *Figure 4-17*. For the longitudinal axis, or the axis which slip will occur, was assigned a stiffness of 1.0 lbf-in. The spring stiffness value of 500,000 lbf-in assigned to the two axes were arbitrarily chosen to model a more rigid connection. As recommended by LUSAS, for a spring stiffness to behave rigidly, the stiffness is sufficient of that 1,000 times that of the adjacent element. Likewise, for a much less stiff spring stiffness, the spring could be modelled with a stiffness of 1/1,000 times that of the adjacent element. In preliminary modelling of the joint element, attempts at a value much lower than 1.0 lbf-in assigned to the “slip” plan, and values much more than 500,000 lbf-in assigned to the other two translation axes resulted in ill-conditioning and/or instabilities and associated warnings/errors within the model. Conversely, joint assignment around the assigned value had no effect in the results of the model. The master assignment was given to the surface of the runway beam while the slave assignment was given to the rail.

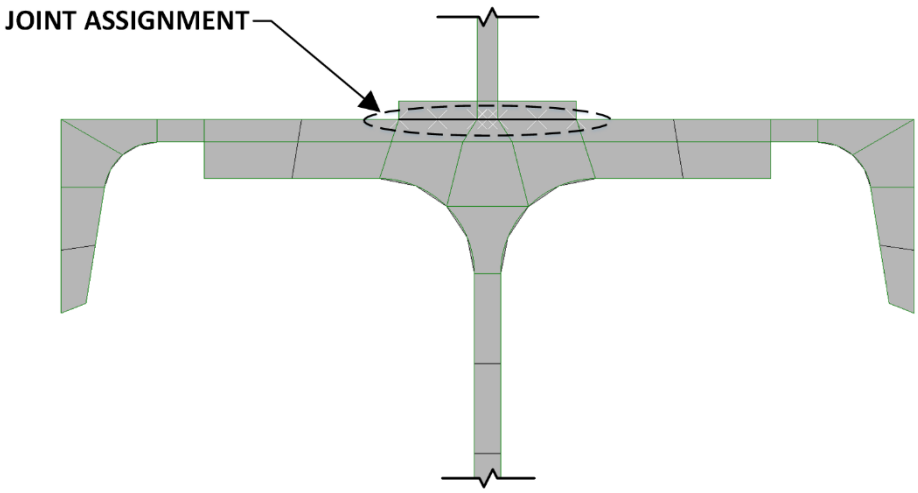

Figure 4-17 Runway/Rail Joint Assignment

The runway beam nearest the building was close enough to provide “tie-back” connections which were mentioned in *Chapter-2*. The tie-back was connected to the channels flange. To account for this restraint of movement, a fixed connection about the translation axis was assigned a similar area of the channel flange as shown in *Figure 4-18* and *Figure 4-19*.

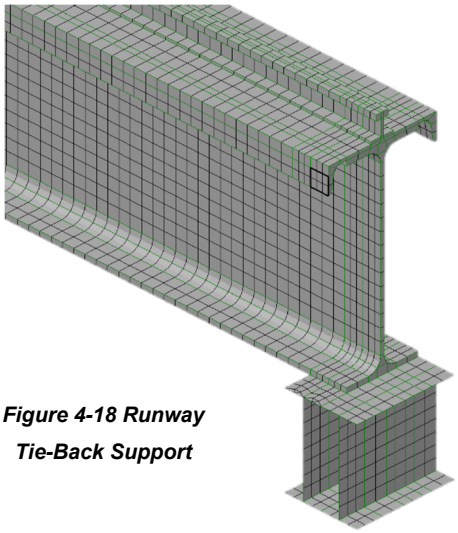

Figure 4-18 Runway Tie-Back Support

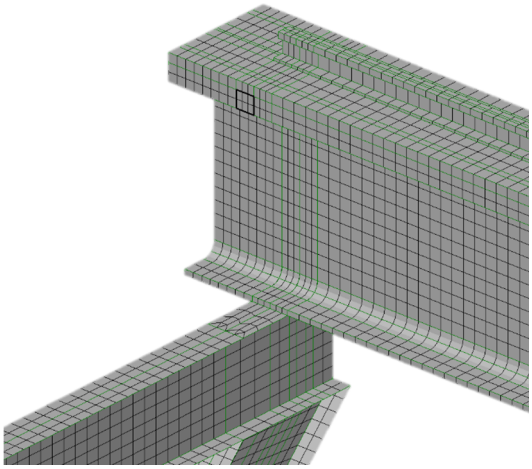

Figure 4-19 Runway Tie-Back Support

The other side of the runway beam was fitted with stiffeners, as shown in *Figure 4-20*, which was used to restrain the top flange movement most likely due to not having space for and tie-back detailing which is common for outdoor cranes. The mesh assignment to the stiffeners was the same as previous surface elements; 3D thick shell quadrilateral elements with a quadratic interpolation order along mesh lines. A thickness was also assigned of 7/16-inch which matched the thickness of the connecting runway beam's web.

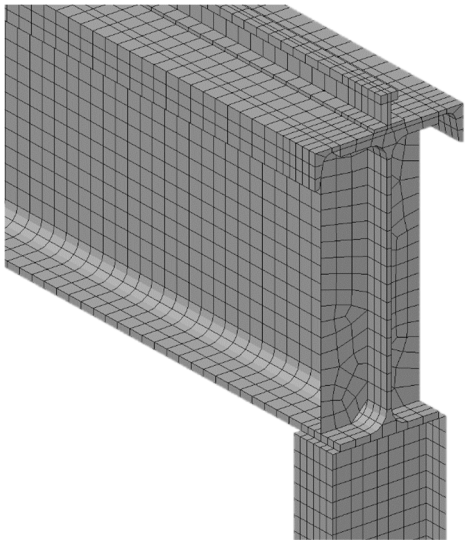

Figure 4-20 Runway with Stiffener

Another area of interest with in the crane system is the end-truck/wheel/rain configuration seen in *Figure 4-21*. The end-truck attachment to the outer wheel (extrusions on each side of the wheel connecting to the end-truck) was modelled with no degree of freedom release and therefore functions as a rigid combined element. In reality, the wheel's outer axel shaft is welded to the end-truck. Although the model does not contain the intricate parts, such as the axels mentioned earlier, the extruded center of the wheel, which can better be seen in *Figure 4-11*, connecting the wheel and end-truck essentially serves the same function. On the same topic, because the wheel does not contain and axel and is connected to the end-truck directly, the wheel no longer has the degree of freedom to move. The degree of freedom for the wheel to rotate freely however is not typical within a realistic crane which is fixed under a gear which powers the wheels. Although the gear will allow move "give" than a rigid connection modelled here, the small influence this movement would have, in a global sense of the model results, is assumed to be insignificant. The wheels also provided difficulty in accurately modelling connection. As mentioned previously

the wheels often contain a “lip” which sits flush with the rail and guides the wheel during travel. The “lip” combined with the contact friction would restrain the translational movement about that axis. The wheel, however, if ever sustained to an uplift would have a degree of freedom released in the gravity axis. To model the wheel supports would require a combination of contact and friction joints. These joint elements would add costly time and increase the file size to an already very large file. To simply the condition, a simple no rotation joint, similar to the joint used in the rail to runway beam connection, was used to model the wheel to rail attachment. Post analysis the stress analyzed to confirm that the translation in each axis did not overcome the static frictional resistance and that the connection had to tension develop. Under these conditions, a translational fixed condition, as modelled, would be sufficiently accurate.

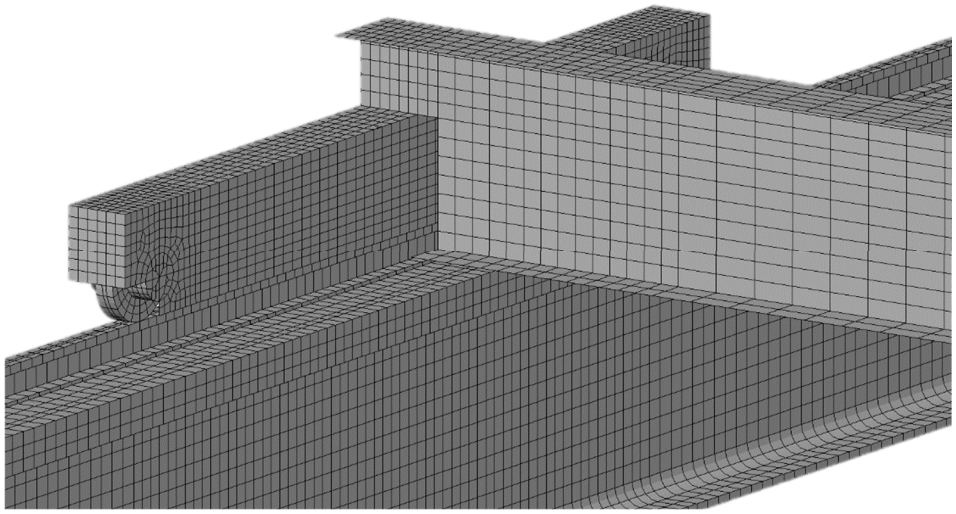

Figure 4-21 End Truck Attachment

4.4 MATERIAL ASSIGNMENTS

All the sections created in this model were attributed with the same material definition. The material definition was selected from the general material library provided by LUSAS and associated properties can be seen in *Figure 4-7*.

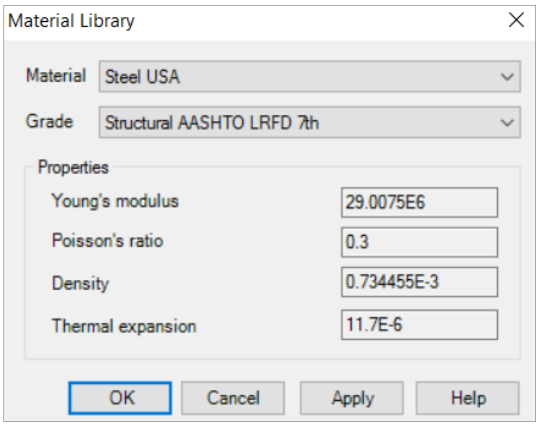

Figure 4-7 Material Property

4.5 LOADING

The crane system as mentioned previously utilized a single bridge with underhung trolley. *Figure 4-22* includes a screenshot of the LUSAS model with a superimposed image of the underhung trolley. The trolley system drawn in *Figure 4-22* is much too complex to be included in this research provided a simplification can be made. In the case-study being examined, only the trolley was being activated and the bridge remained stationary; the only movement in the system was the mass in the gravity direction. Since wind nor seismic was of concern when movement was observed any out of place motion will be ignored. Including the trolley system would result in many natural frequencies being controlled by the rope/chain. Many current crane trolley motors have “smart” control features which allow for smooth acceleration and deacceleration opposed to full torque being applied as the

time of button actuation. The effect of the mass magnitude on the natural modes of vibration will be discussed later. Any mass which pose a threat to progressive structural instability, a mass magnitude which is near the design stress limit and overstressed due to normal stresses developed from the twisting motion or large rotation deformations from the large inertia force from the mass. A structurally significant mass, or at least the mass analyzed in this case-study, has a magnitude which the motor acceleration will not overcome. The motor used in this case-study, which is not known, but can be assumed based on common 5T crane trolley motors. This motor, without including “smart” lifting features, does not possess the acceleration which would overcome the mass of the payload; the system will never go into “slack-rope”. Since the acceleration will never overcome the mass, the wire rope will always be in tension and therefore the system can be replaced by an equivalent mass acting at a node.

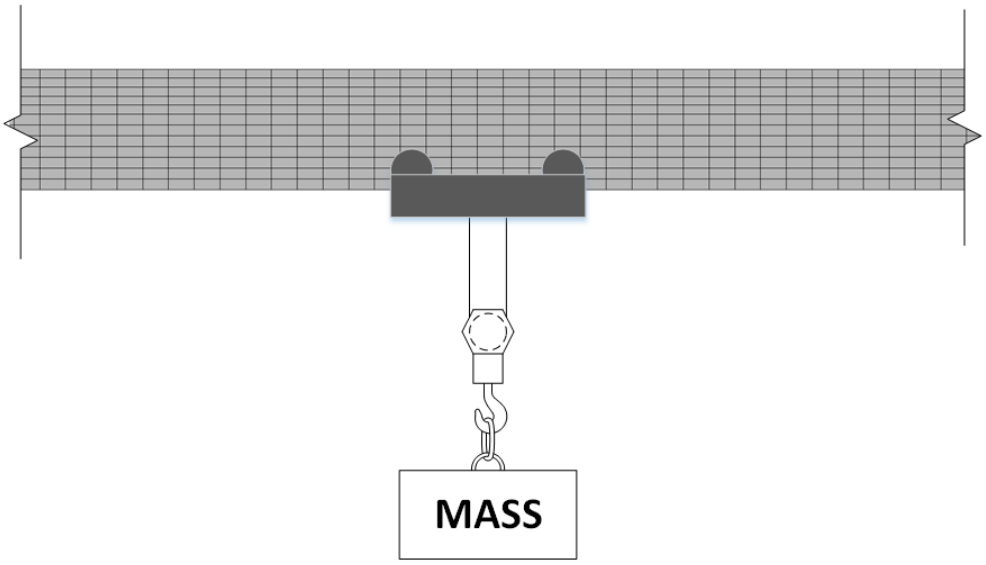

Figure 4-22 Bridge and Trolley

The trolley system is simplified to a single mass of equivalent at the center of the bridge as shown in *Figure 4-23*. While the actual trolley distributes the load along multiple points, the spacing of these wheels is negligible. The magnitude of the mass assigned is 16-18 slinch. The mass assigned is based on the weight of the payload at time of lifting and trolley.

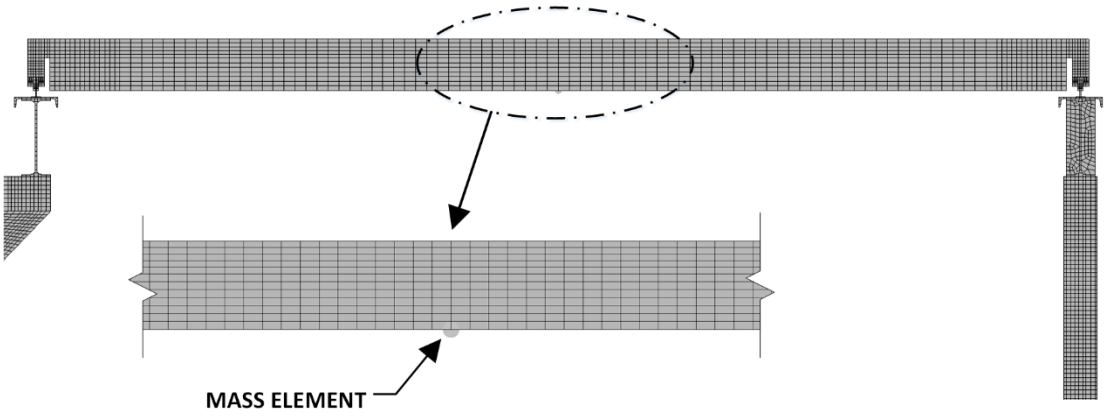

Figure 4-23 Bridge and Mass

CHAPTER 5

FINITE ELEMENT RESULTS

5.1 INTRODUCTION

As stated previously, the crane runway beam, as part of this case study, underwent reported “twisting” motions which was later seen during a site visit. The crane was found to have no issues under static loading, however, when the “inching” process began the runway beam showed noticeable signs of rotation about its longitudinal axis. Due to the difference between static and dynamic deformation overserved in the field the hypothesis is suggested that the twisting motion was due to resonance vibration from the “inching” action when successively lifting the payload.

Three types of analysis were carried out to verify and conclude results from the crane system: static stress analysis, eigenvalue dynamic analysis, and transient dynamic analysis. Each of these analyses will be discussed in more detail further in the chapter.

5.2 VERIFICATION

Another important aspect of the results of the modelling is verifying the structure behaves true to the analytic structure seen in the field. Although a structure could have no warnings or errors in solution, the assignments and assumptions made during the construction of the model may differ than what the structure experiences. Verification is a way to confirm that the constructed finite element model behaves in an acceptable behavior as the analytical structure. Full scale testing can also be used to link experimental results to modelling results. Due to cost, time, and safety issues, building a full-scale crane runway which, in worst case scenario, could collapse was not an option. Fortunately, there was a

short video taken, by an employee of the company using the crane, which shows the crane runway undergoing this motion. The video, however, for copy-right and anonymity reasons, will not be linked or shared at this time in this Thesis. Although at first glance the video, which is just over 21 seconds, does not appear to contain much useful information. However, further investigation reveals two critical pieces of information which can be extracted and used for verification.

5.2.1 CRANE LIFTING TIME

The crane lifting time, presented in *Table 5-1*, was taken from the video previously mentioned. This table was also presented in the *Chapter-3*. The data was extracted from the video by listening to when the trolley was actuated, or when the crane lifting was activated, which makes a unique sound. *Table 5-1* presents the recording of the crane trolley lifts identified under the first column, “LIFT #”. The second column is the time in “space” of the lifts, or the time as it appeared on the video when the trolley was lifted. The third column is the time difference between each crane lift. The third column can be denoted as the period of the lifts. One piece of information which is not known is the type of motor used nor is the duration of the lift known. While these two pieces of information would be helpful, by assuming a common motor for the crane based on the capacity and span, as well as assuming that the duration of each lift is approximately the same, these pieces of information will later be determined as nonvital. As shown in *Table 5-1*, multiple lifts were made, however, only during certain periods, as labeled “most critical lifts”, did the crane runway display increasingly growing deformation rotations. The reader should note that the runway still exhibited slight “twisting” deformations when not within the critical lifting times, however, the a few lifts had to be made before such deformations were visible.

Another critical observation seen from the video was that the last lift, which was outside the critical lifting times, drastically halted the increasing growing “twisting” deformations.

LIFT #	TIME (sec)	Δt_{i-i+1} (sec)
1	11.80	--
Δt_{1-2}	--	1.13
2	12.93	--
Δt_{2-3}	--	1.22
3	14.15	--
Δt_{3-4}	--	1.78
4	15.93	--
Δt_{4-5}	--	0.87
5	16.80	--
Δt_{5-6}	--	0.88
6	17.68	--
Δt_{6-7}	--	0.90
7	18.58	--
Δt_{7-8}	--	0.88
8	19.46	--
Δt_{8-9}	--	1.74
9	21.20	--

MOST CRITICAL LIFTS

Table 5-1 Crane Lift Times

5.2.2 CRANE “TWISTING” PERIOD

Along with the period of the trolley crane lifts, another critical piece of information established from the video was the period of the “twisting” of the crane runway as shown in *Table 5-2*. The reader should note that the “time” column of *Table 5-2* is not the “time in space” but rather an arbitrary time started at the beginning of where the beam started to show the maximum amount of “sway”. The time started at around the beginning of the “Most Critical Lift” phase as shown in *Figure 5-1*, and ended roughly five seconds later near

the end of the “Most Critical Lift” phase. The period of the runway was considerably faster than that of the trolley lifts. The video was slowed down (to 1/8th of the speed) and the periods of the “twisting” or “sway” of the runway beam was measured as shown in *Figure 5-1*. The reader should note that while the video was able to be slowed down to a speed which the “twisting” period of the beam could be counted, the video was not made for scientific nor research puposes; the video was at ground level viewing isometrically from the bottom-side of the beam. So while the twisting could be counted, first column of *Table 5-2*, the exact time of peak twisting, moments shown in *Figure 5-1*, are difficult to determine; opposed to if a cross-section of the beam was viewable. Likewise, the periods of the “twisting” are fractions of seconds so if the peak “twisting” time was recorded slightly before or after the actual peak then this would, in return, results in errors. The reader should also be made aware that serveral recordings of the “twisting” action was made and that none of the “peak” times were perfectly the same, however, all averages were in the 3.5(s) range. Because there are many types of error attributed to *Table 5-1*, the average is presented which is to be used as a general period of the crane twisting. Although the average will be used to describe the period of crane twisting, the range of periods are all plausible twisting periods.

As shown in figures below, the beam “rotation” period was counted from when the beam was fully “twisted” to one side, *Figure 5-1(a),* where the beam reached maximum “twist” on the other side, *Figure 5-1(b),* which can approxiamtely be assumed to the half the period, and finally back to its original deformed position, *Figure 5-1(c).*

Time, t (sec)	Period, T (sec)	Frequency, f (1/sec)
0.000	--	--
--	0.300	3.333
0.300	--	--
--	0.334	2.996
0.634	--	--
--	0.258	3.883
0.891	--	--
	0.275	3.636
1.166	--	--
--	0.313	3.200
1.479	--	--
--	0.280	3.571
1.759	--	--
--	0.300	3.333
2.059	--	--
--	0.279	3.587
2.338	--	--
--	0.304	3.292
2.641	--	--
--	0.250	4.000
2.891	--	--
--	0.296	3.376
3.188	--	--
--	0.241	4.145
3.429	--	--
--	0.318	3.150
3.746	--	--
--	0.316	3.162
4.063	--	--
--	0.241	4.145
4.304	--	--
--	0.275	3.636
4.579	--	--
--	0.280	3.571
4.859	--	--
AVERAGE	**0.286**	**3.531**

Table 5-2 Crane Twisting Periods

As shown in figures below, the beam “rotation” period was counted from when the beam was fully “twisted” to one side, *Figure 5-1(a),* where the beam reached maximum

"twist" on the other side, *Figure 5-1(b),* which can approxiamtely be assumed to the half the period, and finally back to its original deformed position, *Figure 5-1(c).*

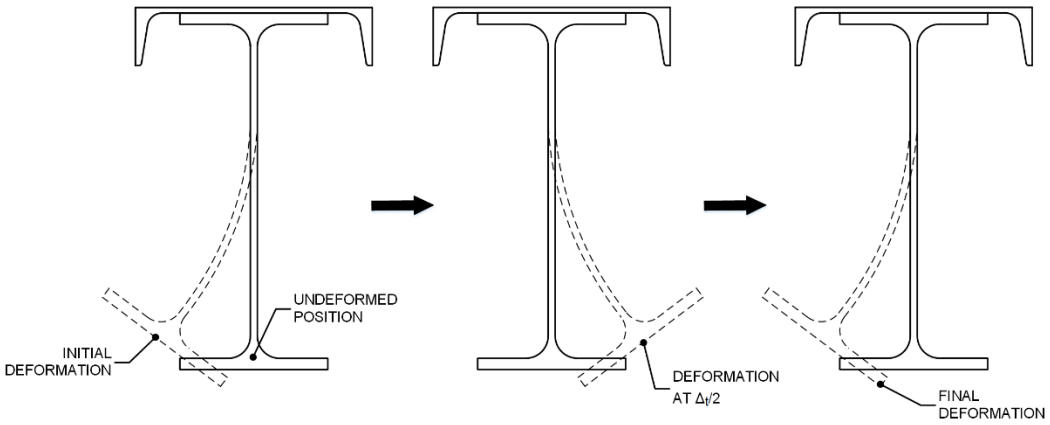

Figure 5-1(a) Twist Period

Figure 5-1(b) Twist Period

Figure 5-1(c) Twist Period

5.3 EIGENVALUE DYNAMIC ANALYSIS

Three primary analyses were carried out to verify the FEA model, find the natural frequencies of the system, iterate possible solutions, and formulate a set of equations: linear static stress analysis, eigenvalue analysis, and transient analysis. The stress analysis was used as a simple test of the model's stiffness matrix as recommended by LUSAS. The static stress analysis, which does not contain any complex dynamic variables as found in the eigenvalue and transient analysis, is much quicker to solve. The stress analysis is also used to verify any assumptions made when assigning properties to the model as mentioned in Chapter-4. The eigenvalue value analysis, or frequency analysis, was used to establish the natural frequency modes of vibration and their respective deformation shapes. Lastly, the transient analysis, also known as time-step or step-by-step

dynamic analysis, is a dynamic analysis which will be used to simulate the effect of an assigned loading.

5.3.1 Analysis Overview

The eigenvalue value analysis, or also known as frequency analysis, is used to find the eigenvalues of the stiffness matrix. The eigenvalues, through relationship, determine the frequencies at which free vibration of the system occurs.

The Fast Lanczos solver was used as the method to solve the eigenvalue analysis. The solver used was the default option set by LUSAS. The modeled system did not fall under any requirements which may require the use of another solver. No material damping was assigned in the eigenvalue analysis.

Twenty eigenvalues were solved and obtained in the analysis as shown in *Table 5-3*. A range could have been established for the suspected frequency (or period) which could have possibly reduced the number of solved eigenvalues and hence reduced file size and solution time, however, a full range of eigenvalues was desired to identify all possible critical vibration modes. Each mode of vibration will be described below, however, not every eigenvalue will be graphically depicted; only the eigenvalues found prevalent to this research will be depicted graphically.

EIGENVALUE ANALYSIS RESULTS			
MODE	EIGENVALUE	FREQUENCY	ERROR NORM
1	129.14	1.8087	7.66E-07
2	164.68	2.0424	5.32E-07
3	370.64	3.0641	1.02E-07
4	580.52	3.8347	2.56E-09
5	678.78	4.1465	1.58E-08
6	734.14	4.3123	6.47E-08
7	1124.88	5.3379	6.91E-08
8	1137.35	5.3674	4.12E-08
9	1392.09	5.9382	1.45E-07
10	1780.80	6.7163	9.12E-08
11	1790.05	6.7337	4.02E-08
12	2561.20	8.0546	4.90E-08
13	3097.46	8.8578	5.20E-08
14	3842.77	9.8660	3.45E-09
15	5410.09	11.7064	3.26E-08
16	6573.06	12.9034	1.10E-08
17	7182.16	13.4880	5.85E-09
18	8021.54	14.2544	1.09E-07
19	9501.88	15.5140	3.33E-06
20	10391.20	16.2238	3.24E-07

Table 5-3 Model Eigenvalues

The reader should note that in some of the figures below, of the deformed shape of the respective natural frequency, the columns or column supports have been hidden in view; In a few of the views the columns blocked the view from accurately seeing the deformation associated with the natural frequency. For similar reasons, the runway beam stiffeners at the end of the span, as previously shown in *Figure 4-20*, have been hidden in all views. All the figures of the eigenvalues deformed shape have a scale factor of 75 which will allow the reader to clearly see the deformation under the respective frequency.

5.3.2 EIGENVALUE-1 (F=1.81 S^{-1})

The first natural frequency mode of the system is associated with a deformation of lateral movement of the runway beams as shown in *Figures 5-2a-Figure 5-2c*. As shown in the figures the deformation is coincident with almost complete lateral translation of the runway beams. Slight twisting of the runway beam and some translation of the columns may be apparent, however, at a scale factor of 75 the amount of movement experienced from the frequency will be negligible to the movement seen in the runway beam.

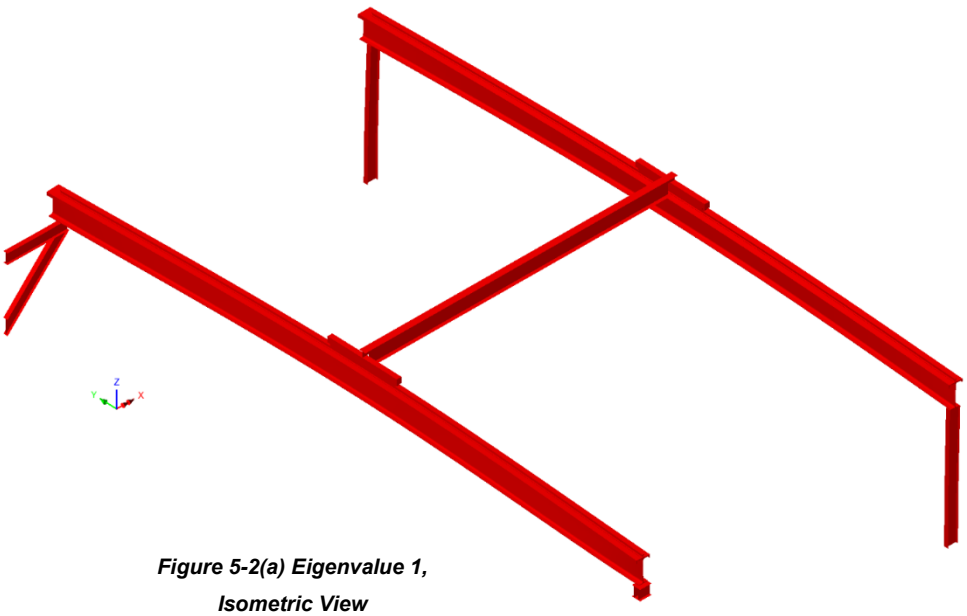

Figure 5-2(a) Eigenvalue 1, Isometric View

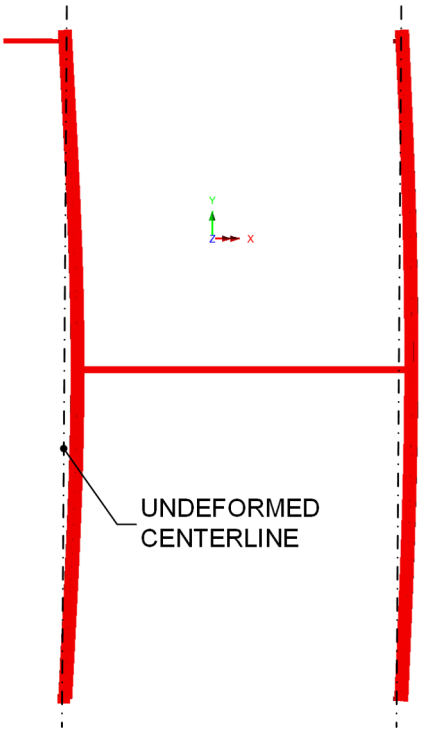

Figure 5-2(b) Eigenvalue 1, Plan View

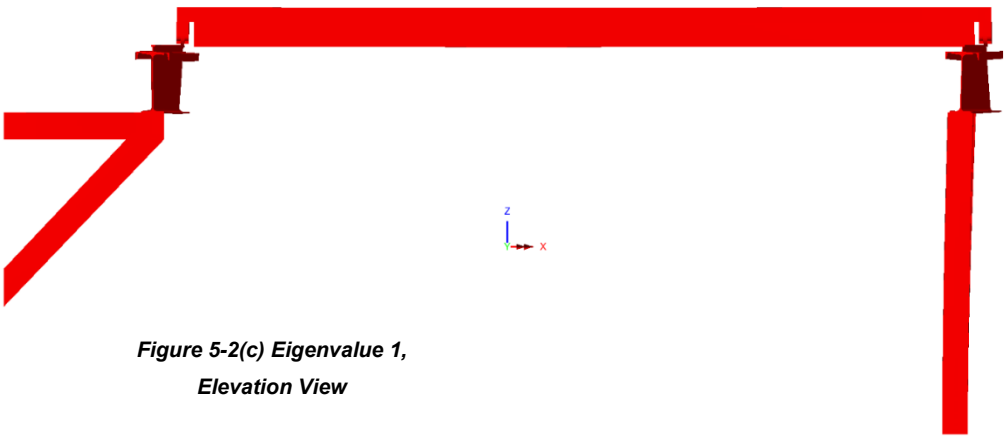

Figure 5-2(c) Eigenvalue 1, Elevation View

5.3.3 EIGENVALUE-4 (F=3.83 S^{-1})

The fourth mode of vibration of the system can be seen in *Figure 5-3(a)-Figure5-3(c)* as dominated by twisting deformation of the runway beam and bridge transverse movement (downward movement). The transverse movement of the bridge can best be seen in the elevation view of Figure 5-3(c). *Figure 5-3(a)* was scaled to a factor of 150. This figure, at the isometric angle viewed, was difficult to see the deformation under its respective frequency at the scale factor of 75. To remind the reader, the runway supports have been turned off in *Figure 5-3(c)* so that the deformation of the runway beam could be more visible. As seen in Figure 5-3(c), the deformation of the outside runway beam, the right-side runway beam in the figure, has a slightly more pronounced twisting deformation. The analytic video was of the left side runway beam and does not show the right-side runway beam. However, from the site-visit, neither runway beam appeared deform more than the other. At a scale factor of 1 the larger deformation may be indistinguishable from the smaller. The larger deformation of the right-side runway beam is likely due to the torsional stiffness of the runway beam. The left-side runway beam utilizes tie-back connections which restrain the top flange while the right-side runway beam utilizes stiffeners which are used to restrain the top flange. The tie-back connection, which restrains the top flange through direct axial (tension or compression), is much stiffer than the stiffeners which are restraining the component forces (axial, bending, shear). Likewise, the columns also a show slight translations in the “x” direction which can be best seen in Figure 5-3(a) (scale factor of 150). The translation the columns exhibit in *Figure 5-3(a)* is faint with a scale factor of 150, and barely noticeable in other figures with a scale factor of 75. The slight movement of the columns, although very minimal, suggests that the columns reduce the stiffness of the runway beam compared to the column supports and runway beam on the contrary side. Because of the reduced stiffness, compared to the other runway

beam, the respective larger deformation of the runway beam is justifiable. The reader should note that because the columns show translation and reduced the stiffness compared to the opposing side or rigid supports, the frequency is therefore affected. The magnitude of the effect the columns have on the frequency is discussed later in this chapter.

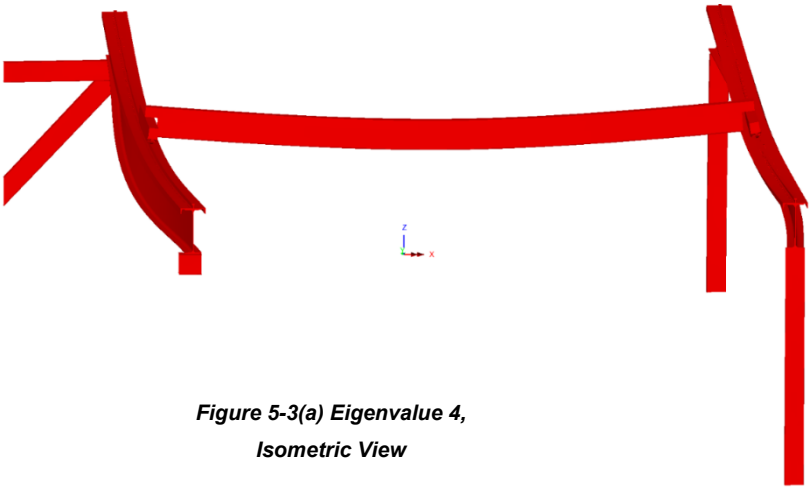

Figure 5-3(a) Eigenvalue 4, Isometric View

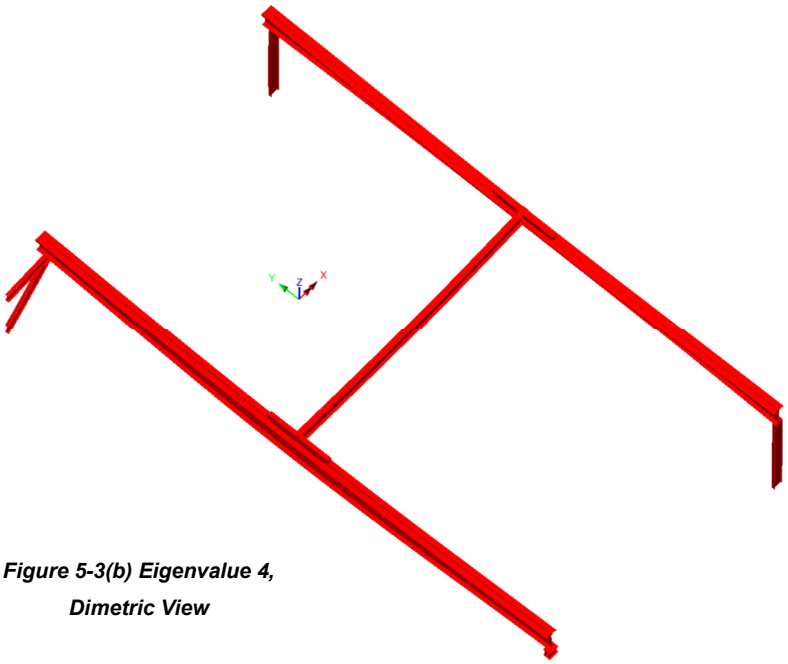

Figure 5-3(b) Eigenvalue 4, Dimetric View

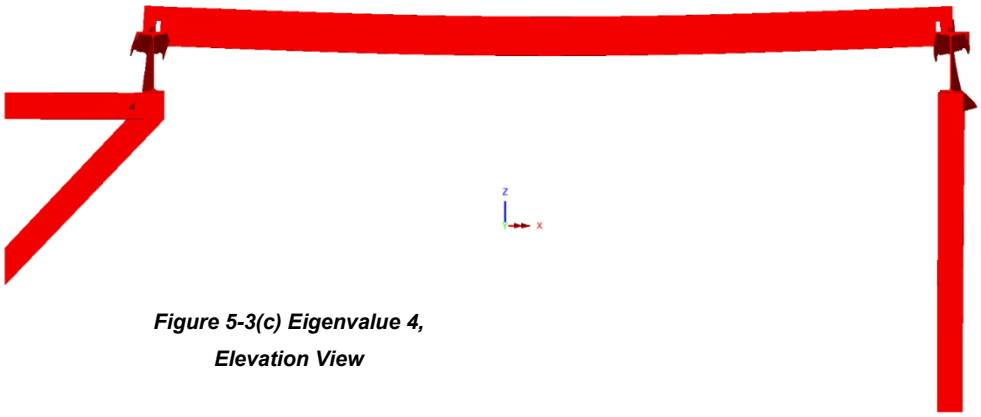

Figure 5-3(c) Eigenvalue 4, Elevation View

5.3.4 EIGENVALUE-5 (F=4.15 S^{-1})

The fifth mode of vibration of the system is characterized by longitudinal twisting (twisting about the “y” axis) of the runway beams as shown in *Figure 5-4(a)-Figure 5-4(c)*. The figures shown for this mode of vibration are scaled with a factor of 50 which was sufficient in accurately showing the deformations. The deformation is very similar to that found in the previous mode of vibration with a few differences, and both frequencies are very close in magnitude. The first major difference between the fourth mode and the fifth mode of vibration is the bridge in this mode, does not appear to have any transverse movement. Another notable difference, although small, is the magnitude of column deformation relative to the runway beam deformation. The reader must remember, as previously mentioned, that the deformation of the structure is normalized and, therefore, the visualized deformation between modes of vibration cannot be compared directly; not to mention that many of the depictions are scaled differently. The relative deformation between individual elements within a mode of vibration can be compared to the relative deformation between individual elements within another mode vibration. Such is the case here, where the deformation of the column relative to the runway beam, best seen in *Figure*

5-4(c), is much larger than that found in the fourth mode. The apparent translation of the column (in the "x"-axis) in this mode suggests that the column, or rather stiffness of the column, does have a direct effect on the frequency. The extent of this effect will be discussed later in this chapter.

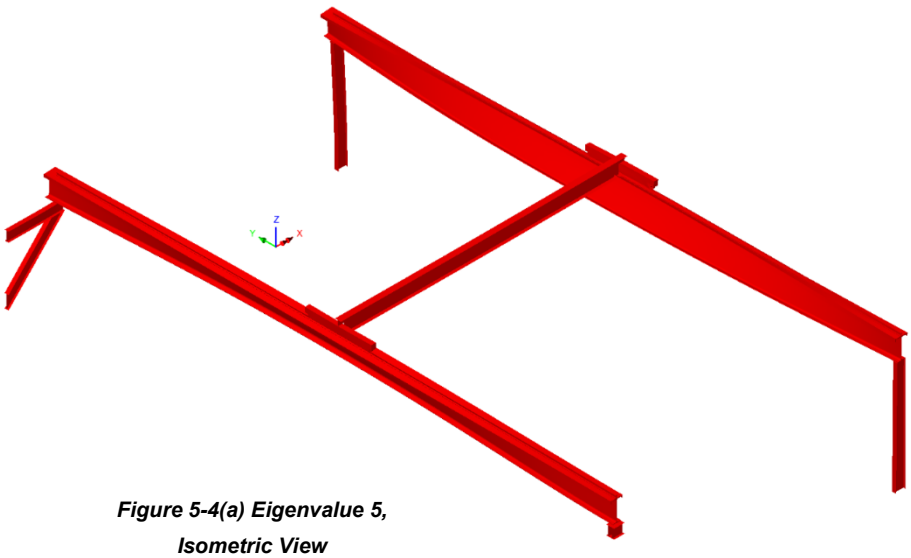

Figure 5-4(a) Eigenvalue 5, Isometric View

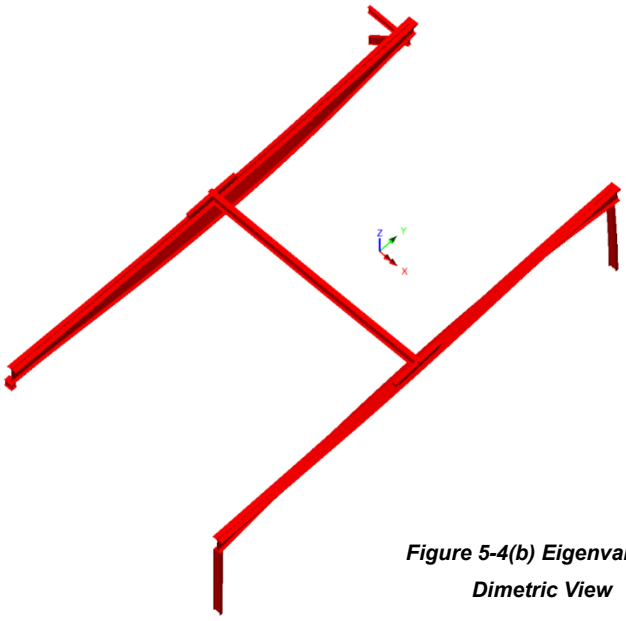

Figure 5-4(b) Eigenvalue 5, Dimetric View

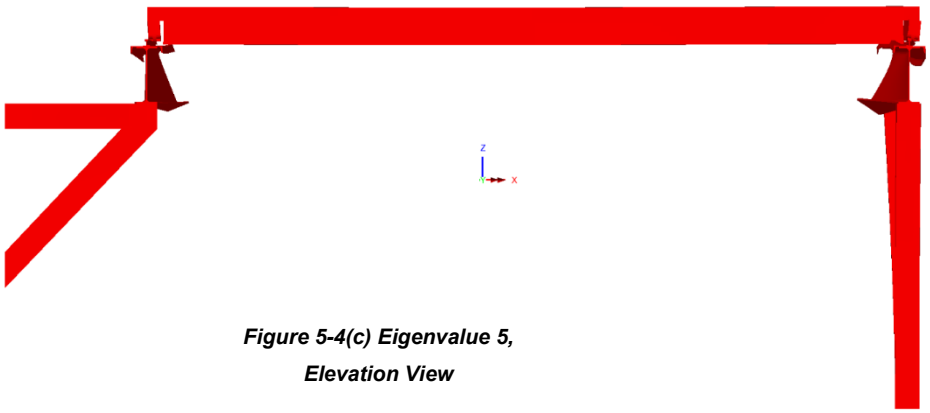

Figure 5-4(c) Eigenvalue 5, Elevation View

5.3.5 EIGENVALUE-7 (F=5.34 S^{-1})

The seventh mode of the vibration of the system is characterized by longitudinal twisting (twisting about the “y” axis) of the runway beams as shown in *Figure 5-6(a)-Figure 5-6(d)*. The seventh mode of vibration is similar in deformation and near the same frequency as the fifth mode of vibration. To accurately portray the deformation, the figures have all been scaled with a factor of 50 except Figure 5-6(d) which the deformation was sufficiently visible when scaled with a factor of 25. One of the most notable difference, up to this point, in this mode of vibration is the relative magnitude of deformation between the runway girders. In previous modes of vibration, the runway beam supported by the two columns, shown on the right side of the figures, has had slightly more pronounced twisting deformation. In this mode of vibration however, the runway beam seen on the left side of the figures is shown to undergo a larger relative deformation best depicted in *Figure 5-6(d)*. Another difference, although small, is the direction of torsion deformation. In the modes, which exhibited twisting of the runway beams, the runway beams both have a deformation of either bottom flange movement “inward” or “outward” as depicted in *Figure 5-5(a)*. In the

seventh mode, one runway beam has a torsional deformation of “inward” while the other runway beam has a torsional deformation of “outward” as depicted in *Figure 5-5(b)*.

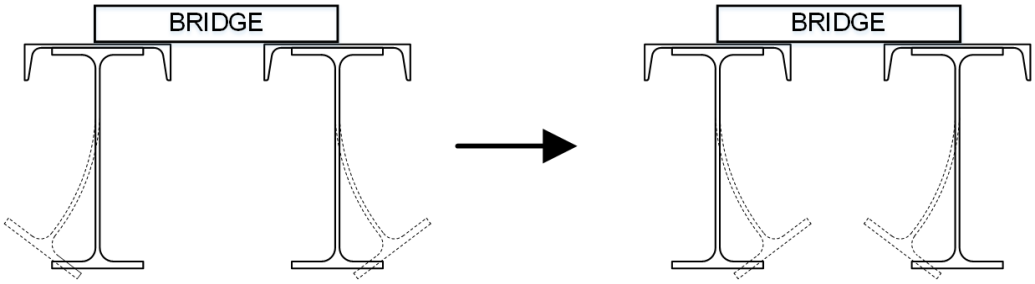

Figure 5-5(a) Runway Deformation

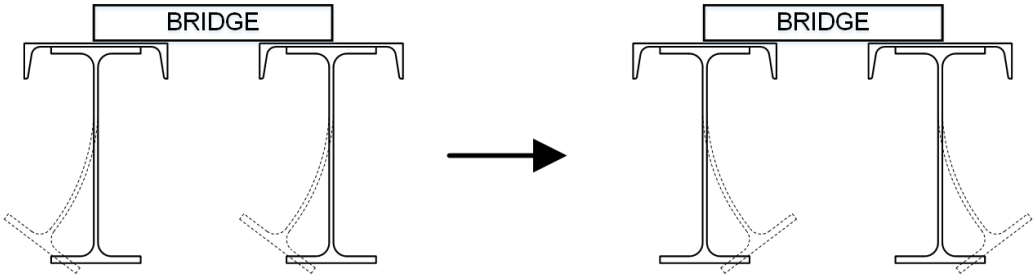

Figure 5-5(b) Runway Deformation

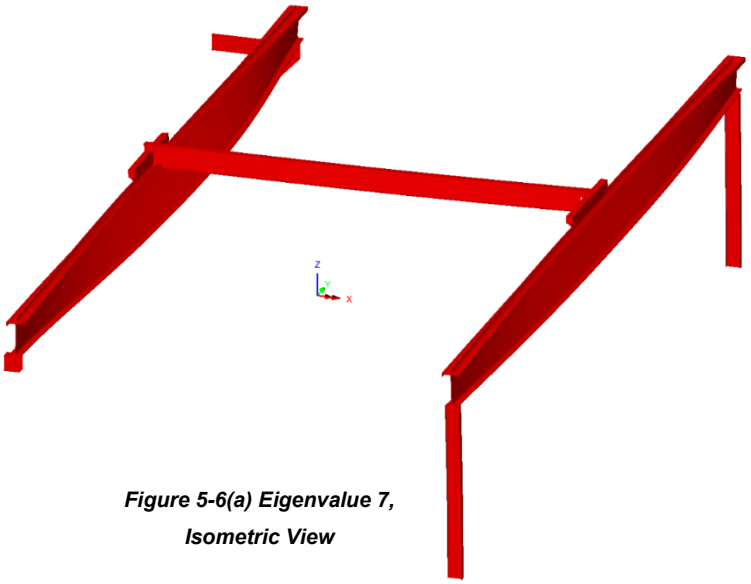

Figure 5-6(a) Eigenvalue 7, Isometric View

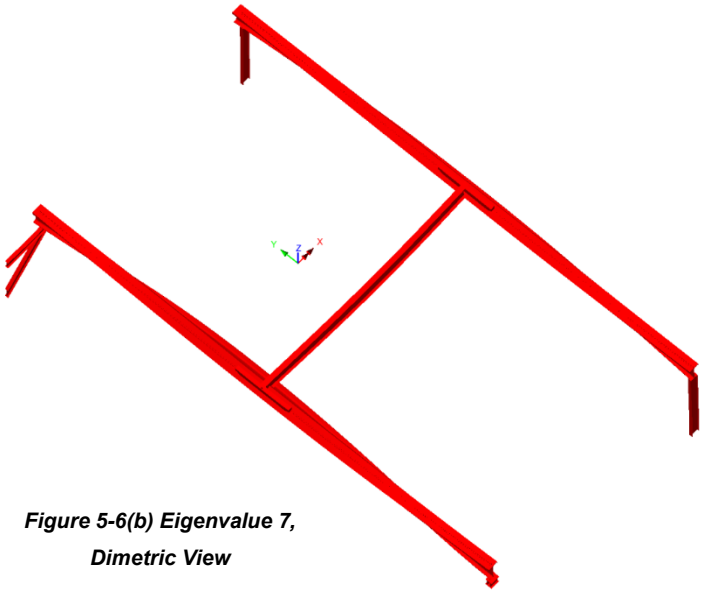

Figure 5-6(b) Eigenvalue 7, Dimetric View

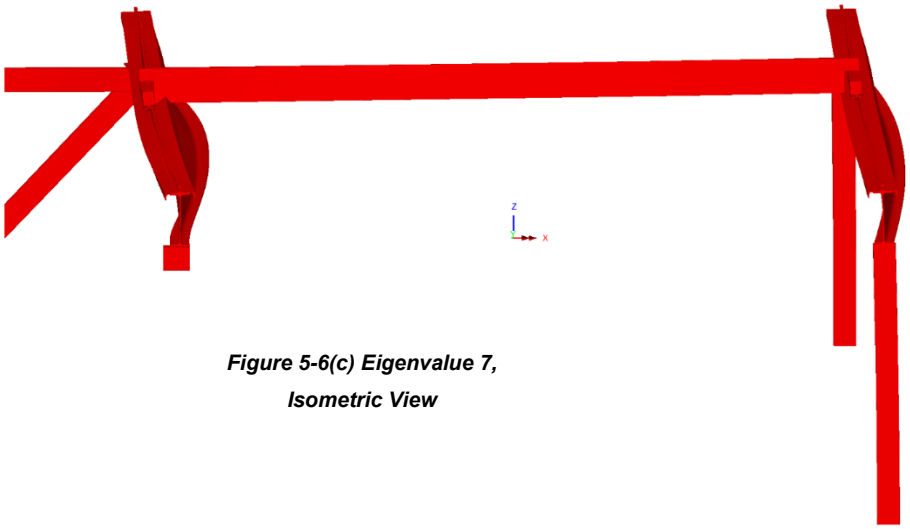

Figure 5-6(c) Eigenvalue 7, Isometric View

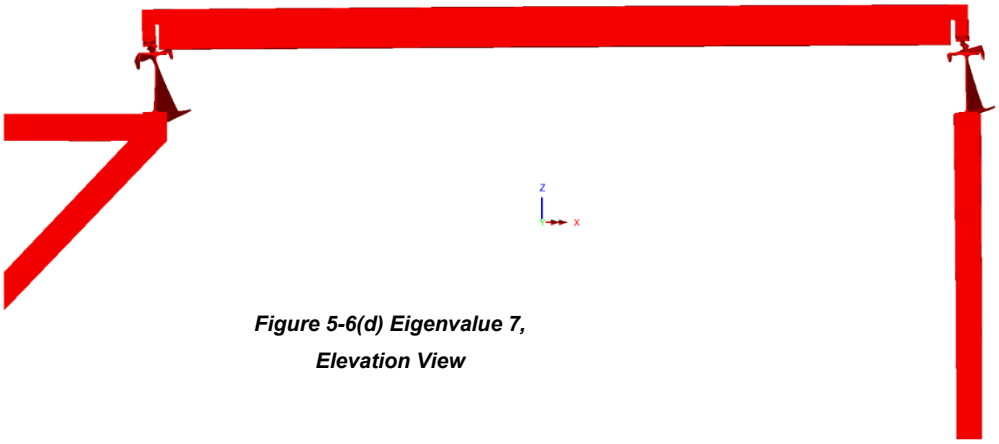

Figure 5-6(d) Eigenvalue 7, Elevation View

5.4 FOURIER ANALYSIS

Recalling the information presented in *Table 5-1*, the "inching" was performed at an average period of 1.18 seconds which is equal to a frequency of 0.85 seconds^{-1}; The average taken of the times in the "most critical lifts" stage equates to a period of 0.88 seconds and a frequency of a frequency of 1.13 seconds^{-1}. The information may come as

surprising because the frequency of “inching” does not coincide with the period of twisting of the runway beam which was found to be 0.286 seconds or, equivalently, a frequency of 3.531 seconds^{-1}. The frequency found in the model of eigenvalue “3”, however, has a frequency of 3.83 seconds^{-1} which is near the frequency calculated in the analytic structure. The information is conflicting; frequency calculated is within a reasonable magnitude to the “twisting” frequency, however, these two frequencies are much greater than the “inching” frequency.

For a periodic or non-periodic force, the frequency (or period) does not necessarily have to coincide with the frequency of the structure for resonance vibration to occur. This is analogous to pushing someone on a swing. To get someone on a swing (swinger) to the maximum height (amplitude) the person pushing (pusher) must push the swinger at the bottom of the swing (period) when the swinger’s velocity is zero. Similarly, the pusher could skip a push (or 2 pushes or 3,4…n) and as the swinger returned to the bottom the swinger could be pushed. The swinger would get to the top quickest if pushed every time they would return; however, the swing would still be able to reach the top if the swinger missed a push considering the swinger did not completely come to a halt before being pushed again.

The “swing” analogy is representative of the “inching” at a different frequency than the natural frequency of the crane system. The compatible forcing frequencies from “inching” can be determined through a Fourier Transformation. The Fourier Transformation, is a representation of any periodic function, through the Fourier Series, using harmonic functions composed of cosine and sine waves. A Fourier Transformation was analyzed to investigate the effects of the “inching” force and evaluate whether a representative frequency matches the frequency of the runway beam or FEA model.

The Fourier Transformation will be performed using Microsoft’s *Excel* which offers an “add-in” to preform Fourier Transformations. The analysis was preformed using 1024

data points; the data used in the Fourier Analysis, as part of the Fourier Series, must be entered in powers of 2. The more data points used the more frequency points will be output in the Fourier Transformation. With 1024 data points, the forcing function could be analyzed per 0.005 second increments for a total time of 5.115 seconds. A forcing function was input, as shown in *Figure 5-7(a)*. The forcing function used in the Fourier Transformation is equivalent to the average frequency of the "inching action". The force within each period was set to have a duration of 0.2 seconds. The duration of the force represents the time the motor, from the crane, pulls on the payload. Current crane motors, with current technology, have motors which ease the acceleration and deacceleration of the motor for safety purposes. The function of the crane force is similar to a parabolic function, however, for simplification reasons, is represented here as a triangular ramping force as shown in *Figure 5-7(a)*. The simplification of the forcing function shape is reasonable; the shape of forcing function (square, parabolic, triangular, etc…) does not affect the Fourier analysis output frequencies, but rather the amplitudes of each frequency. Although the amplitudes of each frequency will be affected by the simplification the peak frequencies will still be the peak frequencies just at a different amplitude. Since the amplitudes are normalized to unity, and since specific amplitudes are not of specific interest in this analysis (only the peak frequencies) the altered amplitudes are of little significance. Likewise, the duration of the crane lift (force) is not known, however, like the shape of the forcing function, the duration of the force only alters the amplitudes. A 0.2 second time was chosen for to maximize the peak amplitudes shown in; the lower duration of force within the period equated to larger amplitudes and higher durations equated to lower amplitudes.

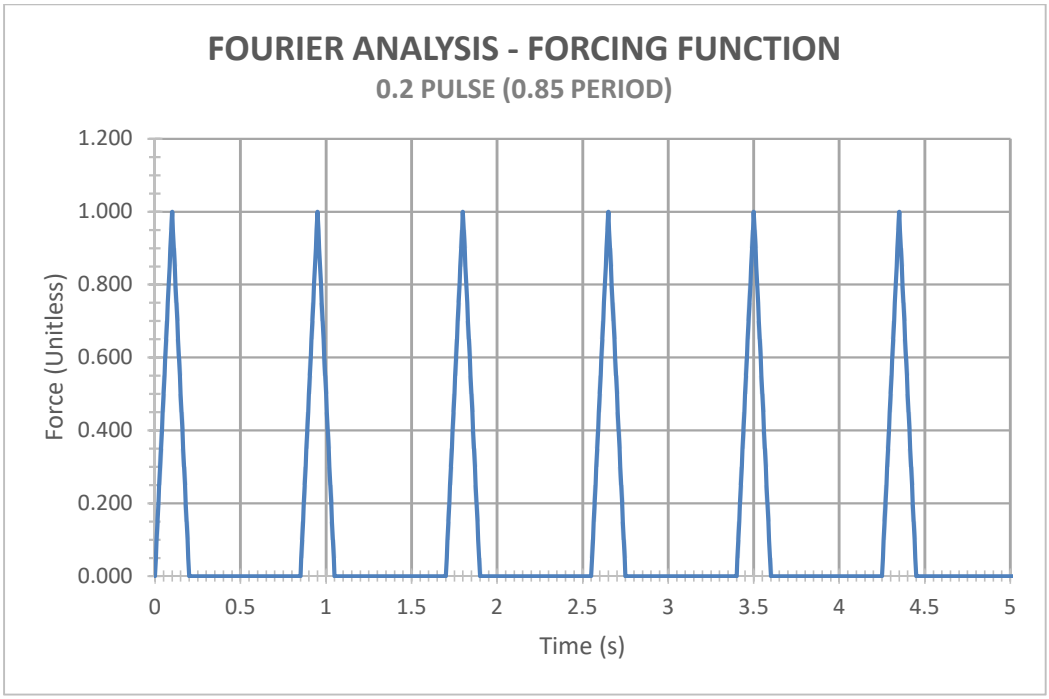

Figure 5-7(a) Fourier Analysis Forcing Function

The results of the Fourier Analysis are shown in *Figure 5-7(b)*. Included in *Figure 5-7(b)* is a numerical table of the peak amplitude frequencies shown in the graph. The Fourier Transformation revealed that there is a peak amplitude corresponding to a frequency of 3.52 seconds^{-1}. Recalling *Table 5-2*, the "twisting" frequency was found to be 3.531 seconds^{-1}. This congruency between the Fourier Analysis and the "twisting" frequency of the runway beam verifies the assumption that the "inching" force can produce an equivalent transformed frequency which, when synced with the natural frequency of the system, caused resonance vibration.

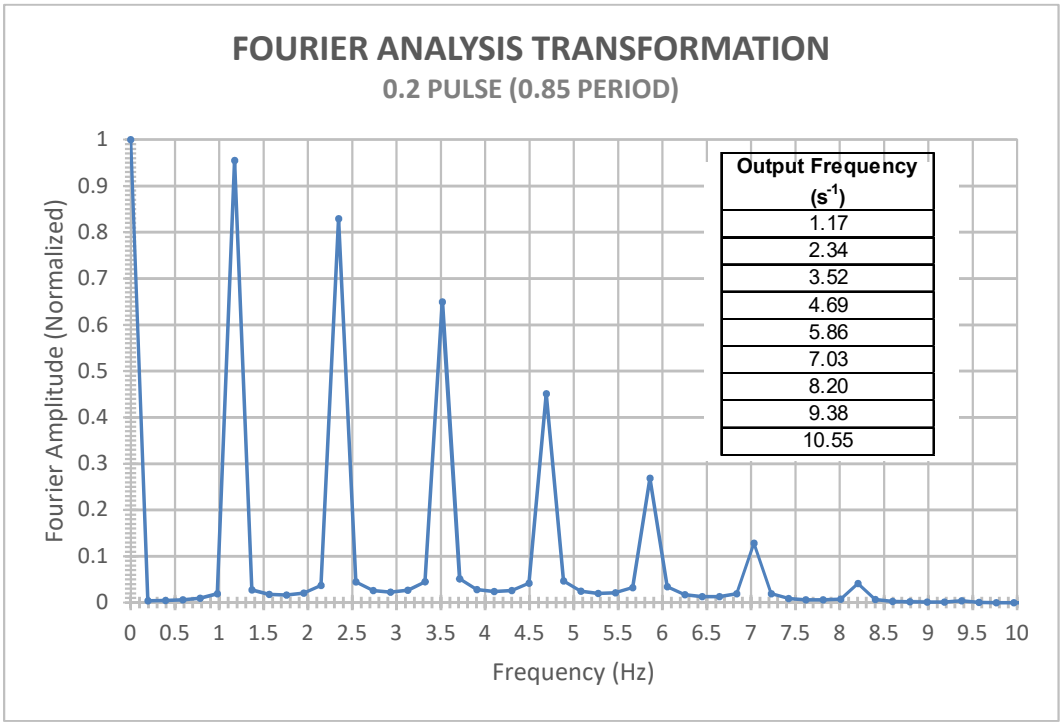

Figure 5-7(b) Fourier Analysis Transformation Results

The congruency between results, although important for verification of resonance vibration, is not the only useful information which can be taken from the Fourier Analysis. As shown in *Figure 5-7(b)*, the energy of the "inching" does not considerably dissipate in amplitude till the peak at a frequency of 9.38 seconds^{-1}. This point of virtually no amplitude translates to the point where no "build-up" of amplitude will occur. Referring to the "swing" analogy, the first "peak" in which the amplitude has, or nearly has, dissipated is equivalent to the "swinger" being initially pushed, and not pushed again till they have come to a complete stop. This concept is vital in understanding the behavior of the runway system and its interaction with the "inching" process. Had the beam's natural frequency been 9.38 seconds^{-1}, or greater, the "twisting" deformation would likely not have ever been noticed. The reader should note that the amplitude at the 9.38 seconds^{-1} peak is technically not

zero, and therefore, resonance vibration is still occurring. Since the amplitude at this frequency is so low, the accumulation of amplitude to reach noticeable effects would take a long time. Another important concept one must understand is for this natural vibration mode alone, if the natural frequency of the system does not equal the frequencies listed in *Figure 5-7(b)* then resonance vibration will not occur. This thinking, however, is risky in terms of design. If the system was designed and the natural frequency was found to be 1.75 seconds^{-1} (midway between two peak frequencies) then resonance vibration, theoretically, would not occur. However, Figure 5-7(b) is an idealized graph of a force through time. In reality, the force may vary in period throughout the lifting process. *Figure 5-8*, like *Figure 5-7*, is another Fourier Transformation in which a 0.2 pulse was alternated between a 0.85 second period and 0.95 second period. Although in real lifting the periods are not likely to repeat, even with one period slightly altered the Fourier Transformation has dramatic results. Although there no frequency peak at the imaginary 1.75 seconds^{-1} assumed previously, there is still considerable amplitude, and no areas in which the amplitude is diminished until a frequency of about 9 seconds^{-1}.

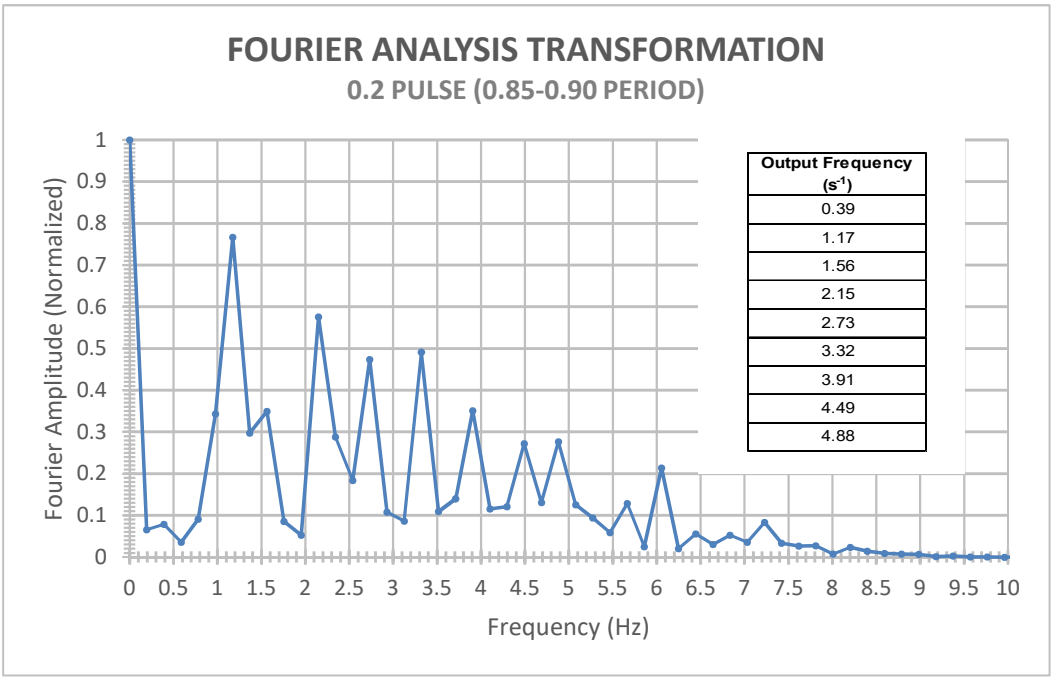

Figure 5-8 Fourier Analysis Transformation Results

5.5 TRANSIENT DYNAMIC ANALYSIS

The two pieces of information possessed for the crane system is the "inching" period, presented in *Table 5-1*, and the "twisting" of the crane beam which was presented in *Table 5-2*. The Eigenvalue Analysis verified the congruency between the "twisting" of the runway beam and natural frequency of the system. The Fourier Transformation provided an explanation to the possibility of how "inching" period caused resonance vibration in a structure with a different period. To prove this theory a Transient Dynamic Analysis (TDA) in LUSAS was performed. The TDA, or more commonly known as a time-history analysis, is an analysis of the model through time. This type of analysis is known having lengthy solving times because of the nature of the analysis. Likewise, because of

the relatively small period and pulse of the “inching” which must be included in the analysis, the time step increments, for an accurate analysis and results, must equally be small. The large model with a small increment time step results in a very lengthy solution time. Initially, the TDA was performed using an increment of 0.20 seconds. The solution took over three days of continuous analysis. The solution revealed that more data points were required for a more accurate analysis. The support staff from LUSAS also ran the model, however, due to the time, the analysis was not able to be completed. The time required to solve the analysis under the current model is not reasonable. A model of a single runway was produced with the same assignments as the full-size model.

The fourth natural mode of vibration of the crane system is a function of the crane bridge was previously mentioned opposed to other modes which consisted of only “twisting” of the runway beam. Likewise, the exclusion of the columns, which was mentioned influencing the natural modes of vibration, is likely to change compared to the simple beam model.

The natural modes of vibration for the simple beam model, shown in *Table 5-4*, are slightly different than that of the full-size crane system. For this model, the second mode of vibration was found to be for torsion as pictured in *Figure 5-9*. The torsion mode of vibration in this model most closely resembles the torsion natural modes of five (4.15 $seconds^{-1}$) and seven (5.34 $seconds^{-1}$) of the full-size model. Although two modes of vibration in the full-size model closely resemble mode 2 of the simple beam model, the natural vibration mode 7 of the full-size model is most likely the most congruent. For the torsional mode of vibration, the torsional stiffness of the crane system, composed of two runway beams in series circuit with the bridge, is greater than the single runway beam. Since the torsional stiffness of the crane system is larger the frequency is likely to greater as reflected in the data.

MODE	EIGENVALUE	FREQUENCY	ERROR NORM
1	292.78	2.72	5.71E-07
2	929.41	4.85	1.54E-07
3	1395.25	5.94	1.03E-07
4	3020.63	8.75	6.85E-08
5	3661.00	9.63	6.19E-08
6	5683.37	12.00	3.06E-08
7	11523.90	17.09	2.44E-08
8	21755.30	23.47	7.10E-09
9	23729.30	24.52	1.78E-08
10	29461.20	27.32	1.90E-07

Table 5-4 Simple Beam Eigenvalue Analysis Results

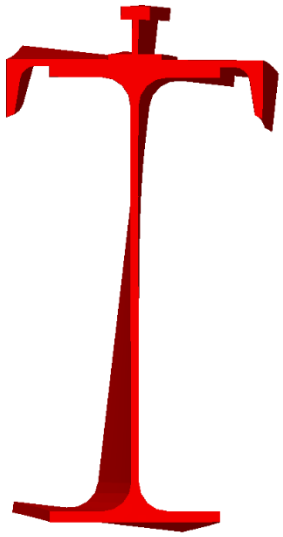

Figure 5-9 Mode 2, Elevation View

The simple beam model is not a perfect representation of the crane system. As mentioned previously, due to the exclusion of the bridge member in the simplified model, the mode of vibration which resulted in the “twisting” deformation in the analytic crane system is not represented in the simple model. However, other torsional modes of vibration in both the full-size model and simplified are well within a reasonable “inching” time. *Figure 5-8* graphically represents this possibility; with a few second shift in the lifting period large

amplitudes, which could cause resonance vibration, is existent until a frequency of about *8.0 seconds^{-1}*. So, although other torsional modes of vibration were possible, the vibration experienced in the analytic modes was most likely due to it being the lowest frequency of the torsional modes. Likewise, the concern is ultimately not matching the exact torsion frequency between the two models, but to prove that a small incremental "inching" period can interface with a torsion period at a different period.

To test whether an "inching" period can cause resonance vibration for a different period of vibration a Transient Dynamic Analysis was performed. Because the TDA utilizes the simple beam model some equivalent alterations were made. The natural frequency of the crane system was found to match a peak frequency in the Fourier Transformation Analysis. To match this relationship in the simple beam model, a Fourier Transformation was performed with different periods until a peak frequency was found which matched the torsional natural frequency. As shown in *Figure 5-10*, a Fourier Transformation Analysis revealed a peak frequency of *5.08 seconds^{-1}.* The 5.08 *seconds^{-1}* peak frequency is not an exact match as the simple beam's torsional frequency, however, as shown in *Figure 5-10*, the torsion natural frequency is within an area of large amplitude and will further signify the results; a natural frequency does not have to necessarily be at a peak amplitude for resonance vibration to occur.

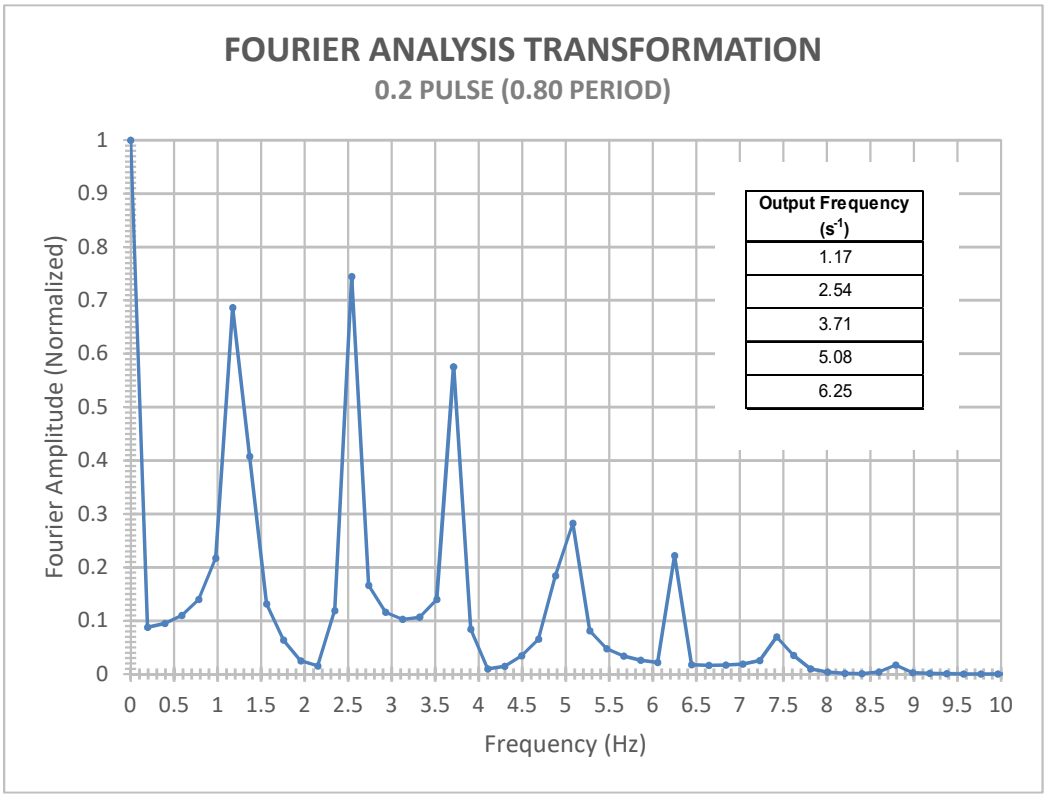

Figure 5-10 Fourier Analysis Transformation Results

Two load curves were established in LUSAS. The first for a unit force (1 kip) which had a triangular pulse of 0.2 seconds over a period of 0.8 seconds similar to *Figure 5-7(a)*. The other load case was specified for gravity with a constant factor of unity over the entire time. The time-period set was for five seconds. The time-period selected was to match the analytic model's critical lifting period. To analyze the results of the Transient Analysis and to verify the period of the runway beam. One way to analyze the period of the runway beam from the possible results is analyzing the displacement of the nodes. The torsion deformation can be characterized by an "x" displacement of the node on the bottom center of the runway flange as shown in *Figure 5-11*.

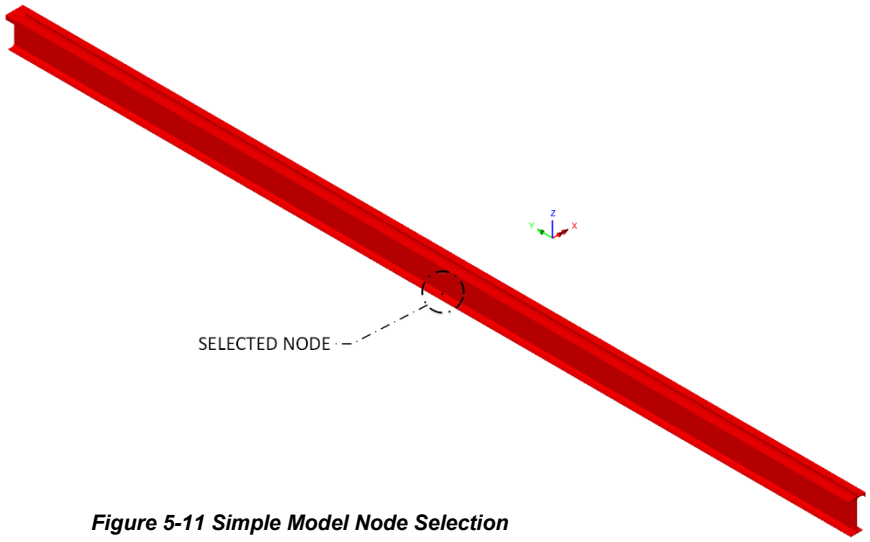

Figure 5-11 Simple Model Node Selection

Figure 5-12 reveals the results of center bottom flange node of the runway beam's "x" displacement. *Figure 5-12* is not a perfect representation of the torsional movement of the runway beam because the graph is capturing the "x" displacement of the node while the torsional rotation is a component of "x" and "z" displacement (using the coordinate system in *Figure 5-11*). The rotation of the runway beam will move in a circular motion with the radius approximately equally the center flange point to bottom flange point. When viewing the "x" displacement of the rotation, the results are revealing the "x" displacement on a polar circular path and not a linear one. Likewise, the graph is also considering the "x" displacement due to lateral torsional buckling. The runway beam is braced only at the ends and completely unbraced through the span and well beyond the plastic lateral buckling limit so lateral torsional buckling is an issue. Another concept the reader must keep in mind is the magnitude of displacement which must be ignored. A loading of 100 pounds was arbitrarily used. An arbitrary value was selected based on a few reasons: 1) the motor used in the analytic model is not known, 2) Whether the full acceleration of the motor was

reached which would be difficult even if the motor was known, and 3) the acceleration graph of the motor throughout the lifting cycle. However, the magnitude of the force is not of concern if the chosen loading is kept reasonable and not induce a case where nonlinearities would need to be considered.

The analysis was carried out using a loading with a 0.2 second pulse within a 0.8 second period over 5 seconds. From *Figure 5-12*, one can easily determine that the "x" displacements of the bottom flange are must quicker than 0.8 seconds. The major peaks or the periods of the displacement within the figure range between 0.18-0.22 seconds on average. This equivalently represents a frequency of 4.54-5.56 seconds^{-1}. This result is well within considerable range for the torsional natural mode of vibration frequency found to be 4.85 seconds^{-1}. The correlation between the results suggests that an "inching" period must consider alternate transformed periods when considering the investigation or design of the runway beam or crane system.

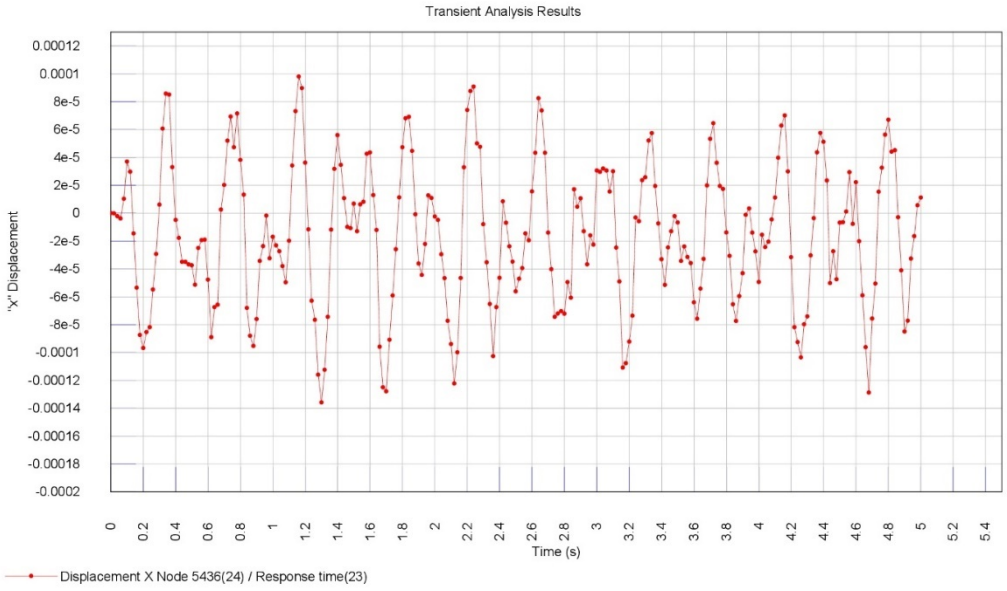

Figure 5-12 Transient Analysis "X" Displacement Graph

CHAPTER 6

STRUCTURAL SOLUTION

6.1 INTRODUCTION

In structural design when considering vibration and vibration resonance, the structure should be designed such that the natural frequencies are past the equivalent transformed frequencies where considerable amplitude exists. If this method is adopted, even if the frequencies falls on a transformed amplitude peak, the resulting energy transformed through each period will be minimal and no considerable deformation will be noticed. Unfortunately, many crane standards and designs do not consider such vibration and result in retrofits to the structure to accommodate the vibration such as the case with this thesis. For this reason, two solutions will be explored in the structural design for crane runway beams; the first for the retrofit of existing cranes focusing on the crane system presented in this thesis and another for the design of crane runways yet to be constructed.

6.2 RETROFIT SOLUTION

6.2.1 INTRODUCTION

Shown in *Figure 6-1(a)* and *Figure 6-1(b)* are the force curve for the “inching” lift times and Fourier Transformation Analysis for the force in the analytic model respectively. *Figure 6-1(a)* includes all the “inching” times included in the analytic model, opposed to the previous chapter which was focused on the “critical lifting times”

discussed previously. *Figure 6-1(b)* is the Fourier Transformation of the "inching" forcing function. The figure reveals that most of the amplitude is dispersed shortly after 5.5 seconds^{-1}. From the previous chapter, in an ideal case of uniform periods, the amplitude is dissipated around 8.5 seconds^{-1}. A uniform period, such as *Figure 5-7(b)* presented in the previous chapter, is more likely to carry amplitude through a system for a longer amount of time since the force is more rhythmic.

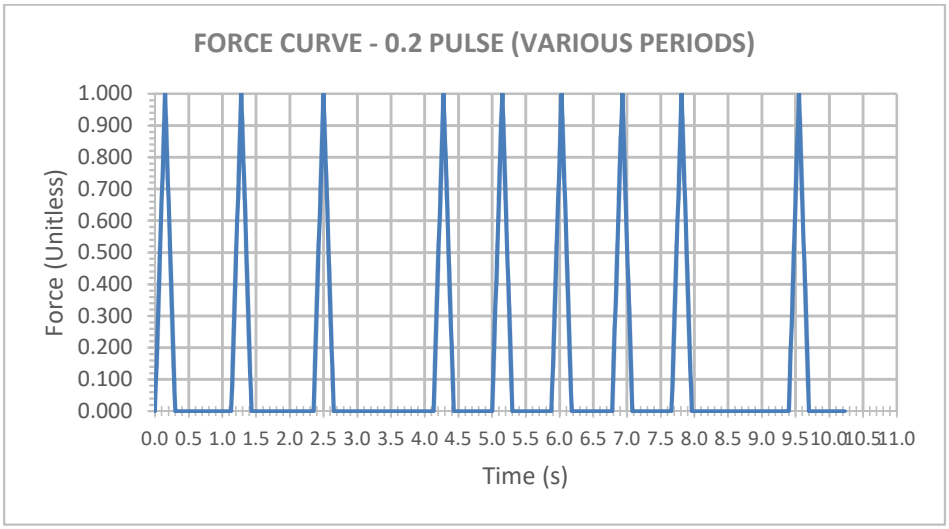

Figure 6-1(a) "Inching" Forcing Function Graph

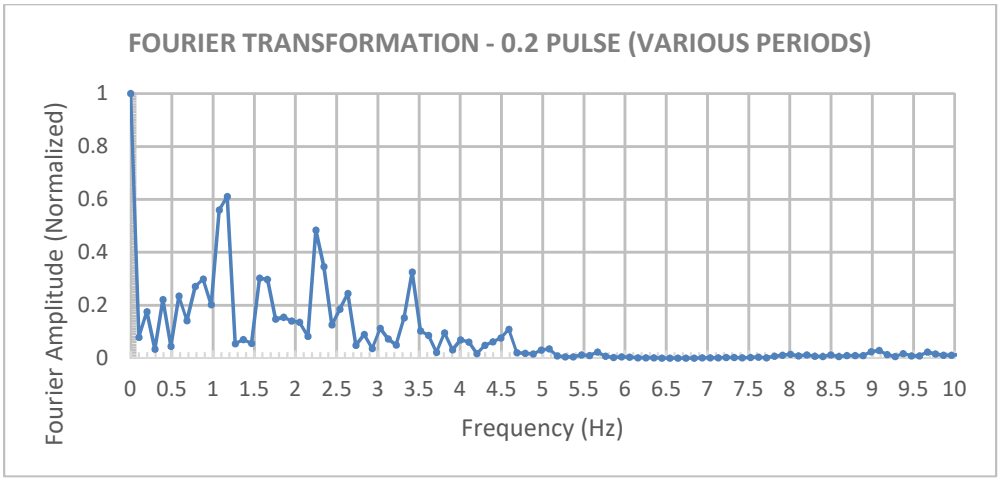

Figure 6-1(b) "Inching" Forcing Function Fourier Transformation

Similar to the AASHTO Pedestrian Bridge Design (AASHTO, 2009), which was previously discussed, the runway beam should be designed such that the torsion natural modes of vibration are greater than 8.5 seconds^{-1}. While the 8.5 seconds^{-1} was based on the Fourier Transformation of the idealized forcing function for a period of 0.8 seconds, many of the quicker “inching” actions will have a similar amplitude dissipation at approximately the same frequency. To provide an adequate retrofit design to meet the 8.5 seconds^{-1} frequency, the crane system will be stiffened. The supporting structure for the crane (runways beams and column supports) are often designed by one engineer while the crane system (crane, bridge, trolley, and hoist) are designed and provided by a crane company. For this reason, both the retrofit and preconstruction designs will be based on the crane supporting system which the design engineer will have more direct control over primarily in the preconstruction design phase.

To increase the torsional stiffness of the crane system three options will be explored. The first will be the addition of intermediate stiffeners which was the first solution discussed during the site visit suggested by the crane companies engineer. The addition of intermediate stiffeners is often a solution for similar torsional vibration issues of runway beams as told by one of the third-party engineers who had dealt with this issue before. The next option will be the inclusion of side plates to the runway beam between the channel flanges. This solution will be explored based on the concept of the general torsion theory; adding side plates to part or all of the runway beam will produce a closed section capable of resisting torsion compared to an open section. The last solution explored will be the strengthening of the columns. The columns, which are lightly designed for the structure to begin with, exhibited signs of deformation within many of the natural frequencies. This solution aims at the possibility of increasing the torsional stiffness by simple stiffness

increase of the columns. Another use in this method is to find the implication the columns have on the natural frequency of the crane system which will be useful in equation development.

6.2.2 INTERMEDIATE STIFFENERS

As previously stated, a common retrofit for crane runways exhibiting torsional resonance vibration is to add intermediate stiffeners to the runway beam as suggested by the crane manufacturers engineer. Intermediate stiffeners were added under the wheel locations of each runway beam on each side as shown in *Figure 6-2*. *Figure 6-2* reveals only one side of one runway beam, however, the intermediate stiffeners are on the other side of the and runway beam as well. The stiffeners were assigned a thickness of 5/16" which matches the web of the runway section for welding accommodations. The stiffeners were modelled as surfaces. The mesh of the stiffeners was created using 3D thick shell quadrilateral elements with a quadratic interpolation order along mesh lines. The material assignment is identical to the other elements in the model. Since the stiffeners will be welded, the connection between the runway and stiffener are assumed rigid.

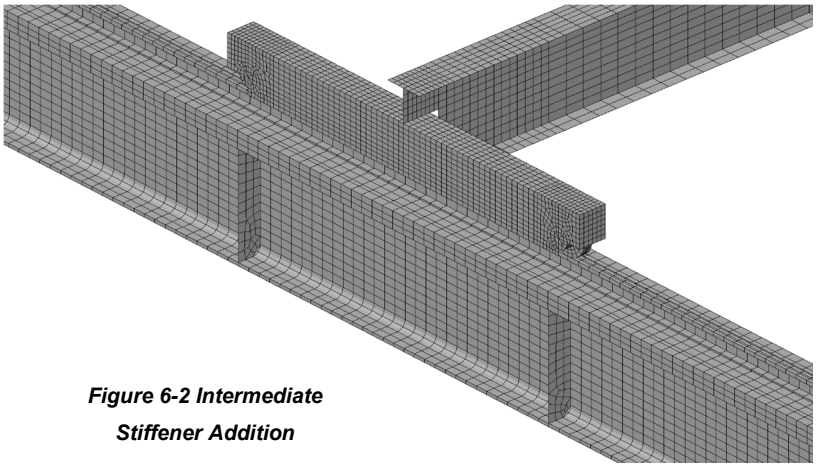

Figure 6-2 Intermediate Stiffener Addition

An eigenvalue analysis was performed on the model with the intermediate stiffeners. For ease of access, the unmodified natural frequencies have been relisted in this chapter and found in *Table 6-1*. *Table 6-2* is the results of the Eigenvalue Analysis for the crane system with added intermediate stiffeners. The reader should note that in the tables below displaying the eigenvalues, the four critical eigenvalues associated with lateral deformation (the first mode) and torsional deformation (fourth, fifth, and seventh mode) have been highlighted grey. The addition of stiffeners has an insignificant effect on any of the modes in question. In the first and fourth mode of vibration the frequency drops with the addition of stiffeners. The reduction in frequency is only a few thousandths, and is likely due to the slight differences in “error norm”; because the difference is so minimal the modes are likely unaffected by the stiffeners and the solution different due to the nature of the Eigenvalue Analysis solution.

BASELINE ANALYSIS (UNMODIFIED)

MODE	EIGENVALUE	FREQUENCY	ERROR NORM
1	129.183	1.809	9.32E-07
2	164.737	2.043	4.52E-07
3	370.644	3.064	7.88E-08
4	580.674	3.835	3.16E-09
5	682.858	4.159	2.00E-08
6	734.649	4.314	7.62E-08
7	1133.08	5.357	6.44E-08
8	1138.05	5.369	8.84E-08
9	1392.98	5.940	1.53E-07
10	1781.91	6.718	1.04E-07

Table 6-1 Eigenvalue Analysis

INTERMEDIATE STIFFENERS ADDED

MODE	EIGENVALUE	FREQUENCY	ERROR NORM
1	128.052	1.801	9.02E-07
2	163.521	2.035	4.91E-07
3	370.646	3.064	7.86E-08
4	578.987	3.830	3.62E-09
5	696.537	4.200	2.16E-08
6	737.451	4.322	5.38E-08
7	1136.900	5.366	6.97E-08
8	1189.840	5.490	1.05E-07
9	1386.750	5.927	1.57E-07
10	1790.050	6.734	4.15E-08

Table 6-2 Eigenvalue Analysis

6.2.3 INTERMEDIATE STIFFENERS & SIDE-PLATES

6.2.3.1 Intermediate stiffeners & Side-Plates (1 runway)

Side-plates were added between the stiffeners to completely enclose the center area of the runway between the bridge wheels. The bridge wheels are where any lateral of torsional stresses will be transferred into the runway beam. In this analysis, the section has been boxed off (both sides of the runway beam) for only a single runway beam as shown in *Figure 6-3*. The intermediate stiffeners on the adjacent runway beam have not been removed. The stiffeners were not removed to maximize the torsional stiffness at the center; based on the authors rational, increasing the torsional stiffness at the center of the beam is not likely to be a solution. The addition of extra side-plates requires expensive additional fabrication costs, and therefore, this analysis will first examine the addition of side-plates to one runway and then both. The side plates were first arbitrarily assigned on the runway beam supported on the column supports. The side-plates were assigned a thickness of 5/16” which matches the web of the runway section for welding accommodations. The side-plates were modelled as surfaces. The mesh of the side-plates was created using 3D thick shell quadrilateral elements with a quadratic interpolation order along mesh lines. The material assignment is identical to the other elements in the model.

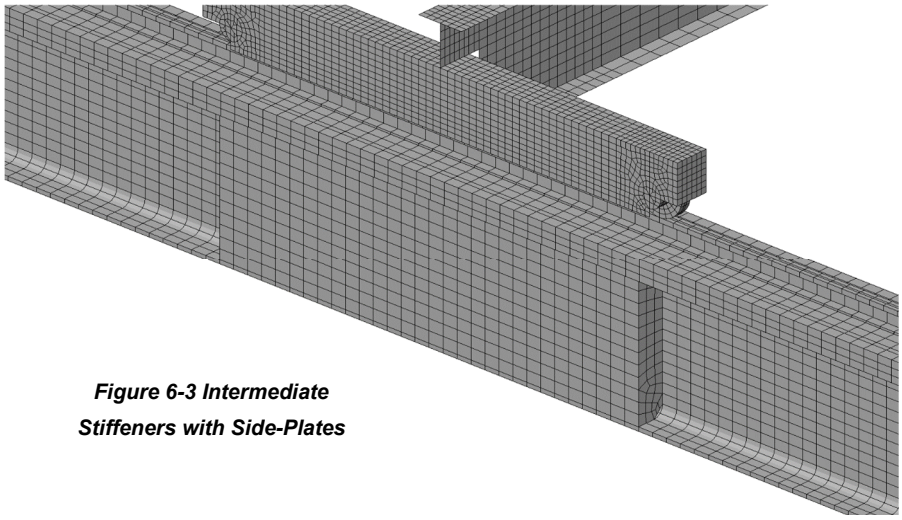

Figure 6-3 Intermediate Stiffeners with Side-Plates

The results of the Eigenvalue Analysis are similar to the previous as shown in *Table 6-3*. All the lateral and torsional modes of vibration are relatively unchanged. The lateral mode of vibration (mode 1) is slightly increased. The increase in frequency of the lateral mode of vibration could likely be due to the very minimal increase in stiffness from the additional side-plates. The slight difference could also be due to a slight different in the "error norm". The torsional modes of vibration are all slightly decreased. Since the addition of the intermediate stiffeners, the torsional modes of vibration have all seen a decrease. The "error norm" could be the cause, however, although a possible coincidence, the influence of "error norm" never results in a slight increase. The addition of the stiffeners and side-plates could result in a redistribution of stresses and result in the decreased frequency.

INTERMEDIATE STIFFENERS W/ SIDE-PLATES (1 RUNWAY)

MODE	EIGENVALUE	FREQUENCY	ERROR NORM
1	129.808	1.813	8.98E-07
2	163.521	2.035	4.41E-07
3	370.671	3.064	9.76E-08
4	578.729	3.829	3.37E-09
5	668.330	4.114	1.61E-08
6	734.509	4.313	8.10E-08
7	1132.680	5.356	5.49E-08
8	1138.790	5.371	9.97E-08
9	1348.040	5.843	6.05E-08
10	1786.590	6.727	1.10E-07

Table 6-3 Eigenvalue Analysis

6.2.3.2 Intermediate stiffeners & Side-Plates (Both runways)

The following analysis utilizes the side-plates on each side of the runway beam on each runway beam. The analysis is similar to the previous, however, *Figure 6-3* applies to both runway beams; the previous analysis only operates side-plates on a single runway beam.

As shown in *Table 6-4*, all modes under investigation were decreased. As previously suggested, the addition of the intermediate stiffeners and side-plates maybe undesirably redistributing the stress in such a way which has adverse effects on the crane system. Although only three analysis were conducted on the center of the runway beams, stiffening the center of the runway beam has led to a decrease in frequency, opposite of the desired outcome, and possibly not the more economic option to avoid resonance vibration from “inching”. The deformation of the critical eigenvalues (4,5,7) can be found in the figures below. As depicted in the *Figure 6-4(a)* through *Figure 6-4(c)*, the inclusion of the stiffeners and side plates have no change on the deformation of the structure.

INTERMEDIATE STIFFENERS W/ SIDE-PLATES

MODE	EIGENVALUE	FREQUENCY	ERROR NORM
1	126.587	1.791	8.99E-07
2	154.316	1.977	4.93E-07
3	370.685	3.064	1.46E-07
4	575.994	3.820	3.65E-09
5	638.956	4.023	1.05E-08
6	736.570	4.319	1.31E-07
7	1105.430	5.292	8.60E-08
8	1137.300	5.367	6.41E-08
9	1316.540	5.775	1.44E-07
10	1790.090	6.734	8.19E-07

Table 6-4 Eigenvalue Analysis

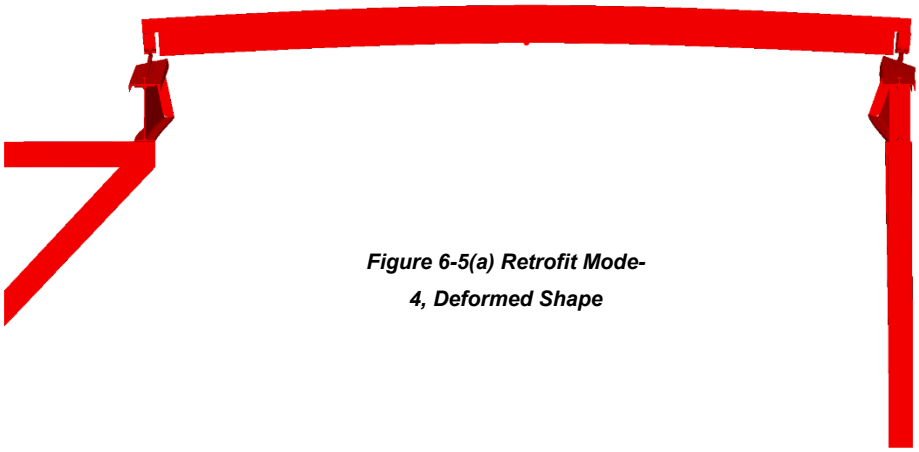

Figure 6-5(a) Retrofit Mode-4, Deformed Shape

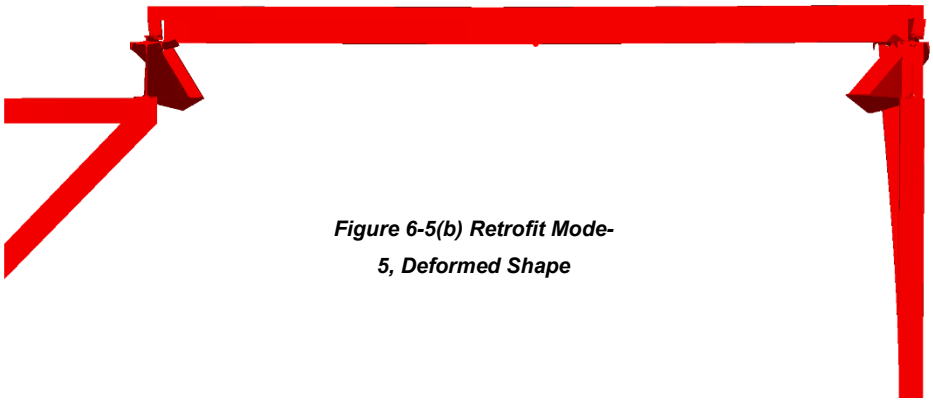

Figure 6-5(b) Retrofit Mode-5, Deformed Shape

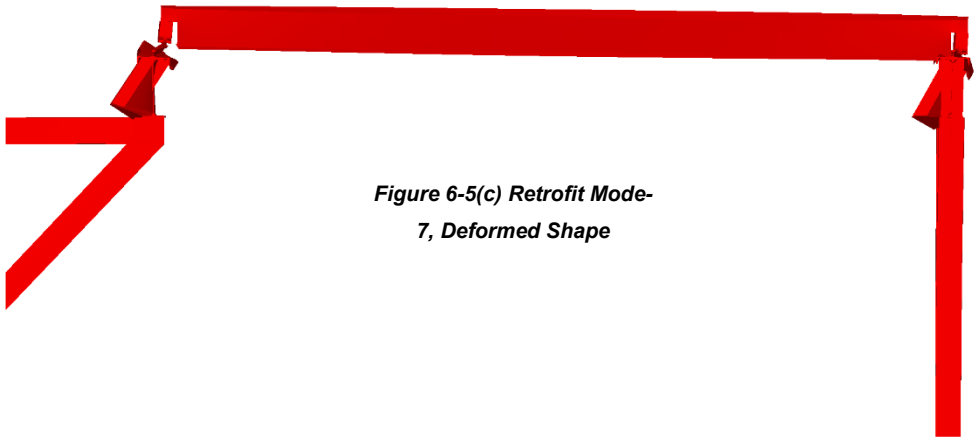

Figure 6-5(c) Retrofit Mode-7, Deformed Shape

6.2.4 END SPAN SIDE-PLATE

6.2.4.1 End Span Side-Plate (1 Side-1 Runway)

A side plate was added to a single runway beam from the column support to the wheel location as shown in *Figure 6-6.* Due to the geometry of the model in which the model was created, the addition of the side-plate from the column support to wheel location was done for simplicity reasons. The addition of material may seem excessive, but each solution will be evaluated based on the results. The material, thickness, and mesh was assigned identical to the previous. The results of the eigenvalue analysis can be found in *Table 6-5*.

Figure 6-6 shows the side-plate within the crane system. The top portion of the figure (crane system in red) is a solid view of the geometry of the crane; red was chosen which best showed the difficult-to-see side-plate. The side-plate has been outlined in black to view the extend of the plate. The called-out portion (grey) is a zoomed in portion as shown in the figure. The called-out section is a mesh view of the system.

SINGLE END-SPAN SIDE-PLATE

MODE	EIGENVALUE	FREQUENCY	ERROR NORM
1	141.629	1.894	7.19E-07
2	164.737	2.043	4.36E-07
3	370.742	3.064	1.01E-07
4	584.549	3.848	3.10E-09
5	721.495	4.275	4.10E-08
6	748.765	4.355	3.07E-08
7	1137.280	5.367	3.97E-08
8	1352.940	5.854	6.89E-08
9	1710.190	6.582	1.42E-06
10	1790.060	6.734	2.90E-06

Table 6-5 Eigenvalue Analysis

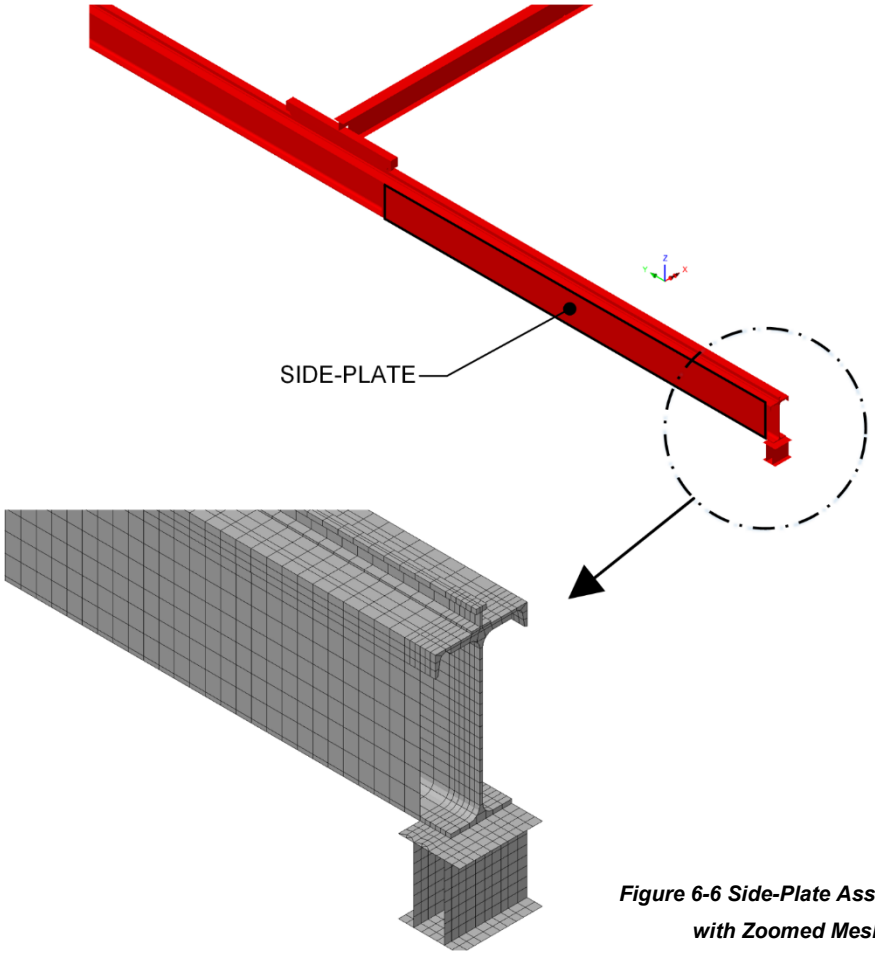

Figure 6-6 Side-Plate Assignment with Zoomed Mesh

Previously, in the analysis which focused on stiffening the center of the runway beam(s) where the torsion on the runway beam originates from the bridge wheels, there had been relatively no change in frequencies. For this analysis, which focused on the intermediate area between the bridge wheels and column supports, all the frequencies had an increase. The increase for most of these were found to be very insignificant with respect to the goal value. The largest increase in frequency was found for mode five. *Figure 6-7(a) – Figure 6-7(c)* shows the deformation of the three primary modes which involve runway torsion; modes 4,5,7. As shown in the figures below, the modes are now converging to their respective primary deformation. For example, mode 4, which was previously thought to be a torsional mode of vibration, appear to be a transverse bridge mode of vibration which was resulting in the runway lateral torsional deformation. Likewise, mode 5 in the previously eigenvalue analyses was composed of primarily torsional rotation of the right runway beam (oriented to figure) with little respective column translation (x-direction). However, from the increased torsional stiffness from the runway beam with the side-plate added, the columns are now the primary deformation with the beam developing slight torsional rotation. Mode 7 of the analysis is now converging to a torsional rotation of the bridge. The torsional rotation of the bridge, although torsional rotation, is not investigated in this research.

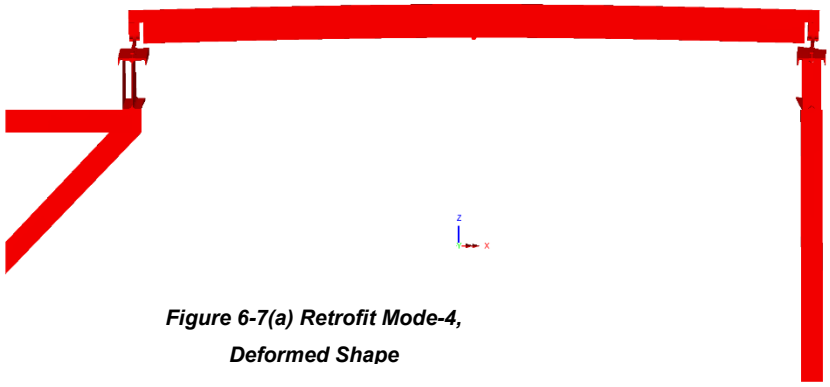

Figure 6-7(a) Retrofit Mode-4,
Deformed Shape

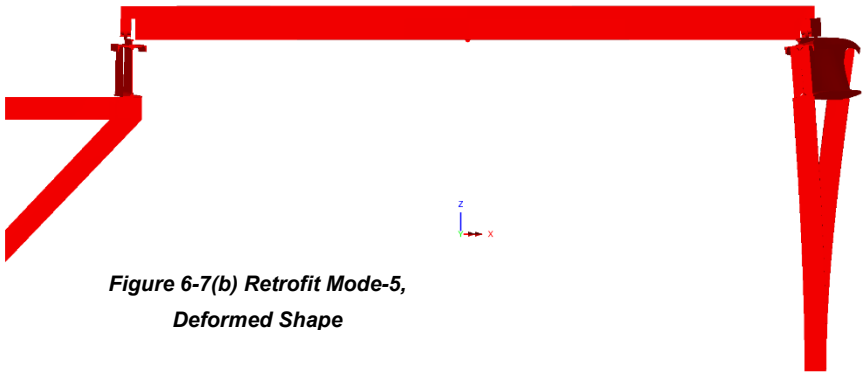

Figure 6-7(b) Retrofit Mode-5,
Deformed Shape

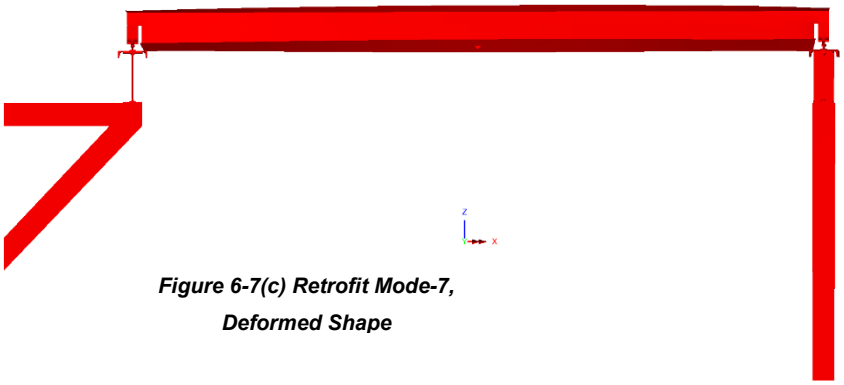

Figure 6-7(c) Retrofit Mode-7,
Deformed Shape

SINGLE END-SPAN SIDE-PLATE

MODE	EIGENVALUE	FREQUENCY	ERROR NORM
1	141.629	1.894	7.19E-07
2	164.737	2.043	4.36E-07
3	370.742	3.064	1.01E-07
4	584.549	3.848	3.10E-09
5	721.495	4.275	4.10E-08
6	748.765	4.355	3.07E-08
7	1137.280	5.367	3.97E-08
8	1352.940	5.854	6.89E-08
9	1710.190	6.582	1.42E-06
10	1790.060	6.734	2.90E-06

Table 6-6 Eigenvalue Analysis

6.2.4.2 End Span Side-Plate (1 Side-2 Runways)

In this analysis, a side-plate was assigned to both runways to the outside flange of each runway similar to *Figure 6-4*. The results of Eigenvalue analysis are found in *Table 6-7*. The lateral and torsional modes of vibration both show an increase in frequency compared to the analysis where only 1 side-plate was applied. For the first, fourth, and fifth mode the increase in frequency is very negligible. The increase in frequency for the seventh mode is much greater. Overall, the frequencies compared to the target value to avoid resonance vibration is still very far away. The lateral natural frequency, mode 2, does not need to meet the same requirements as the torsional ones. In crane operation, the trolley can accelerate along the length of the bridge. For this reason, the lateral mode of vibration is frequently presented. “Inching” the motor parallel to the bridge is not common to the authors knowledge, but still possible. Pedestrian bridges similarly give requirements for lateral modes of vibration as well as transverse for the main supporting girders as previously mentioned in Chapter 2. Although the lateral mode of vibration was not an issue in the analytic model. Since the lateral mode is possible and mentioned in similar structures, the analysis will discuss the lateral natural frequency. The deformation of this

analysis is not shown due to the almost exact relationship with the previous analysis using a single side plate.

SINGLE END-SPAN SIDE-PLATE (2-RUNWAYS)

MODE	EIGENVALUE	FREQUENCY	ERROR NORM
1	142.327	1.899	8.03E-07
2	147.041	1.930	4.94E-07
3	370.757	3.065	9.77E-08
4	588.363	3.860	2.95E-09
5	713.167	4.250	5.77E-08
6	1137.210	5.367	4.27E-08
7	1326.110	5.796	1.98E-07
8	1466.700	6.095	7.94E-07
9	1790.060	6.734	2.91E-06
10	2059.020	7.222	2.14E-06

Table 6-7 Eigenvalue Analysis

6.2.4.3 End Span Side-Plate (2 Sides-2 Runways)

In previous analysis, a single side-plate was applied to one side of a single runway beam per analysis. Because the results of the Eigenvalue Analysis are still far from the target value, analysis may be skipped. Larger structural modifications are now evident to reach the torsional modes of vibration to an acceptable limit. In this analysis side-plates are placed on each side of each runway beam as shown in *Figure 6-5*. The results of the Eigenvalue Analysis for this analysis can be found in *Table 6-8*. Surprisingly, the addition of the side-plates to fully box the member has very little effect compared to a single side-plate placed on each member.

END-SPAN SIDE-PLATES (2-RUNWAYS)

MODE	EIGENVALUE	FREQUENCY	ERROR NORM
1	133.453	1.839	4.93E-07
2	144.733	1.915	8.11E-07
3	370.823	3.065	1.67E-07
4	594.851	3.882	2.85E-09
5	688.695	4.177	1.13E-07
6	1137.040	5.367	5.52E-08
7	1288.000	5.712	1.42E-07
8	1406.260	5.968	1.08E-07
9	1790.080	6.734	3.14E-06
10	2240.740	7.534	3.40E-07

Table 6-8 Eigenvalue Analysis

6.2.4.4 End Span Side-Plate (2 Sides-2 Runways) & Column Stiffening

In previous analysis, which focused on the stiffening of the runway beam, there has been a convergence of the modes to reveal the true mode of vibration. Mode 4 has converged to one of bridge transverse movement which, due to the initial low torsional stiffness in the analytic model, led to the lateral torsional twisting of the runway beams. Similar to mode 4, mode 7 revealed to be a primary vibration mode of bridge torsional rotation. Mode 5, which initially was primarily a torsion mode of the runway beam, became a mode dominated by column translation. From torsion theory, one way to increase the torsional stiffness (i.e. reduce the rotation or angle of twist) is to change the restraints of the beam. This, however, is not an idealized simple supported beam, and the restraints of the beam, in this case, is composed of the runway beam and column. Previously, the runway beam's torsional stiffness was lower than the columns translation and the torsion mode dominated. When the side plates were added to the runway beam, the translation stiffness of the columns became lower and the translation dominated. To correct this issue,

and essentially fix the end restraints of the runway beam, the column stiffness will be increased. The reader should not that while the torsion degree of freedom is mentioned as being fixed (or warping prevention of the restraint), this is more a simplification of increase the stiffness of the beam and column together; the major bending axis degree of freedom will remain assumed pinned.

To prevent the torsional mode of vibration, which is what the previous mode 5 has been shown converging to, dominating the column translation, the columns have been stiffened in this analysis. The column's flanges and webs were increased such that the resulting moment of inertia equaled approximately 500 in^4. This target value is reasonable, although high, because a common retrofit to stiffen the columns would be to attach a channel to the existing columns. The channel was not modelled for simplicity reasons. The single side plate on each of the runways, as in the previous analysis, was kept. The analysis results can be seen in *Table 6-9* and the accompanying deformation of the investigated modes in *Figure 6-8(a)* through *Figure 6-8(c)*. As shown in *Table 6-9*, all the natural frequencies of the investigated modes have increased. As shown in *Figure 6-8(a)*, the natural frequency of mode 4 is still dominated by transverse bridge movement. Although the frequency is still not at a target value, the torsional deformation of the runway beam has been virtually eliminated. Because the bridge is a component of the runway manufacturer, the investigation to stiffen the bridge, to increase this mode's natural frequency will not be investigated. As shown in *Figure 6-8(b)*, mode 5 is dominated by bridge torsion which was seen in previous analyses as mode 7. As stated previous, this mode may not be realistic and is a result of the load simplification. As shown in *Figure 6-8(c)*, mode 7 is depicted as dominated by runway torsion. The natural frequency of this mode, as shown in *Table 6-9*, is approximately 6.142 $seconds^{-1}$. From *Figure 5-10* in the previous chapter, a frequency of 6.142 $seconds^{-1}$ is roughly at the fifth harmonic of the

idealized pulse. Where “inching” will not be perfectly uniform, the frequency is far past the fifth harmonic. Although the natural frequency of the beam is not at a harmonic (from the Fourier Series Transformation) which has energy fully dissipated, the natural frequency is at the last harmonic with amplitude.

END-SPAN SIDE-PLATES (2-RUNWAYS) & COLUMN STIFFENING

MODE	EIGENVALUE	FREQUENCY	ERROR NORM
1	169.540	2.072	5.56E-07
2	237.162	2.451	3.03E-07
3	370.918	3.065	9.85E-08
4	603.728	3.911	2.80E-09
5	1136.670	5.366	4.63E-08
6	1370.720	5.892	7.11E-08
7	1489.110	6.142	8.02E-08
8	1790.060	6.734	3.49E-08
9	1966.570	7.058	2.96E-08
10	3018.290	8.744	3.60E-07

Table 6-9 Eigenvalue Analysis

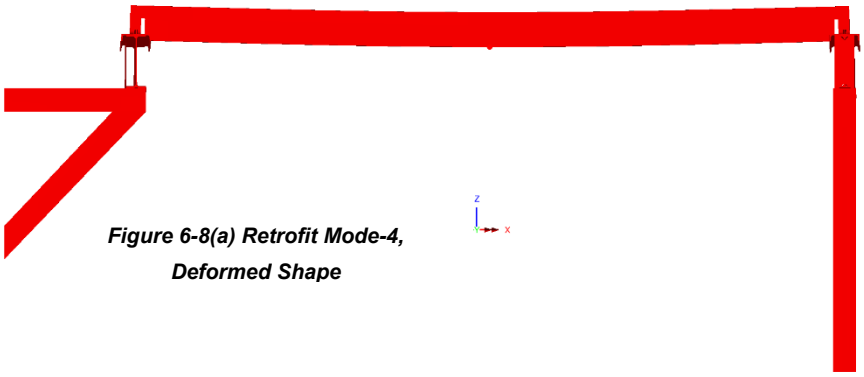

Figure 6-8(a) Retrofit Mode-4, Deformed Shape

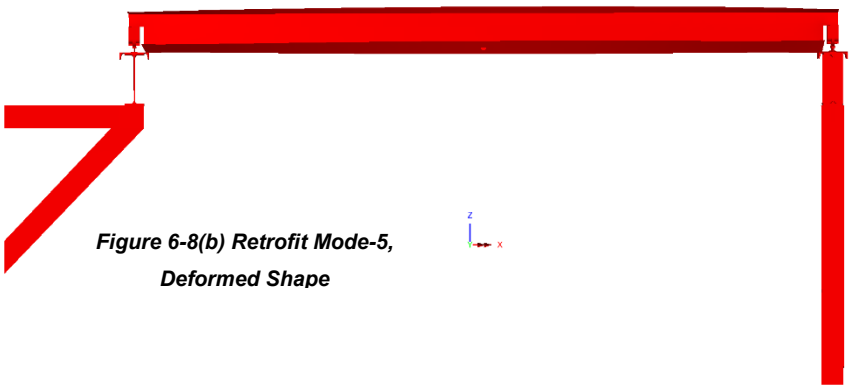

Figure 6-8(b) Retrofit Mode-5, Deformed Shape

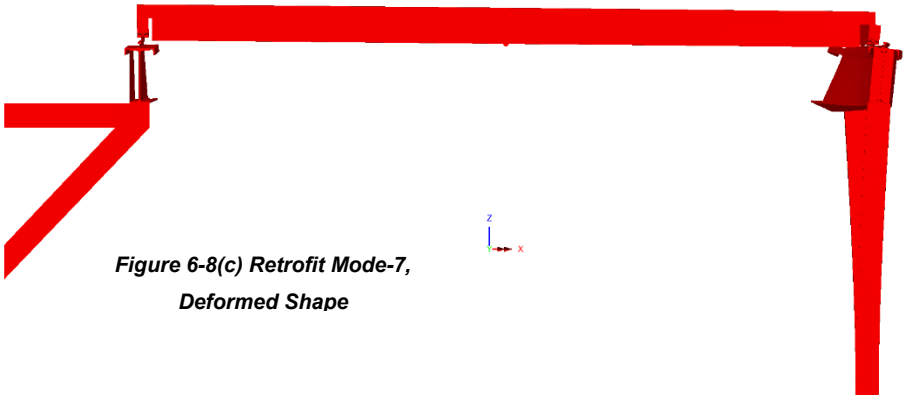

Figure 6-8(c) Retrofit Mode-7, Deformed Shape

6.3 PROPOSED EQUATIONS

6.3.1 INTRODUCTION

To produce a three-dimensional model, as done in this thesis, for every crane system to check for torsional vibration is not reasonable or economical for an engineer. Such as done in other codes (AASHTO Pedestrian Bridge Design and seismic provisions

of ASCE) equations should be used to check if torsional vibration of the runway beam is of concern. Based on these results would conduct the designer to which method of analysis and to what degree of analysis should the designer preform. The next two sections will discuss possible equations to determine if torsional vibration is an issue in a crane system. The analytic model was the result of the bridge transverse natural vibration (mode 4 in the unmodified crane system) which resulted in the torsional rotation of the runway beam as a secondary effect. The equations presented here, however, will focus on the torsional mode of vibration which when converged in the retrofit solutions was found to be mode 5 with respect to the unmodified crane system. If the equations are used to design or check the runway beams for possible runway for the torsional mode, the resulting torsional stiffness increase is likely to negate rotational secondary effects from the bridge of other elements as in the analyses in *Chapter 6*. Likewise, the torsion mode of vibration (mode 5 in the analytic model) was not found to be the cause of the runway rotation, however, since the frequency is within the harmonic spectrum of considerable amplitude, the mode could have equally been an issue if the inching frequency would have coincided.

6.3.2 TORSION THEORY EQUATIONS

The first approach towards a simplified approximation to the torsional vibration of the runway beams is using the general torsion theory to develop approximate equations. From general vibration theory, *Equation 6-1* will be used as the base. *Equation 6-2*, however, is not in useful terms for our purposes. Using *Equation 6-2* and *Equation 6-3*, from general vibration theory, the circular frequency, ω_n, can be converted to frequency or period.

$$\omega_n = \sqrt{\frac{k}{m}} \qquad (6\text{-}1)$$

$$f_n = \frac{\omega_n}{2\pi} \qquad (6\text{-}2)$$

$$T_n = \frac{1}{f_n} \qquad (6\text{-}3)$$

Where,

ω_n = The natural circular frequency of vibration

k = Stiffness

m = Mass

$0 \le z \le \alpha l$

The stiffness of the runway beam, k, has not yet been defined. Using the stiffness method (or also known as the displacement method) we can define the stiffness, or rather rotational stiffness, as a unit of torsion which results in the runway's rotation as shown in *Equation 6-4*.

$$k = \frac{T}{\theta} \qquad (6\text{-}4)$$

Where,

θ = Runway beam rotation

T = Torsion force

The rotation of the runway, which has not yet been defined, must take into account the possible warping of the open cross-section. The derivation of general torsion for an open cross-section can be very difficult and time consuming. Fortunately, a close approximation can be used from ASIC's Design Guide 9 (DG-9) (Seaburg & Carter, 2003).

Equation 6-5 and *Equation 6-6* are both from DG-9 found in the appendix. *Equation 6-5* is for a simply supported beam and *Equation 6-6* is for a fixed-fixed beam. The equations are based on a unit or torque acting at a point on the beam. For simplification purposes our equations will define the torque to act at the center of the beam; this will be accomplished by setting α=0.5.

$$\theta = \frac{Tl}{GJ} \cdot \left[(1.0 - \alpha) \cdot \frac{z}{l} + \frac{a}{l} \cdot \left(\frac{\sinh\left(\frac{\alpha l}{a}\right)}{\tanh\left(\frac{l}{a}\right)} - \cosh\left(\frac{\alpha l}{a}\right) \right) \cdot \sinh\left(\frac{z}{a}\right) \right] \qquad (6\text{-}5)$$

$$\theta = \frac{Ta}{(H+1)GJ} \left\{ [H \cdot A + B] \times \left[\cosh\left(\frac{z}{a}\right) - 1.0 \right] - \sinh\left(\frac{z}{a}\right) + \frac{z}{a} \right\} \qquad (6\text{-}6)$$

Where,

$$A = \left(\frac{1}{\sinh\left(\frac{l}{a}\right)} + \sinh\left(\frac{\alpha l}{a}\right) - \frac{\cosh\left(\frac{\alpha l}{a}\right)}{\tanh\left(\frac{l}{a}\right)} \right)$$

$$B = \left(\sinh\left(\frac{\alpha l}{a}\right) - \frac{\cosh\left(\frac{\alpha l}{a}\right)}{\tanh\left(\frac{l}{a}\right)} + \frac{1}{\tanh\left(\frac{l}{a}\right)} \right)$$

$$a = \sqrt{\frac{EC_w}{GJ}}$$

$$z = \alpha \cdot l$$

α = 0.5

The stiffness can now be defined, and all other variables are now available to solve for the stiffness. Because *Equation 6-1* is derived from a force and unit displacement, the equation must be adapted for a torque and unit rotation as done in *Equation 6-7*. The modification essentially uses the mass polar moment of inertia.

$$\omega_n = \sqrt{\frac{k}{I_p \rho l}} \qquad (6\text{-}7)$$

Where,

I_p = Polar moment of inertia

ρ = mass density of bar

l = length

If the stiffness is doubled in *Equation 6-7*, assuming the stiffness are in parallel, then the resulting frequency obtained, rotation using *Equation 6-5*, is found to be 3.71 seconds^{-1}. Using *Equation 6-6*, the frequency was found to be 4.78 seconds^{-1}. From the equations, the fixed-fixed condition represents the natural frequency found in the unmodified analytic system. The fixed-fixed boundary condition equation most likely represented the frequency found in the model do to the restraint of warping at the beam ends due to the column, stiffener, and tie-back connections. The torsion natural frequency of the unmodified analytic model was found to be 4.158 seconds^{-1}. The lower frequency obtained in the model, compared to that of the fixed-fixed condition equation, is highly likely due to the decreased rotation stiffness from the supporting columns.

6.3.3 GERE EQUATIONS

Another method which may be useful in approximating the torsion natural frequency of the runway beams will use equations derived by Gere (Gere, 1954) for the torsional vibration of open-walled sections. The torsion natural frequency derived by Gere is presented as *Equation 6-8*.

$$\omega_n = \frac{n\pi}{l^2} \cdot \sqrt{\frac{n^2\pi^2 EC_w + l^2 GJ}{m \cdot I_p}} \qquad (6\text{-}8)$$

Using the equation directly gives a torsional natural frequency of 3.77 seconds^{-1}. The reader should note that both the equation methods presented give values close to mode 4 of the transverse bridge movement. The similarity between values is a coincidence. Although the equations are not a perfect solution, each of the methods presented (aside from *Equation 6-6*) all give conservative values. If one was to use the equations for the design of the beam, the actual torsional natural frequency would be much greater.

CHAPTER 7

RESULT'S SUMMARY & CONCLUSION

The extent of the authors knowledge of the crane system's retrofit is confined to the discussion at the facility. The solution retrofit for the torsion of the runway was to plate each side of each runway beam; plates would be added from wide-flange bottom flange to top flange, on each side, for both runway beams. In addition, the columns were to be reinforced with a channel oriented to the major axis about the "x-axis" direction as shown in the above figures. From a material and a welding/fabrication stand-point, this cost would be enormous. From the above analyses, however, the solution uses significantly less material and fabrication. For the proposed retrofit solution, the side plates would call for approximately 240 linear feet of side plate. The last eigenvalue analysis preformed, which used a side plate from the column to the nearest wheel on each runway, requires approximately 54 linear feet of side plate. The solution found in the LUSAS model which produced a reasonable frequency is approximately 23% of the material used for the proposed retrofit discussed on site.

The equations presented in Chapter-6 provide useful approximations in determining the torsional natural frequency of the system. Using these conservative equations, the resulting torsional stiffness is likely to negate any other modes which torsional rotation is of concern. Equations to approximate the torsional natural frequency when only partial modification is made to the cross-section (as opposed to the entire span) as presented as the retrofit solution would be difficult if not nearly impossible to solve. The designer, if wanting to retrofit a crane system for increased torsional stability, should either make the costly decision to modify the cross-section along its entire span or run an in-

depth finite element analysis. The results of the finite element, however, may lead the designer to modify the cross-section along its entire span anyways. With the little research done on torsional natural frequency of runway beams makes prediction of frequencies and deformations difficult. The key to designing a runway beam without torsional resonance is in the preliminary design stages; selecting an initial cross-section which will not be susceptible to resonance vibration especially torsional vibration. The reader and runway designer should also strive for more communication between the use of the crane and the effect of the crane members; the bridge should be checked for vibration concerns.

APPENDIX A

RUNWAY CALCULATION EXAMPLE

A.1 DESIGN EXAMPLE

The following design example will be a repeat of the example provided by Fisher in DG-7 (Fisher, DG 7, 2004), however, using the suggested design procedure provided by Ellifritt and Lue (Elifritt & Lue, 1998). Although the same example is provided in (Elifritt & Lue, 1998), the yield strength of the runway beam was taken as 36-ksi opposed to the design example in DG-7, which was taken as 50-ksi. The yield strength of material in this example will be taken as 50-ksi as to directly compare the results between the suggested design procedures provided here and the commonly used AISC equations based off the 3-plate section. In addition, the example here will slightly differ from (Elifritt & Lue, 1998); updates to current standards and computer based section properties.

A.1.1 GIVEN DESIGN INFORMATION

The following information is based on the crane information provided in DG-7 Example 18.1.1 (Fisher, DG 7, 2004).

- Crane Capacity = 20 tons (40 kips)
- Bridge Span = 70 ft
- Type of Control – Cab Operated
- Bridge Weight = 57.2 kips
- Combined Trolley and Hoist Weight = 10.6 kips
- Maximum Wheel Load (without impact) = 38.1 kips
- Wheel Spacing = 12 ft.
- Runway Girder Span = 30 ft.
- Assume no reduction in allowable stress due to fatigue.

- Use AISC criteria and A992 steel for the beam section and A572 Grade 50 channel cap.
- Recall from Section 2.3.5; Use a load factor of 1.2 for the bridge weight and a load factor of 1.6 for the hoist and trolley weight.

The intent of this design example is strictly for comparison purposes. For this reason, a W27×94 w/ C15×33.9 will be checked.

A.1.2 CALCULATION OF FORCES AND MOMENTS

The forces listed previously for this design were based on the total weight per the respective member. The forces must be per each wheel must be determined. Likewise, the weight of the bridge must be separated from the weight of the capacity and weight of the trolley and hoist. The separation of the weights will be needed later when finding the factored point loads and the lateral force.

The weight of the bridge can be found per wheel as follows;

$$W_{bridge} = 57.2/4 = 14.3\ kip$$

Recall from ASCE, the lateral force is to be taken as a percentage of the sum of the capacity and the weight of the trolley and hoist. The reader should note the maximum wheel loadings listed by the manufacturer include, from the authors experience, will be slightly larger than the sum of the full weight of the capacity, bridge, trolley, and hoist to account for other components that make up the crane. For this reason, when finding the vertical loading, the designer should subtract the maximum wheel load from the weight of the bridge.

$$W_{trolley+hoist+capacity} = P_{max} - W_{bridge} = 38.1 - 14.3 = 23.8\ kip$$

For the factored vertical loads (using ultimate load combination 1-eq-4),

$$P_u = 1.2 \cdot \left(W_{bridge}\right) + 1.6 \cdot \left(W_{trolley+hoist+capacity}\right) = 1.2 \cdot (14.3) + 1.6 \cdot \left(23.8\right) = 55.2\ kip$$

$$P_{impact} = f_{impact} \cdot \left(P_{max}\right) = 0.25 \cdot \left(W_{bridge}\right) + 0.25 \cdot \left(W_{trolley+hoist+capacity}\right)$$

$$P_{u.impact} = 0.25 \cdot \left(1.2 \cdot 14.3\right) + 0.25 \cdot \left(1.6 \cdot 23.8\right) = 4.29 + 9.52 = 13.8\ kip$$

$$P_{u+impact} = P_u + P_{u.impact} = 55.2 + 13.8 = 69.0\ kip$$

For the lateral loads,

$$P_{lateral} = 0.20 \cdot \left(W_{trolley+hoist} + W_{load}\right) = 0.20 \cdot \left(10.6 + 40\right) = 10.1\ kip$$

$$P_{u.lateral} = 1.6 \cdot P_{lateral} = 1.6 \cdot \left(10.12\right) = 16.2\ kip$$

$$P_{u.lateral} = 4.05\ kip$$

For the self-weight dead load, assume a girder weight (and rail) weight of 148 plf (the weights will be checked after the design),

$$P_{girder+rail} = 148\ plf$$

$$P_{u.girder+rail} = 1.2 \cdot \left(P_{girder+rail}\right) = 1.2 \cdot \left(148\right) = 178\ plf$$

Because of the popularity in computational programs, the author of this thesis would suggest setting up an array to find the maximum moment quickly and effectively—Use AISC's moment diagram in AISC Steel Construction Manual (Table 3-23 pg.3-216) to calculate the moment due to the wheel loads along an interval of points and superimpose the results with the moment along the same interval with the moment due to the self-weight of the runway and rail. In the calculations provided below an interval of 0.25-ft was used: Results may improve if your interval is reduced. The array analysis along interval points was performed in *MATHCAD 3.0*.

Using diagram 10 *Simple Beam – Two Equal Concentrated Loads Unsymmetrically Placed* (unsymmetrically placed loads due to the fact the crane is moving along the runway) (ASIC, 2010).

$$M_1 = M_{max} = R_1 \cdot a$$

Where, $R_1 = \frac{P}{l} \cdot (l - a + b)$

The following two equations can be written in terms of our variables;

$$R_1 = \frac{P_{u+impact}}{L} \cdot (L - a + b)$$

Plugging R_1 into the moment equation,

$$M_1 = \left[\frac{P_{u+impact}}{L} \cdot (L - a + b) \right] \cdot a$$

Also, from the assumed self-weight of the girder and rail,

$$M_x = \frac{w \cdot x}{2} \cdot (l - x)$$

Or written in terms of our variables,

$$M_x = \frac{w_{u.girder+rail} \cdot x}{2} \cdot (L - x)$$

$$M_u = \left[\frac{P_{u+impact}}{L} \cdot (L - a + b) \right] \cdot a + \frac{w_{u.girder+rail} \cdot x}{2} \cdot (L - x)$$

The maximum moment at any point as the crane travels along the runway can be found as,

$$M_{ux} = 681.58\ kip \cdot ft$$

The deflection analysis of the example will not be provided here. The intent of this example is to introduce another strength design method; the deflection or serviceability of

the member is not the topic. Likewise, the deflection will be calculated the same way as shown in DG-7.

Section Properties WC:

Z_x = 357 in.^{4}

Z_y = 89.6 in.^{4}

S_{xc} = 435 in.^{3}

S_{xt} = 268 in.^{3}

Section Properties W:

A^w = 27.6 in.^{2}

d^w = 26.9 in.

b_f^w = 10.0 in.

t_w^w = 0.490 in.

t_f^w = 0.745 in.

I_y^w = 124 in.^{4}

$Z_y^w = 38.8$ in.^{3}

J^w = 4.03 in.^{4}

C_w^w = 21300 in.^{6}

Section Properties C:

A^c = 10.0 in.^{2}

t_w^c = 0.400 in.

b_f^c = 3.40 in.

I_y^c = 8.07 in.^{4}

I_x^c = 315 in.^{4}

J^c = 1.01 in.^{4}

$Z_x^c = 50.8$ in.^{3}

A.1.3 SOLUTION ANALYSIS 1

$$M_P = Z_x \cdot F_y \le 1.6 \cdot S_{xc} \cdot F_y \quad \text{(Eq-7)}$$

$$M_P = (357) \cdot (50) \le 1.6 \cdot (435) \cdot (50) = 17850 \le 34800$$

$$M_P = 17850 - kip \cdot in = 1487.5\ kip \cdot ft$$

$$M_r = min(F_L \cdot S_{xc}, F_y \cdot S_{xt}) \quad \text{(Eq-8)}$$

$$F_L = F_y - F_R \quad \text{(Eq-9)}$$

Where residual stress per the 1999 Specification (AISC),

F_R (residual stress) = 16.5-ksi (10-ksi suggested satisfactory per (Elifritt & Lue, 1998))

The residual stress was changed from a constant 16.5-ksi in the 1999 Specification to the 0.3F_y found in the 2005 Specification. This change, to update to current standards, will be adopted in this thesis. (Elifritt & Lue, 1998) suggested using a residual stress of 10-ksi because of a low heat input required to join the two members. The 10-ksi residual stress was lower than the suggested value of 16.5-ksi, which the specification recommends.

Fisher (Fisher, DG 7, 2004)used the value the Specification recommends of 16.5-ksi. The value of $0.3F_y$ will be used in this thesis in lieu of a reduced equivalent used by Ellifritt and Lue.

Therefore, the residual stress can be defined as,

$$F_R = 0.3F_y$$

$$F_L = 0.7F_y \qquad \text{(Eq-9)}$$

$$F_L = 0.7F_y = 0.7 \cdot (50) = 35\ ksi$$

$$M_r = min(35 \cdot 435, 50 \cdot 268) = min(15225, 13400) = 13400\ kip \cdot in$$

$$M_r = 13400\ kip \cdot in. = 1116.7\ kip \cdot ft$$

$$M_n = M_p - (M_p - M_r) \cdot \left(\frac{L_b - L_p}{L_r - L_p} \right) \qquad \text{(Eq-10)}$$

$$I_{yc} = \frac{I_y^w}{2} + I_x^c \qquad \text{(Eq-13)}$$

$$I_{yc} = \frac{I_y^w}{2} + I_x^c = \frac{124}{2} + 315 = 377\ in^4$$

$$r_{yc} = \sqrt{\frac{I_{yc}}{A^c + (b_f^w \cdot t_f^w)}} = \sqrt{\frac{377}{10 + (10 \cdot 0.745)}} = 4.65\ in$$

$$L_p = \frac{300 \cdot r_{yc}}{\sqrt{F_y}} = \frac{300 \cdot (4.65)}{\sqrt{50}} = 197.2\ in. = 16.43\ ft$$

The next step in the design process is to find the limiting unbraced length, L_r. To find L_r, *Equations 14-16* must be iterated until $M_e = M_r$. To perform the operation to get an exact solution and to eliminate the need for repetitive calculations, the operation was

performed using *MATHCAD 3.0*. Although the solution is already known, an example of the iteration will be performed for clarity.

$$M_e = \frac{\pi}{L_b} \cdot \sqrt{E \cdot I_y \cdot G \cdot J} \cdot \left(B_1 + \sqrt{1 + B_2 + B_1^2} \right)$$

$$B_1 = \frac{\pi \cdot \beta_x}{2 \cdot L_b} \cdot \sqrt{\frac{E \cdot I_y}{G \cdot J}}$$

$$B_2 = \frac{\pi^2 \cdot E \cdot C_w}{L_b^2 \cdot G \cdot J}$$

$$C_w = C_w^w \cdot \left(0.79 + 1.79 \cdot \sqrt{\frac{A^c}{A^w}} \right)$$

$$C_w = C_w^w \cdot \left(0.79 + 1.79 \cdot \sqrt{\frac{A^c}{A^w}} \right) = 21300 \cdot \left(0.79 + 1.79 \cdot \sqrt{\frac{10.0}{27.6}} \right) = 39776.8\ in^6$$

$$R = 2 \cdot \frac{I_{yc}}{I_y} = 2 \cdot \frac{377}{439} = 1.72$$

$$\beta_x = 0.87 \cdot (R - 1) \cdot \left(d^w + \frac{b_f^c}{2} \right)$$

$$\beta_x = 0.87 \cdot (R - 1) \cdot \left(d^w + \frac{b_f^c}{2} \right) = 0.87 \cdot (1.72 - 1.00) \cdot \left(26.9 + \frac{3.40}{2} \right) = 17.85$$

$$J = J^w + J^c + \left(b_f^w \cdot t_f^w \cdot t_w^c \cdot \left(t_f^w + t_w^c \right) \right)$$

$$J = J^w + J^c + \left(b_f^w \cdot t_f^w \cdot t_w^c \cdot \left(t_f^w + t_w^c \right) \right)$$

$$J = 4.03 + 1.01 + \left(10 \cdot 0.745 \cdot 0.40 \cdot (0.745 + 0.40) \right) = 8.45\ in^4$$

From the appendix of this report,

$$J = 7.816\ in^4$$

The torsional constant, J, found through computer analysis will be used. The two torsional constant values may seem different, however, the torsional constant found by *Equation 2-22* was found to be very similar to the computer analysis when a coarse meshed was used.

Also, from the AISC Steel Construction Manual,

$$E = 29000\ ksi,\ G = 11200\ ksi$$

Because L_r will be the unbraced length to which $M_e = M_r$, L_b in *Equations 14-16* must be set to L_r.

To find L_r, first guess $L_r = L_b = 40 - ft. = 480\ in$

$$B_1 = \frac{\pi \cdot \beta_x}{2 \cdot L_r} \cdot \sqrt{\frac{E \cdot I_y}{G \cdot J}} \quad \text{(Eq-15b)}$$

$$B_1 = \frac{\pi \cdot \beta_x}{2 \cdot L_r} \cdot \sqrt{\frac{E \cdot I_y}{G \cdot J}} = \frac{\pi \cdot 17.85}{2 \cdot 480} \cdot \sqrt{\frac{29000 \cdot 439}{11200 \cdot 8.694}} = 0.668$$

$$B_2 = \frac{\pi^2 \cdot E \cdot C_w}{L_r^2 \cdot G \cdot J} \quad \text{(Eq-16)}$$

$$B_2 = \frac{\pi^2 \cdot E \cdot C_w}{L_r^2 \cdot G \cdot J} = \frac{\pi^2 \cdot 29000 \cdot 39776.8}{480^2 \cdot 11200 \cdot 8.694} = 0.508$$

$$M_e = \frac{\pi}{L_r} \cdot \sqrt{E \cdot I_y \cdot G \cdot J} \cdot \left(B_1 + \sqrt{1 + B_2 + B_1^2}\right)$$

$$M_e = \frac{\pi}{480} \cdot \sqrt{29000 \cdot 439 \cdot 11200 \cdot 8.694} \cdot \left(0.668 + \sqrt{1 + 0.508 + 0.668^2}\right)$$

$$M_e = 15054.82 - kip \cdot in. = 1254.57\ kip \cdot ft$$

Recall, $M_r = 1116.7\ kip \cdot ft$

$$M_e \neq M_r$$

In general, we are solving for the unbraced length, L_b, which we defined as L_r in the previous equations. The unbraced length set to L_r returned an elastic buckling moment, M_e, slightly below M_r. The result can be interpreted as the L_b (guessed at 40 feet) returned a moment capacity, M_e, greater than the elastic buckling strength, M_r; with an unbraced length of 40 feet the section is still in the region of inelastic lateral-torsional buckling. The next guess of L_r should be a larger length, which will further lead our section to the elastic buckling strength. The iteration action process is summarized below.

If,

$M_e < M_r \rightarrow$ Decrease guess value of L_r

$M_e > M_r \rightarrow$ Increase guess value of L_r

$M_e = M_r \rightarrow$ Guess value of L_r = actual value of L_r

Based on the above discussion, the next iteration will be performed;

$L_r = L_b = 43 - ft. = 516\ in$ (To eliminate the need for multiple iterations, and because the actual solution is already known (from computer analysis) the length of 43-ft. was chosen.)

Repeating the same steps as previously,

$$B_1 = \frac{\pi \cdot \beta_x}{2 \cdot L_r} \cdot \sqrt{\frac{E \cdot I_y}{G \cdot J}} = \frac{\pi \cdot 17.85}{2 \cdot 516} \cdot \sqrt{\frac{29000 \cdot 439}{11200 \cdot 8.694}} = 0.621$$

$$B_2 = \frac{\pi^2 \cdot E \cdot C_w}{L_r^2 \cdot G \cdot J} = \frac{\pi^2 \cdot 29000 \cdot 39776.8}{516^2 \cdot 11200 \cdot 8.694} = 0.440$$

$$M_e = \frac{\pi}{516} \cdot \sqrt{29000 \cdot 439 \cdot 11200 \cdot 8.694} \cdot \left(0.621 + \sqrt{1 + 0.440 + 0.621^2}\right)$$

$$M_e = 13368.82 - kip \cdot in. = 1114.1\, kip \cdot ft$$

Recall, $M_r = 1116.7\, kip \cdot ft$

$$M_e \approx M_r$$

Since M_e is approximately equal to M_r, the unbraced length of 43 feet is found to be equal to L_r. From program analysis, the actual unbraced length which M_e is equal to M_r is 42.94 feet. The actual unbraced length will be used throughout the rest of this example.

$$L_r = 42.94\ ft$$

Since, $L_p < L_b < L_r$

$$M_{nx} = M_p - \left(M_p - M_r\right) \cdot \left(\frac{L_b - L_p}{L_r - L_p}\right) \quad \text{(Eq-10)}$$

$$M_{nx} = 17850 - \left(17850 - 13400\right) \cdot \left(\frac{30 - 16.43}{42.94 - 16.43}\right)$$

$$M_n = 15572.1 - kip \cdot in. = 1297.7\, kip \cdot ft$$

$$\phi M_{nx} = \phi \cdot M_{nx} = 0.9 \cdot 1297.7 = 1167.9\, kip \cdot ft$$

$$\phi M_{nx} > M_{ux}$$

Likewise, the other solution to the limit state of lateral torsional buckling offered by Ellifritt and Lue, which eliminates the need for iterations,

A.1.4 SOLUTION ANALYSIS 2

$$M_{nx} = M_p - \left(M_p - M_r\right) \cdot \left(\frac{\lambda - 0.49}{1.15 - 0.49}\right)$$

$$\lambda = \sqrt{\frac{M_p}{M_e}}\ ,\ 0.49 < \lambda < 1.15$$

$$F_L = 0.7F_y$$

$$F_L = 0.7F_y = 0.7 \cdot (50) = 35\ ksi$$

$$M_r = min(35 \cdot 435, 50 \cdot 268) = min(15225, 13400) = 13400\ kip \cdot in$$

$$M_r = 13400 - kip \cdot in. = 1116.7\ kip \cdot ft$$

$$M_P = Z_x \cdot F_y \le 1.6 \cdot S_{xc} \cdot F_y$$

$$M_P = (357) \cdot (50) \le 1.6 \cdot (435) \cdot (50) = 17850 \le 34800$$

$$M_P = 17850 - kip \cdot in = 1487.5\ kip \cdot ft$$

$$M_e = \frac{\pi}{L_b} \cdot \sqrt{E \cdot I_y \cdot G \cdot J} \cdot \left(B_1 + \sqrt{1 + B_2 + B_1^2}\right)$$

$$B_1 = \frac{\pi \cdot \beta_x}{2 \cdot L_b} \cdot \sqrt{\frac{E \cdot I_y}{G \cdot J}} = \frac{\pi \cdot 17.85}{2 \cdot 360} \cdot \sqrt{\frac{29000 \cdot 439}{11200 \cdot 8.694}} = 0.891$$

$$B_2 = \frac{\pi^2 \cdot E \cdot C_w}{L_b^2 \cdot G \cdot J} = \frac{\pi^2 \cdot 29000 \cdot 39776.8}{360^2 \cdot 11200 \cdot 8.694} = 0.902$$

$$M_e = \frac{\pi}{360} \cdot \sqrt{29000 \cdot 439 \cdot 11200 \cdot 8.694} \cdot \left(0.891 + \sqrt{1 + 0.902 + 0.891^2}\right)$$

$$M_e = 24610.4 - kip \cdot in. = 2050.9\ kip \cdot ft$$

$$\lambda = \sqrt{\frac{M_p}{M_e}} = \sqrt{\frac{1487.5}{2050.9}} = 0.852$$

$$0.49 < 0.852 < 1.15$$

$$M_{nx} = M_p - \left(M_p - M_r\right) \cdot \left(\frac{\lambda - 0.49}{1.15 - 0.49}\right)$$

$$M_{nx} = 1487.5 - \left(1487.5 - 1116.7\right) \cdot \left(\frac{0.852 - 0.49}{1.15 - 0.49}\right)$$

$$M_{nx} = 15409.5 - kip \cdot in. = 1284.1\, kip \cdot ft$$

$$\phi_b M_{nx} = \phi_b \cdot M_{nx} = 0.9 \cdot 1284.1 = 1155.7\, kip \cdot ft$$

A.1.5 SOLUTION COMPARISON

The percent difference can be found between the two solutions presented above;

$$\%Difference = \frac{\left|\phi_b M_{nx.1} - \phi_b M_{nx.2}\right|}{0.5 \cdot \left(\phi_b M_{nx.1} + \phi_b M_{nx.2}\right)} \cdot 100\%$$

Where,

$\phi_b M_{nx.1}$ = The design moment capacity based on the limit state of lateral torsional buckling found in solution 1.

$\phi_b M_{nx.2}$ = The design moment capacity based on the limit state of lateral torsional buckling found in solution 2.

Therefore,

$$\%Difference = \frac{\left|1167.9 - 1155.7\right|}{0.5 \cdot \left(1167.9 + 1155.7\right)} \cdot 100\% = 1.04\%$$

The percent difference between the two solutions is negligible and very acceptable for most engineering applications.

A.1.5.1 Check Minor Axis Bending

$$M_{uy} = 38.9\ kip \cdot ft$$

Since the section has compact flanges and a compact web,

$$M_{ny} = F_y \cdot Z_x^c + F_y \cdot \frac{Z_y^w}{2} = 50 \cdot 50.8 + 50 \cdot \frac{38.8}{2}$$

$$M_{ny} = 3510 - kip \cdot in. = 292.5\ kip \cdot ft$$

$$\phi_b M_{ny} = \phi_b \cdot M_{ny} = 0.9 \cdot 292.5 = 263.3\ kip \cdot ft$$

$$\phi_b M_{ny} > M_{uy}$$

A.1.5.2 Check Biaxial Bending

$$\frac{M_{ux}}{\phi_b M_{nx}} + \frac{M_{uy}}{\phi_b M_{ny}} \leq 1.0 \text{ (Eq-26b)}$$

$$\frac{681.58}{1167.9} + \frac{38.9}{263.3} = 0.584 + 0.148 = 0.732 \leq 1.0$$

$$0.732 \leq 1.0$$

A.1.5.3 Check Sidesway Buckling

Since the compression flange is not restrained against rotation;

$$\left(h/t_w^w\right)/\left(L_b/b_f^w\right) \leq 1.7$$

Where,

h (by AISC) = clear distance between flanges less the fillet or corner radius for rolled shapes; distance between adjacent lines of fasteners or the clear distance between flanges when welds are used for built-up shapes

$$h = d^w - 2 \cdot k_{des}^w = 26.90 - 2 \cdot (1.34) = 24.22\ in$$

$$\left(h/t_w^w\right)/\left(L_b/b_f^w\right) \le 1.7$$

$$(24.22/0.49)/(360/10.0) = 1.37 \le 1.70$$

$$R_n = \frac{C_r \cdot \left(t_w^w\right)^3 \cdot t_f^w}{h^2} \cdot \left[0.4 \cdot \left(\frac{h/t_w^w}{L_b/b_f^w}\right)^3\right] \quad \text{(Eq-28b)}$$

Recall,

$$M_y = M_r = 13400\ kip \cdot in$$

$$M_{ux} = 681.58\ kip \cdot ft$$

$$M_y > M_{ux} \rightarrow C_r = 960000\ ksi$$

Note that the laterally unbraced length, L_b, for the sidesway buckling equations, applies to the unbraced length along either flange, tension or compression. In this example, the unbraced length is 30' for each flange (only braced at the column supports-assumed)

$$R_n = \frac{C_r \cdot \left(t_w^w\right)^3 \cdot t_f^w}{h^2} \cdot \left[0.4 \cdot \left(\frac{h/t_w^w}{L_b/b_f^w}\right)^3\right]$$

$$R_n = \frac{960000 \cdot (0.490)^3 \cdot 0.745}{24.22^2} \cdot \left[0.4 \cdot \left(\frac{24.22/0.490}{360/10.0}\right)^3\right]$$

$$R_n = 148.06\ kip$$

$$\phi R_n = \phi \cdot R_n = 0.85 \cdot 148.06 = 125.85\ kip$$

Recall the maximum factored wheel load (including impact) found previously,

$$P_{u+impact} = 69.0\ kip \qquad \phi R_n > P_{u+impact}$$

REFERENCES

AASHTO. (2009). LRFD Guide Specifications for the Designof Pedestrian Bridges. *American Association of State Highway and Transportation Officials*.

AISE. (2003). Guide for the Design and Construction of Mill Buildings. *Association of Iron and Steel Engineers*(13).

ASCE. (2010). Minimum Design Loads for Building and Other Structures. *American Society of Civil Engineers*, ASCE 7-10.

ASIC. (2010). *Manual of Steel Construction* (14 ed.). Chicago, Il: American Insttitue of Steel Construction.

Bachman, H., & Walter, A. (1987). Vibrations in Structures: Induced by man and machines. *Zulrich: International Association for Bridge and Structural Engineering* .

Bradford, M. A., Woolcock, S. T., & Kitipornchai, S. (2002). Lateral Buckling Design of Crane Runaway Beams . *Structural Stability and Dynamics*.

Bucholdt, H. A., & Nejad, M. (2012). Structural dynamics for engineers. (T. Telford, Ed.) *2nd*.

CMAA. (2010). Specifications for Top Running & Under Running Single Girder Electrical Traveling Cranes Utilizing Under Running Trolley Hoist. In *Crane Manufactures of America.* Charolette, NC: CMAA 74.

Code of Standard Practice for Steel Buildings and Bridges. (2010). In *American Institute of Steel Construction* (14 ed.). Chicago, Illinois: AISC.

Elifritt, D. S., & Lue, D.-M. (1998). Design of Crane Runaway Beam with Channel Cap. *AISC Engineering Journal*, 41-49.

Fisher, J. M. (2004). *Industrial Buildings: Roofs of Anchor Rods* (2nd ed.). ASIC.

Fisher, J. M., & Van De Pas, J. P. (2002). New Fatigue Provisions for the Design of Crane Runaway Girders. *Engineering Journal, 29*(2).

Galambos, T. V. (2008). *Structural Stability of Steel: Concepts and Applications for Structural Engineers.* Hoboken: John Wiley & Sons, INC.

Gere, J. M. (1954). Torsional Vibration of Beams of Thin-Walled Open Section. *Journal of Applied Mechanics*, 381-387.

Goldman, C. (1990). Design of crane runaway girders for top running and underrunning cranes and monorails. *Canadian Journal of Civil Engineering* , 987-1004.

Haupt-Karp, A. V., Urian, G., Campian, C., & Pop, M. (2013). Reinforcing Solutions of Existing Crane Runaway Beams in a Steel Warehouse. *Design, Fabrication, and Economy of Metal Structures*, 443-48.

Hrabovsky, L. (2015). Action on Crane Runaway Caused by Horizontal Forces due to Crane Skewing. *KEM Key Engineering Materials*, 391-99.

Hsu, W. T., Dung, L. M., & Chen, F. Y. (2012). Design Aid for Moment Strength of Built Crane Runaway Girders. *International Journal of Steel Structures*, 403-17.

Inching. (2017). Retrieved from Kone Cranes: http://www.konecranesusa.com/equipment/overhead-cranes/smart-features-for-overhead-cranes/inching

MacCrimmon, R. (2009). *Guide For The Design Of Crane-Supporting Steel Structures.* Niagara Falls, Ontario: Canadian Institute of Steel Construction.

MBMA. (2006). *Low Rise Building Systems Manual.* Cleveland, OH: Metal Building Manufacturers Association.

Mueller, J. E. (1965). Lessons from Crane Runaways. *Engineering Journal, 2*(1).

Nethercot, D. A., & Rockey, K. C. (1972). A Unified Approach to the Elastic Lateral Buckling of Beams. *American Institute of Steel Construction Engineering Journal*, 96-107.

Occupational Safety and Health Administration. (n.d.). Retrieved from United States Department of Labor: https://www.osha.gov/pls/oshaweb/owadisp.show_document?p_table=INTERPRETATIONS&p_id=19732

Rao, S. S. (2004). *Mechanical Vibrations* (5th ed.). Upper Saddle River: Pearson Prentice Hall.

Ricker, D. T. (1982). Tips for Avoiding Crane Runaway Problems. *AISC Engineering Journal*, 181-205.

Seaburg, P. A., & Carter, C. J. (2003). *Torsional Analysis of Structural Steel Members.* American Institute of Steel Construction, Inc.

Sepp, J. (1992). Discussion: Design of crane runaway girders for top running and underrunning cranes and monorails. *Canadian Journalof Civil Engineering*.

Specification for Structural Steel Buildings. (2010). In AISC, *Manual of Steel Construction* (14th ed., pp. 1-552). Chicago, Illinois: AISC. doi:ANS/AISC 360-10